In presenting this dissertation as a partial fulfillment of the requirements for an advanced degree from Emory University, I agree that the Library of the University shall make it available for inspection and circulation in accordance with its regulations, governing materials of this type. I agree that permission to copy from, or to publish, this dissertation may be granted by the professor under whose direction it is written, or, in his absence, by the Dean of the Graduate School when such copying or publication is solely for scholarly purposes and does not involve potential financial gain. It is understood that any copying from, or publication of, this dissertation which involves potential financial gain will not be allowed without written permission.

_____

Jennifer L. Sorrells

Synthesis and Characterization of Unusal Amphiphiles
Part I. Nonsteroidal Facial Amphiphiles
Part II. Diketopiperazine Derived Surfactants

By
Jennifer L. Sorrells
Doctor of Philosophy
Department of Chemistry

_____
Dr. Fredric Menger, Advisor

_____
Dr. Frank McDonald, Committee Member

_____
Dr. Dennis Liotta, Committee Member

Date
Accepted:

_____
Lisa A. Tedesco, Ph.D.

_____
Date

Synthesis and Aggregation of Unusal Amphiphiles
Part I. Nonsteroidal Facial Amphiphiles
Part II. Diketopiperazine Derived Surfactants

By
Jennifer L. Sorrells

B. A., The College of Wooster, 2002

Advisor: Dr. Fredric M. Menger Ph.D.

An Abstract of
A dissertation submitted to the faculty of the Graduate
School of Emory University in partial fulfillment
Of the requirements for the degree of

Doctor of Philosophy.

Department of Chemistry

2008

Abstract

Surfactants have dual functionalities which are able to interact with both water and oil. Designing new surfactants allows for probing the relationship between structure and function in amphiphile self-assembly. In an attempt to strive for a greater understanding of the delicate balance between hydrophobic and hydrophilic structure, this dissertation focuses on new surfactant synthesis and characterization. In Part I, a rigid hydrophobic molecule was studied and there were significant changes to the packing of the molecules in water as compared to a standard surfactant. In Part II, a traditional long alkyl chain was used in combination with a unique diketopiperazine head group. This research has shown that alterations to the standard amphiphile structure greatly impact surfactant assembly in water.

Synthesis and Characterization of Unusal Amphiphiles
Part I. Nonsteroidal Facial Amphiphiles
Part II. Diketopiperazine Derived Surfactants

By
Jennifer L. Sorrells

B. A., The College of Wooster, 2002

Advisor: Dr. Fredric M. Menger Ph.D.

A dissertation submitted to the faculty of the Graduate
School of Emory University in partial fulfillment
Of the requirements for the degree of
Doctor of Philosophy.

Department of Chemistry

2008

Acknowledgments

I would first like to thank my adviser, Dr. Menger. His support, enthusiasm, and guidance during this whole process were invaluable. Dr. Menger was always one to appreciate the unconventional. His willingness to allow me to design my own project and run with it was a freedom rarely accorded to graduate students. As such, it was one of the most influential aspects of my graduate career, and I thank Dr. Menger for the experience. I would also like to thank Lib Menger for graciously hosting a number of lab parties over the years. It was at these parties that I got to enjoy home cooked meals, and listen to stories from the boss about his expeditions in far remote locations.

My committee members, Dr. Liotta and Dr. McDonald, have been an indispensible source of support throughout graduate school. Dr. Liotta's willingness to support students in whatever they find interesting has not gone unnoticed. Without a doubt, Dr. McDonald is one of the best teachers I have encountered in my career; I have learned a lot from him. I also want to thank Tracy Morkin, who supervised me on the HHMI curriculum development grant. The faculty members of the chemistry department have been phenomenal, and I have truly enjoying learning from all of them during my time here.

The research I accomplished could not have been completed without the help of many people: the late Dr. Rob Apkarian; Dr. Hardcastle; Dr. Prasad; Dr. Strobel, members of the Liotta and Liebeskind labs; Patty, Steve, and Sarah in the stockroom; and the entire chemistry department staff.

In terms of the day to day graduate school experience, I would like to thank the people in my lab. I have gotten to work with many people over the years, and my life has

been enriched by them. Mary Chlebowski was a fantastic mentor and lab mate for the first two years. Also, Lei Shi, who I had the pleasure of working with for three years, is an amazing chemist and a great person to have in the lab. Hailing Zhang has also been a wonderful colleague, both while she was here at Emory and in her current position as a faculty member at Mercer University. I also enjoyed working with Ashley Galloway and Hao Lu. I want to thank Syed Rizvi for setting up and working with me on the surface balance experiments. And of course, the lab was not complete without our post-docs Fabs Pertusati and Dan Lundberg, whose assistance and friendship were greatly appreciated.

My graduate career would not have been complete without my friends inside and outside the department. My two best friends in the department, Ana Alcaraz and Uliana Danilenko, have been a wonderful source of support throughout my five years at Emory. I thoroughly enjoyed the chemistry poker crowd (Andy Flick, Erika Milczek, Cara Mosley, Ernest Murray, Annette and Rob Neuman, Dave Stockwell, Shana Topp and Valarie Truax) for all the great games. Brad Balthaser, my always loyal coffee buddy, has helped me through a lot of the tough times. I have enjoyed many late nights with my fellow Atwood penthouse dwellers, in particular Tom Coombs, Reese Lee, and Janette Villalobos. Anil Mehta has been a wonderful mentor and colleague. I would like to thank my friends from college, Andrea Frueh and Maggie Harrod, for their support.

I have been truly blessed to have a wonderful family. My parents have been a constant source of support throughout my life. I would like to thank them both for all of the opportunities they have provided for me. My mom is the strongest, most amazing woman I know, and my father is a natural-born leader and a person of outstanding

character. It is wonderful to be able to have them as my parents as well as two of my best friends. I also want to thank my brother, Jeff, for his support throughout grad school, and I admire his zest for life.

I would like to thank my extended family: the Borlins, the Chases, the McGannons, the McNalleys, the Sylvania Renners, the Tipp City Renners, and the Zingales. Spending holidays and family gatherings with them have always been a welcomed break from the stress of graduate school. Additionally, I would like to thank my grandparents, Bill and Audrey Renner, and Bertha Chase for all of their love and support. Beyond my blood-related family, I have been very fortunate to have a fantastic extended Bowling Green Family. The Dunns (Terry, Theresa, Rachel, and Matthew), the Daltons (Chris, Ellen, and Kathryn), the Nanningas (Nate, Linda, Andy, Nick, and Adam), and the Zhangs (Robert, Yan, and Tian) have always made it wonderful to go home.

Last, but definitely not least, all of this would never have been possible without the love and support of Amy Liu. She has been there for the good times, the bad times, and all of the times in between. Without her, I never could have done this.

Dedicated to My Family

Table of Contents

List of Figures

List of Schemes

List of Equations

List of Tables

List of Abbreviations

PEG	Polyethylene glycol
CMC	Critical micelle concentration
CPP	Critical packing parameter
Orange OT	l-o-tolylazo-2-naphthol
SDS	Sodium dodecyl sulfate
DMF	Dimethylformamide
HOBT	1-hydroxybenztriazole
DCC	Dicyclohexylcarbodiimide
EtOAc	Ethylacetate
DMA	Dimethylacetamide
NMR	Nuclear magnetic resonence
HRSEM	High resolution scanning electron microscopy
HPLC	High pressure liquid chromatrography
ELSD	Evaporative light scattering detector
p-TSA	Para-Toluene sulfonic acid
DMSO	Dimethysulfoxide
Pd/C	Palladium on carbon
DMAP	Dimethylaminopyridine
BOC	tert-Butoxycarbonyl
CBZ	Carbobenzyloxy
SdeS	Sodium decyl sulfate

Introduction

Amphiphiles and Surfactants

Amphiphilic compounds possess two distinctly different regions affecting the chemical properties. These molecules have a hydrophobic region (usually a long chain alkyl group) as well as a hydrophilic portion containing a polar functionality (Figure 1). Surfactants are the one of the most common amphiphiles and are extensively used for industrial applications including food and beverages, paints, cosmetics, detergents, and adhesives.[1] There is substantial interest in studying these molecules, considering the extensive commercial use.

Figure 1. The hydrophobic portion is illustrated in red while the hydrophilic portion of the amphiphile indicated in blue.

Structure

The properties of amphiphilic compounds are strongly dictated by the structure of the molecule. The hydrophobic portion of an amphiphile traditionally contains a long hydrocarbon chain that is often more than 10 carbons in length. The hydrophilic portion, however, can have many different polar functionalities including sulfate, ammonium, or polyethylene glycol (PEG).[1] Surfactants are characterized by the polar characteristics of

the head group including anionic, cationic, zwitterionic, or nonionic (Figure 2).[1] These structural elements combine to create compounds with unique properties. The location of the hydrophilic head relative to the hydrophobic tail has an influential role in the characteristics of the molecules. A surfactant with a hydrophilic group in the center of a 16-carbon alkyl chain would be drastically different from the traditional amphiphilic structures illustrated in Figure 2. The influence of chemical structure on the aqueous solution properties of amphiphiles is the focus of this dissertation.

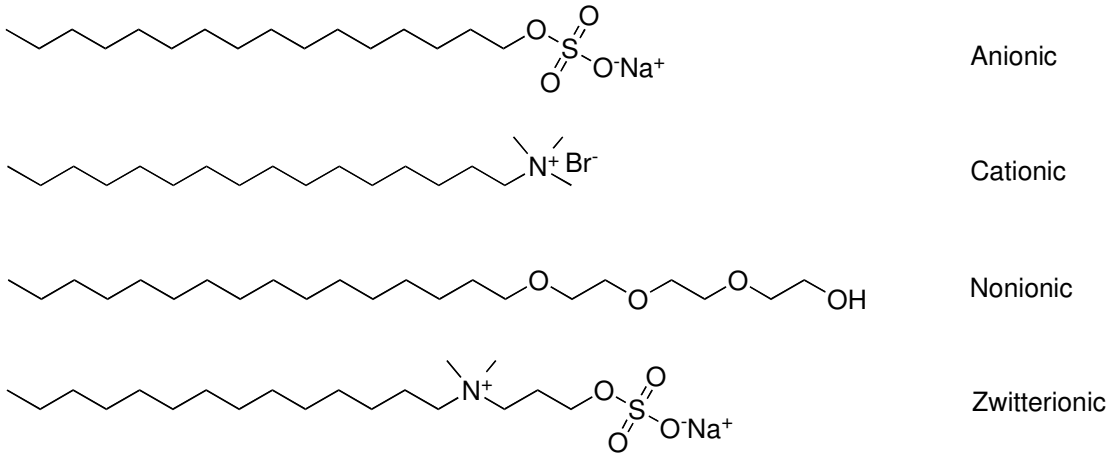

Figure 2. Major types of surfactants based on polar head groups

Surface Activity

The word surfactant is short for surface active agent.[1] Adsorption at the air-water interface is due to the chemical structure of these amphiphiles. At the air-water interface, surfactants align with their hydrophilic head groups in the water layer and their hydrophobic tails protruding into the air (Figure 3). This occurs because the hydrocarbon tails have a more favorable interaction with air than with the polar water molecules.

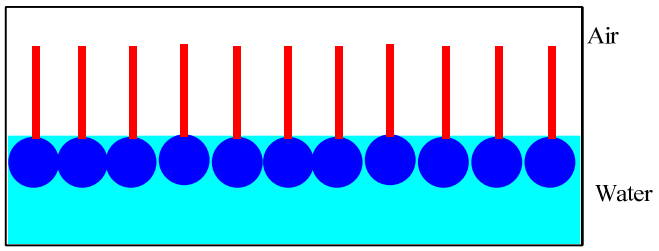

Figure 3. Surfactants at the air-water interface

Surfactants' adsorption at the air-water interface results in a significant decrease in the surface tension of water.[1] Two major factors influence the surface tension of water: (1) the strong attractive forces between the water molecules including hydrogen bonding, London-dispersion, and dipole-dipole interactions; (2) the unbalanced forces between the air and water molecules at the surface. Water molecules in solution feel equivalent forces in all directions (Figure 4). On the surface, the water molecules have stronger interactions with the molecules in the bulk solution than with the air-vapor phase above the surface of the solution. This dissymmetry of forces results in the surface tension of aqueous solutions. When a surfactant adsorbs at the air-water interface it interacts favorably with both the water and the air-vapor phase. This results in a net lowering of the surface tension of the liquid.

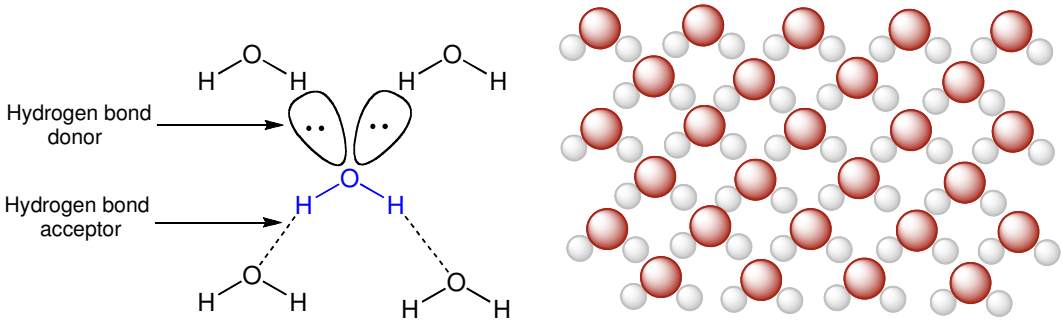

Figure 4. Attractive forces of water molecules

Aggregation and Critical Micelle Concentration

There is a limit to the number of molecules that can associate at the surface of a liquid. In the case of surfactants, once the surface becomes saturated, aggregation occurs in the bulk solution.[1] The driving force for aggregation is the unfavorable interactions of the lipid portion of the surfactant with the bulk aqueous solution.[2] Aggregation occurs in solution at specific concentrations depending on the structure of the surfactant. The number of amphiphiles in the bulk solution increases once the surface is saturated with molecules packing at the air-water interface. The molecules aggregate in a cooperative event once a critical concentration is reached. Many surfactant molecules will come together through favorable interactions of the hydrophobic tails. As the hydrocarbon tails come together the hydrophilic head groups form a protective shell separating the water from the hydrophobic interior of the aggregate. The association of many surfactant molecules into an aggregate is called a micelle.[3] Micellar aggregation is often associated with a spherical shape (Figure 5); however, many different aggregate shapes are possible. Aggregation of surfactants allows for the encapsulation of hydrophobic guests into the interior. Surfactants are one of the major components of detergents assisting in the solubilization of grease.

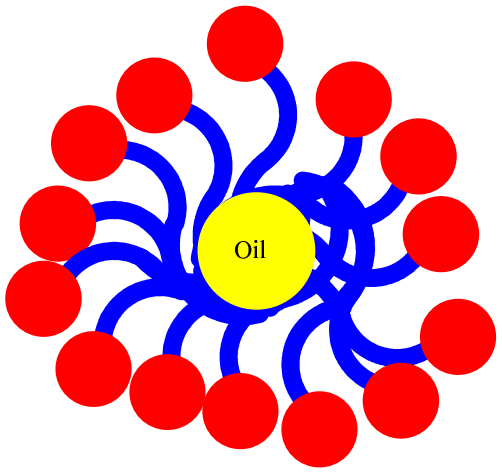

Figure 5. Spherical micelle illustrating the encapsulation of a hydrophobic guest

Types of Aggregates

Beyond the simple spherical micelle, many different shapes of aggregates are possible. The structure of the molecule plays a critical role in the type of aggregate formed. The critical packing parameter (CPP) is a theory based on the effect of surfactant structure on aggregation.[4,5] This predicts aggregate shape based on head-group area, extended chain length, and hydrophobic volume.

The CPP is a number without units that can explain trends in aggregate formation based on the structure of the surfactant. As seen in Equation 1, the CPP is a ratio of the volume of the hydrophobic portion compared to the maximum chain length and the area of the head group.[4,5] This results in a number which can predict a possible aggregate structure (Figure 6). A number greater than 1 predicts a reverse micelle, while a number below 1/3 indicates a traditional spherical micelle. In between, 1 and 1/3 often a bilayer structures are observed.

$$CPP = \frac{v}{l_{\max} \cdot a}$$

Equation 1

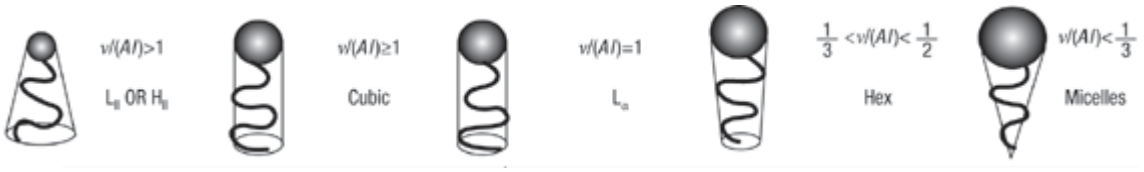

Figure 6. Critical packing parameter as a prediction of aggregate shape[6]

Facial Amphiphiles

Traditional amphiphiles and surfactants have been extensively studied and explored for various solution properties. The purpose of this dissertation is to expand beyond the traditional amphiphile and examine alterations of the basic molecular structure on aggregation in aqueous solution. One unusual class of amphiphilic species is facial amphiphiles, which display different properties from their long chain analogs.

A common facial amphiphile is cholic acid, a steroid. There are three hydroxyl groups on the bottom face of the molecule and the top face is all hydrocarbon functionalities (**Figure 7**). This distinct type of division between hydrophilic and hydrophobic functionalities is the characteristic feature of facial amphiphiles. There have been extensive studies into the aggregation properties of cholic acid and comparable derivatives. I will highlight a few important examples here and then focus on some of the various nonsteroidal facial amphiphiles.

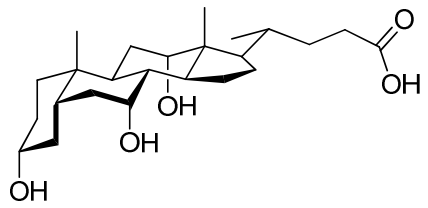

Figure 7. The structure of cholic acid

Easy and readily accessible derivatives of cholic acid are alterations to the hydroxyl or carboxylic acid functional groups. However in terms of facial amphiphilicity, there have been more alterations to the hydroxyl functionalities reported.[7-10] An interesting example is esterification of the hydroxyl functional groups with an alkyl chain bearing a terminal quaternary ammonium (Figure 8).[11] The length of the hydrocarbon chain was varied to contain 3-5 or 7 ethylene groups (indicated by **m**). Additionally, a hydrocarbon chain was placed on the carboxylic acid portion containing 8, 10, 12, or 16 carbons (indicated by **n**). The CMC decreased with increasing spacer length (**m** and **n**) which is the same trend found with traditional surfactants.

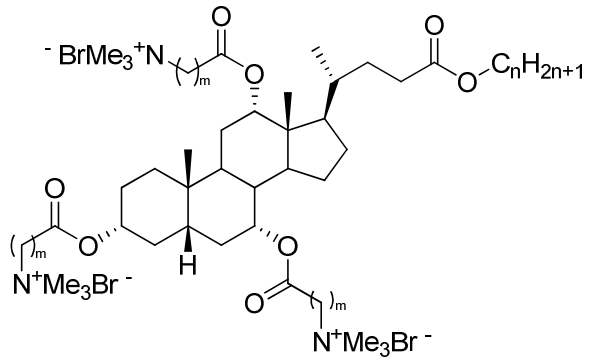

Figure 8. Cholic acid derivatives with quaternary ammonium functionalities as well as varied alkyl spacers **m** and **n**[11]

Cholic acid has also been altered with poly-hydroxyl functionalities, amino alcohols, quaternary ammonium, as well as sodium sulfonate (Figure 9).[12] The CMC of the various compounds has been determined using l-o-tolylazo-2-naphthol (Orange OT) dye solubilization experiments. The reported CMC of these molecules varies significantly (3mM to 25mM). Additionally, the pH dependence has also been examined, and it was observed that the CMC could be tuned based on the combination of pH and structure of the molecule. There have been many other derivatives of cholic acid;[7-10] however, there are other non-steroidal facial amphiphiles.

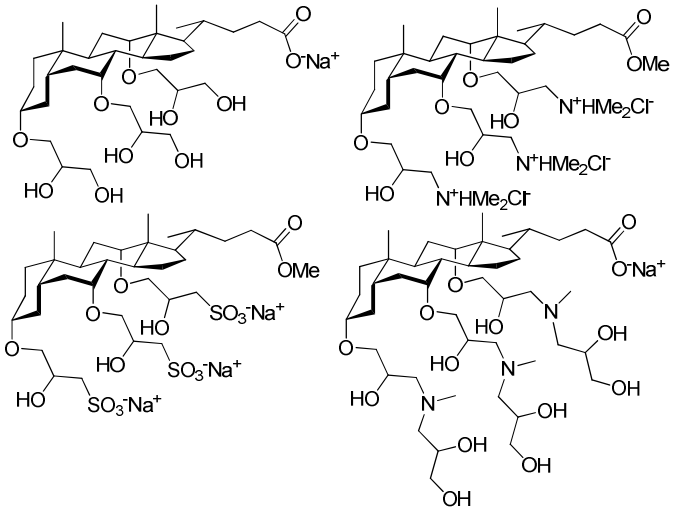

Figure 9. Cholic acid derived facial amphiphiles[12]

Gellman and Barrette synthesized several contrafacial amphiphiles (Figure 10) and examined the aggregation properties in aqueous solution.[13,14] These molecules did not aggregate in a cooperative fashion; however, concentration dependent ^{1}H NMR spectra indicated that there was a gradual change in the chemical shift with respect to concentration. Aggregation occurred anywhere from 20-40 mM (**1a** and **4a**) or 5-10 mM (**2a** and **3a**) depending on the molecule. The authors also used dye solubilization

experiments to probe the hydrophobic core of the aggregate. Their CMC values derived from the dye solubilization experiments differed from those obtained in the NMR experiments. For **1a** aggregation was not observed while in **2a**, **3a**, and **4a** a much higher aggregation concentration was reported (from 60-330 mM).

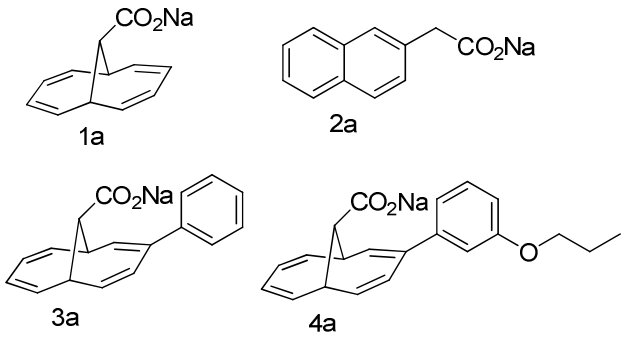

Figure 10. Contrafacial amphiphiles[13,14]

Thus far there has been limited research on the aggregation of non-steroidal rigid amphiphiles. The work by Gellman[13,14] is the first major contribution into the examination of rigid amphiphiles with unique topologies. Part of this dissertation focuses on the preparation and study of new rigid amphiphiles.

Amide-Based Surfactants

Development of new surfactants allows for examining the effects of surfactant structure on assembly properties. One common alteration is the incorporation of unique functionalities into surfactant structure. Traditional surfactants rely on ether, sulfate, carboxylate, amino, and ammonium functionalities to impart water solubility. Many novel surfactants incorporate ester functionalities for their cleavable nature.[15] Amide based surfactants have been developed for their hydrogen bonding capabilities and biodegradability.[15,16]

The amide functional group is a border-line hydrophilic functionality.[17] The hydrophobicity and hydrophilicity of a functional group is described by the octanol/water partition coefficient, referred to as the Hansch parameter. The Hansch parameter for the amide indicate greater hydrophilicity then the alcohol or carboxyl functional groups.[18] However, the amide is significantly less hydrophilic than ionic functionalities such as the quaternary ammonium and the sulfate. This functionality has been of interest in the development of novel surfactants for the hydrophilic behavior as well as the associative hydrogen-bonding interactions.

Menger and Zhang synthesized polyamide based non-ionic surfactants, named peptoads (Figure 11).[15,19,20] The CMC and aqueous solution properties of these di and triamide surfactants has been determined. The length of the hydrophobic segment for the 12 compounds affected the solubility of the molecules.[20] Additionally, the solubility of the molecules was influenced by number of possible intermolecular amide bonds. Three intermolecular amide bonds greatly inhibited solubility, while two intermolecular amide bonds had a strong positive effect on solubility. The peptoad illustrated in Figure 11 showed very high water solubility (> 10M) and dissolved Taxol. The solubilizing power was as efficient as Cremophor EL (the emulsifier used in the formulation of Taxol).

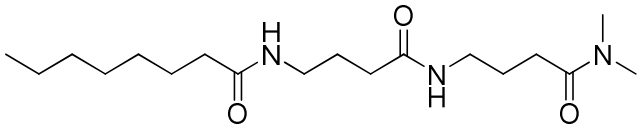

Figure 11. One example of a nonionic Peptoad surfactant[19,20]

A PEG surfactant which incorporated an amide functionality was examined for adsorption to the air-water interface (Figure 12).[21] The exchange of the amide for an ether functionality raised the hydrophilicity of the molecule as well as the CMC. Examining surface pressure isotherms revealed that attractive interactions between the amide containing surfactants were present. This indicated that associative hydrogen bonding through the amide was taking place at the air-water interface.

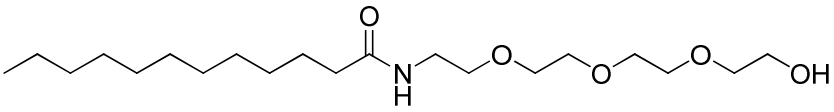

Figure 12. Tetra(ethylene oxide) dodecyl amide[21]

Beyond non-ionic surfactants, amides have also been incorporated into ionic surfactants. Cationic surfactants with an amide group spacer have been studied and the molecules were found to form hydrogen bonds via the amide functionality within the micelle (Figure 13).[22] Additionally, the surface tension and conductivity data point to the conclusion that a traditional spherical micelle is formed displaying a cationically charged surface.

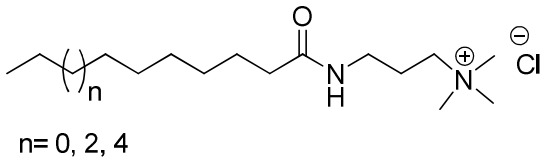

Figure 13. Cationic amide-based surfactants[22]

There have been many amino-acid based surfactants studied for the effect of hydrogen bonding and chirality on aggregation.[16,23-25] Additionally, there has been substantial interest in chiral amino-acid based surfactants for chiral separations.[26-28] The purpose here is not to examine every amino acid based surfactant, but to highlight a few examples and examine the effect of amino acid based surfactants on aggregation and surface adsorption.

The temperature where micellization occurs is known as the Krafft temperature (Figure 14). The Krafft temperature of several enatiomerically pure L and racemic DL amino-acid based surfactants bearing hydrophobic residues has been reported (Figure 15).[29] The Krafft temperatures of all the molecules were very low (below 0ºC). Additionally, the molecules displayed low melting points (78-120°C). Most of the molecules had a CMC near 15mM with no difference between optical isomers. This indicated a more traditional micellar system.

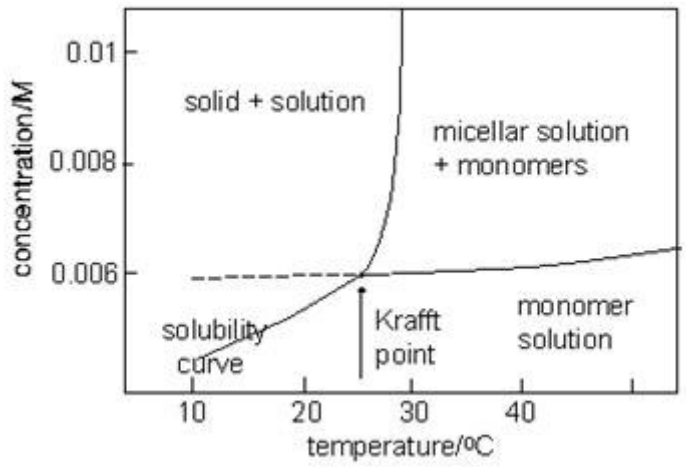

Figure 14. The Krafft phenomenon in surfactant solutions[30]

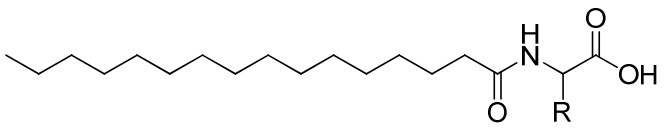

Amino Acid	-R
Gly	-H
Ala	$-CH_3$
Val	$-CH(CH_3)_2$
Leu	$-CH_2CH(CH_3)_2$
Ile	$-CH(CH_3)CH_2CH_3$
Phe	$-CH_2C_6H_5$

Figure 15. Amino acid based surfactants with hydrophobic residues[29]

Roy et al. prepared a series of amino acid based surfactants bearing hydrophilic head groups including serine, arginine, and glutamine (Figure 16).[25] Surface tension data revealed that the molecules formed micelles and transitioned to vesicle formation. The arginine and glutamine both have an additional amide bond in the head group which aided in the formation of micelles. Both displayed lower CMC values than the serine derivative.

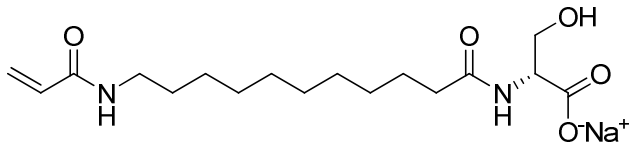

Figure 16. Amino acid based surfactants with hydrophilic residues (serine shown here)[25]

The presence of amides in amphiphiles has led to the development of new surfactants which show increased associations at the air-water interface as well as traditional surfactant self assembly. These structures have furthered the understanding of structure function relationships in surfactant aggregation and have broadened the field. Part of this dissertation will focus on further expanding the scope of amide based surfactants.

Part I

Non-Steroidal Facial Amphiphiles

Preface

Synthesis of polycyclic facial amphiphiles has largely been restricted to steroids, nature's template. There has been significant work on synthesizing new derivatives of cholic acid. However, little work has been done to probe alterations of the hydrophobic surface. As such, we designed a new system which examined changes to the hydrophobic template. Maintenance of a polycyclic hydrophobic core structure was imperative for examining the effect of rigidity on facial amphiphilic aggregation in aqueous solutions. Several charges were placed on the core structure in an attempt to increase water solubility.

To probe the effect of hydrophobic rigidity on facial amphiphilic behavior, we chose to synthesize **A** and **B**. The structures possess a large, rigid, hydrophobic backbone and have evenly spaced charged groups. Comparing the properties of **A** verses **B** allowed us to probe the effect of facial amphiphilicity.

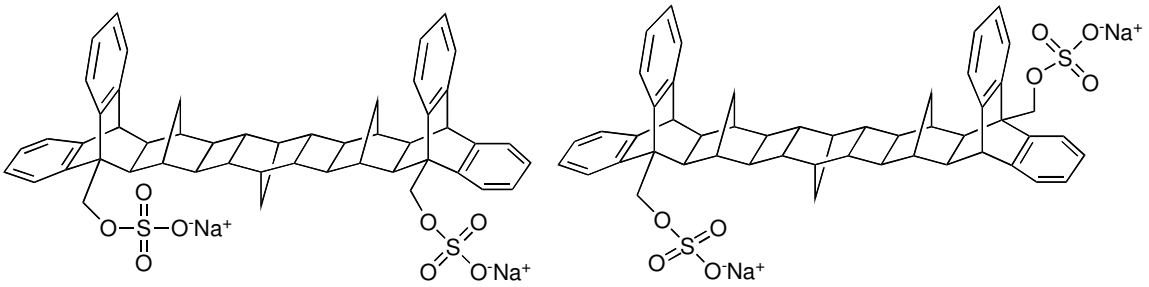

Figure 17. Nonsteroidal facial amphiphiles

The synthesis of these molecules built on the work of Feldman et al., where they synthesized a rigid hydrophobic polycyclic molecule for template controlled polymerization of acrylate monomers (Figure 18).[31] Their synthesis of this molecule

provided an excellent basis for our study of nonsteroidal rigid amphiphiles. The aqueous solution behavior of non-steroidal rigid amphiphiles has been largely uncharacterized. For this project we examined the solution phase properties of the molecules and explored the uncharted "waters".

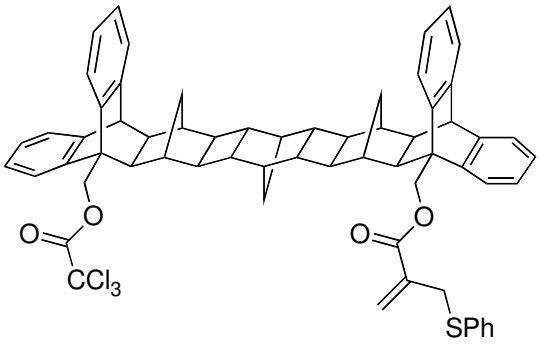

Figure 18. Template synthesized for the polymerization of acrylate monomers[31]

Synthesis

The synthesis of **A** and **B** was completed using the multistep sequence outlined in Scheme 1. A five step sequence was employed to prepare a gram of the final product by starting from commercially available 9-anthracene carboxylate and norbonadiene. The reaction yields were not fully optimized. Upon isolation the products were analyzed using ^{1}H and ^{13}C Nuclear Magnetic Resonance (NMR), High Resolution Mass Spectrometry (HRMS), and/or elemental analysis.

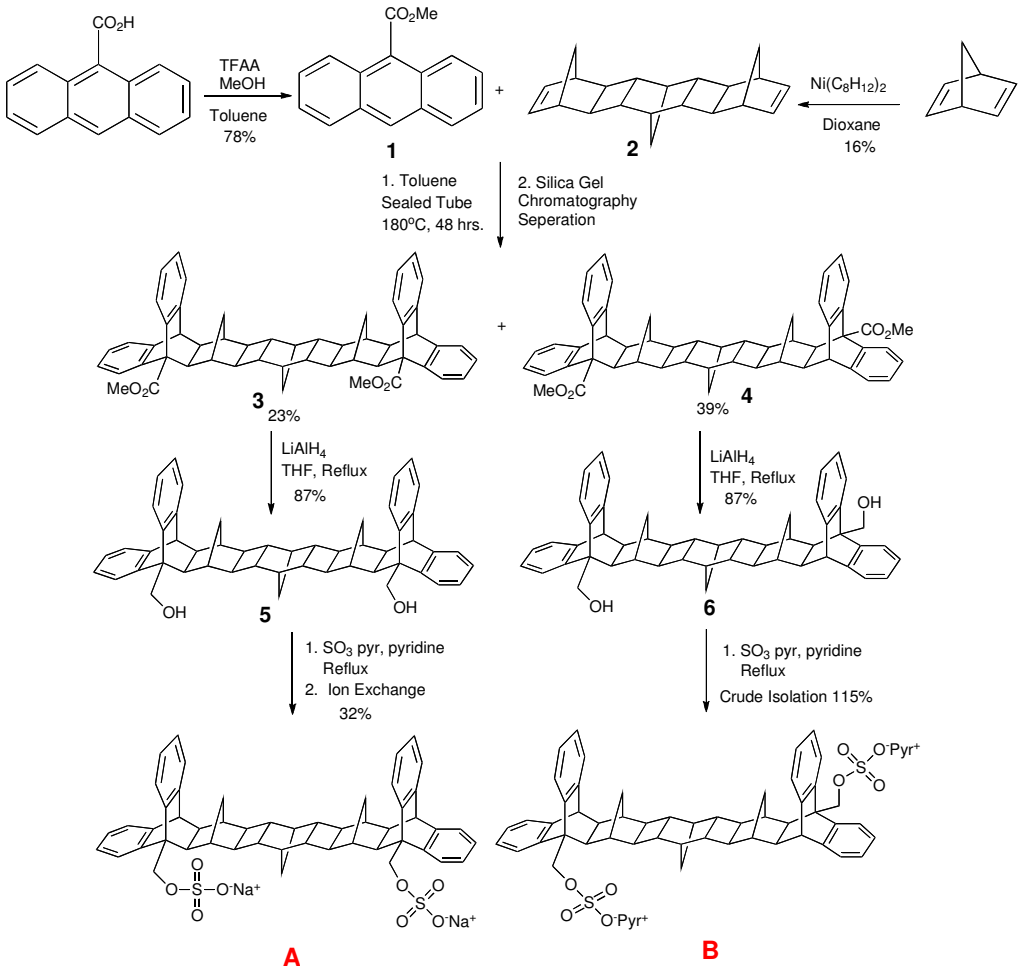

Scheme 1. Synthesis of Non-Steroidal Rigid Amphiphiles

Discussion

Formation of the 9-methylanthracenecarboxylate was easily obtained by reacting the corresponding carboxylic acid with trifluroacetic anhydride and methanol.[31] The norbornadiene oligomerization reaction to form the trimer posed some difficulties. The bis-cyclooctadiene (COD) nickel catalyst was extremely reactive with water, which destroyed the compound. High moisture content in the air caused problems; therefore, a glove bag was employed using nitrogen gas. Due to the reactivity with water, weighing out the catalyst was not attempted, and the entire amount (1.0 g) was used directly from the bottle purchased. The reaction was completed on ~90 gram scale of the norbornadiene.[31] This resulted in a mixture of oligomeric products including dimeric norbornadiene (obtained in 49.2% yield), **2** isolated in 16.1% yield, as well as higher order oligomers (not isolated).

A subsequent double Diels-Alder reaction of the **2** with **1** was attempted using several different methods including different high pressure apparati as well as using a microwave reactor. The microwave reactor produced the product in good yield; however, it was found that heating in an oil bath worked just as efficiently. Purification required benzene/hexane (75/25) elutent in silica gel chromatography. Toluene/hexane was also attempted, although ineffective.[31]

Complete reduction of the methyl esters using lithium aluminum hydride to form the primary alcohol was efficient (87% yield) and simple extraction yielded pure product.[31] Functional group inter-conversion of the alcohol to form tosylates, sulfates, and protected phosphates were synthetically accessible; however, several substitution

reactions to form bromides did not result in product formation. The overall reactivity trend observed found that substitution of that alcohol was not possible.

The primary reason for this observation was due to the large steric barrier prohibiting the S_N2 attack at the methylene carbon. The neopentyl center has an extremely slow rate of substitution. Due to the lack of a hydrogen on the adjacent carbon atom, the common problem of an elimination pathway was not encountered.[32] The slow reaction rates were most likely prohibitive in the formation of product.

Final preparation of the sulfates employed the procedure of Chlebowski et al.[33] The starting alcohol was refluxed in pyridine with sulfur trioxide pyridine complex and formed the sulfate compounds as pyridinium salts. This product precipitated from the reaction mixture, was filtered, and rinsed with excess hexanes. To obtain the purified sodium salts, the product was dissolved in methanol and stirred for 10 minutes with Dowex (sodium form) ion exchange resin. This resulted in the exchange of one of the two pyridinium counter ions for sodium. Dissolving the solution in 0.1 M sodium hydroxide solution with subsequent dialysis resulted in purified product.

Upon isolation, the compounds were examined for water solubility and potential aqueous solution aggregation.

Characterization

Compound **B** was found to be completely water insoluble and therefore was not subjected to further examination. However, compound **A** was found to be water-soluble and thus indicated that facial amphiphilicity was important for solubility! To compare

the aqueous solution behavior of amphiphile **A** with traditional surfactant amphiphiles, the standard sodium dodecyl sulfate (SDS) was employed.

Physical Characteristics

Crystal Structure

A crystal structure of a precursor compound of **A** (the syn trimer diester) provided an idea of favorable hydrophobic interactions in the solid state. A very ordered packing array was noticeable when looking at the crystal structure (Figure 19). The molecules appeared stacked onto one another through interactions of the aromatic rings. The π–π interactions of the system have been known to be very stable. As seen in the crystal structure, there is little other intermolecular interaction. With such a rigid structure this was not surprising. This information could provide an idea of the favorable solution-state interactions; however, associations in the solid state are not directly related to aqueous phase behavior.

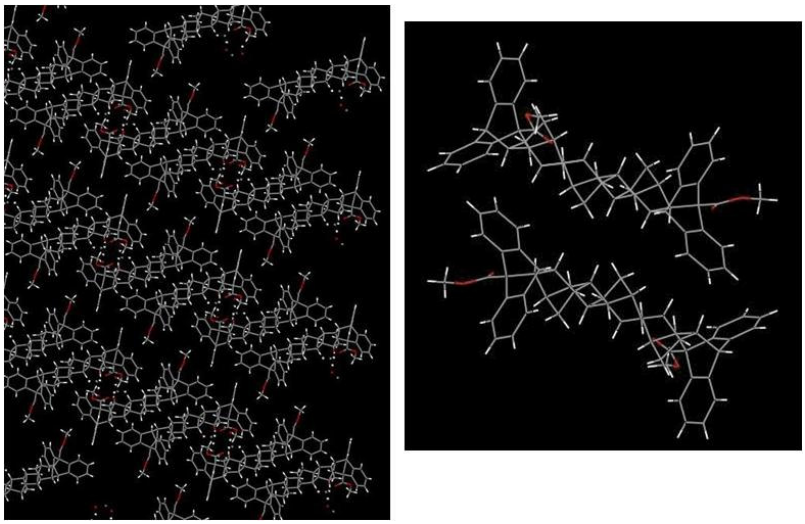

Figure 19. Crystal structure images of the syn trimer diester

Surface Tension

Examining the surface tension of the amphiphile allowed for exploration of how the molecules interact at the air-water interface. An amphiphilic molecule that significantly lowers the surface tension of a liquid is highly surface active.[1] In many surfactant systems, it is possible to also explore the critical micelle concentration or CMC. It was possible to begin understanding the basic aqueous solution properties by examining the surface tension of **A**.

The traditional method of exploring air-water interface interaction of an amphiphilic species has been to measure the surface tension at a constant temperature across many different concentrations. Plotting the surface tension versus the log of concentration gives a graph as seen in Figure 20.[1] The graph illustrates that at low concentrations there is a significant drop in the surface tension and then abruptly the surface tension remains constant.[34] The abrupt change in the plot is the CMC, where aggregates in the solution are formed. This happens because the surface is saturated and in a cooperative event micelles form in the bulk solution.

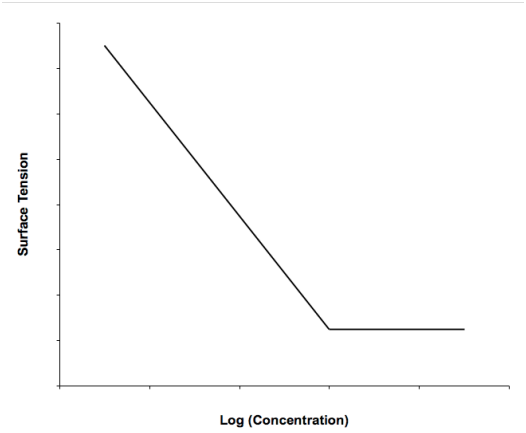

Figure 20. General plot of the surface tension vs. log of concentration

Although there were many methods to choose from, measurement of the surface tension of **A** was completed using the Du Noüy Ring method. This simple and reliable method for measuring the surface tension of a liquid allowed for efficient and accurate results. The surface tension of a liquid was obtained from resting a platinum-iridium ring on the surface of a liquid. The force required to pull the ring upward off the surface indicated the surface tension of the liquid (Figure 21).[34] This technique is accomplished using a surface tensiometer (Figure 21).

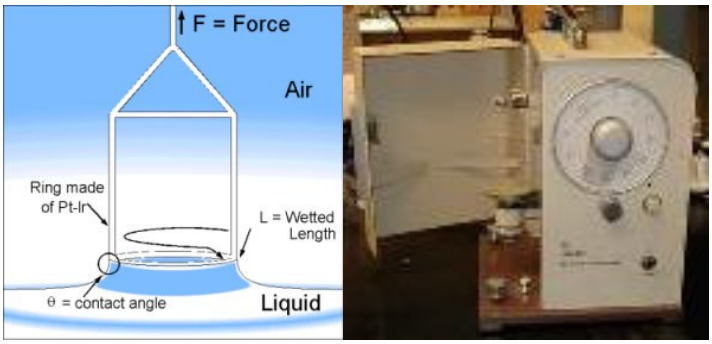

Figure 21. Illustration of the Du Noüy Ring Method and the surface tensiometer

Measurement of the surface tension of **A** resulted in the plot illustrated below (Figure 22). It is initially evident that **A** displayed no precipitous break in the surface tension indicating no CMC. SDS on the other hand, showed a break and therefore a CMC of 8 mM. Additionally, the lack of a break in the plot of **A** indicated that any possible aggregation is non-cooperative. Looking at the relative values of the surface tension, one can note that SDS was much more efficient in decreasing the surface tension of water compared to **A**. This was largely due to the packing at the interface; SDS can pack very tightly at the interface.[35] However, **A** with a very rigid hydrophobic region

cannot pack as densely at the interface and therefore its ability to decrease the surface tension of water is diminished.

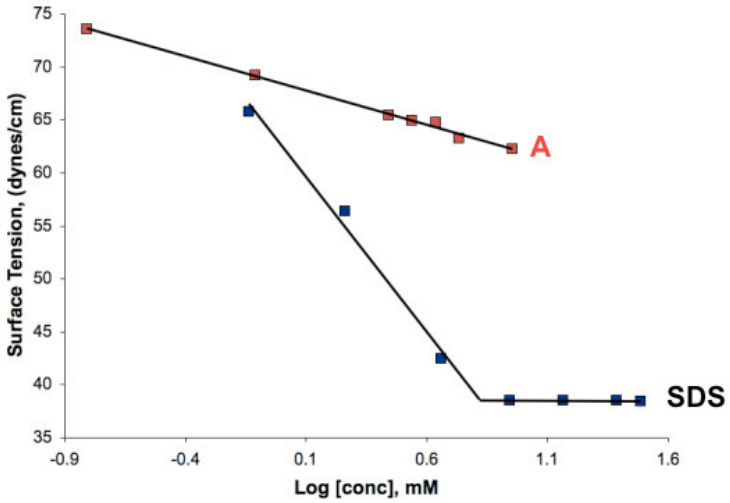

Figure 22. Surface tension of **A** vs. log concentration

Emulsion

Interactions at the liquid-liquid interface can be informative in understanding how the separate hydrophobic and hydrophilic regions of the molecule interact in oil or water. One experiment employed to probe that interaction was emulsion stabilization. When a surfactant or amphiphile is vigorously combined with both oil and water, a stable emulsion forms.[36]

Emulsions are solutions which combine two immiscible liquids. Droplets of a solution (oil) are suspended in another (water) or vice versa. The suspended solution is considered the dispersed phase while the bulk solution is considered the continuous phase. Emulsions are inherently unstable, unless an additive is present to stabilize the two solutions. The instability is due to the interfacial tension between the two liquids. The

presence of a surfactant slows down the kinetics of these processes. It does so by having both the hydrophobic and hydrophilic regions interact at the interface. Just as surfactants interact at the air-water interface to lower the surface tension of a liquid, the amphiphile is decreasing the tension between the two immiscible liquids.

As illustrated in Figure 23, there are many states an emulsion goes through in transitioning from a stable emulsion to two separate solutions.[36] The primary emulsion is where one phase is evenly dispersed within the other. Two droplets can combine to form larger droplets in a process called coalescence (Figure 23A).[36] Droplets can bunch together but not combine in what is referred to as flocculation (Figure 23C). Phase separation can occur when there is a difference in densities. This is called creaming and Figure 23D illustrates the particles phase separating on the surface. The entire collapse of an emulsion where the liquids separate into two phases is called breaking (Figure 23B).

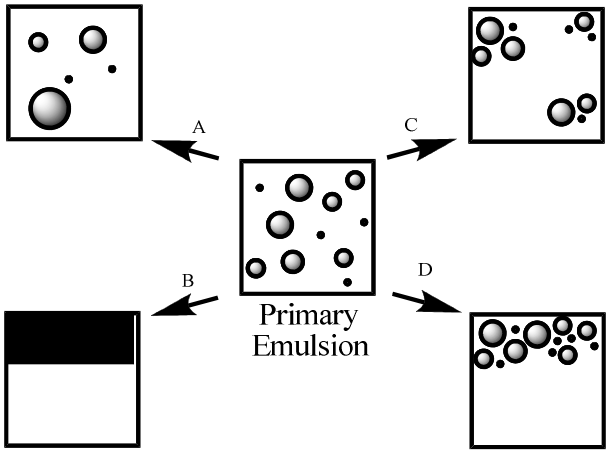

Figure 23. Stages of the emulsion process[36]

The ability of **A** to stabilize an emulsion was examined by dissolving 3 mg in 2.5 mL of water. Vortexing this solution for 10 minutes with 2.5 mL of toluene produced an oil/water emulsion that was stable for more than 6 months. No significant change in the

particle size was noted, and the evenly dispersed particles can be observed in Figure 24. It was interesting that **A** was able to stabilize the oil-water interface considering its rigid hydrophobic region. The facial orientation of the hydrophilic groups probably aided in the interaction of the interfacial region.

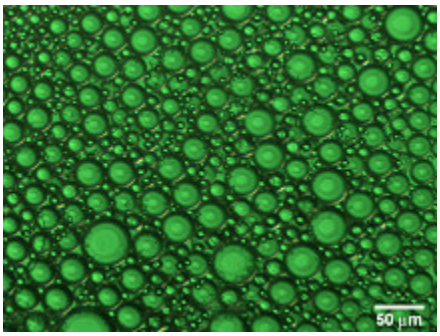

Figure 24. Oil in water emulsion light microscope image of **A** under 20X magnification

Nuclear Magnetic Resonance

NMR can be utilized to examine the size and shape of aggregates in solution. With compound **A** having potentially unique aggregates based on the unusual structure this technique was used to probe the aggregate structure. When a proton NMR spectrum of a small molecule in solution is obtained, the appearance is usually the presence of sharp peaks.[37] This is the result of averaging from the molecules freely tumbling in solution. When an aggregate is formed the molecules are tumbling as a large macromolecular unit. This unit will tumble significantly slower and from this the resulting spectrum often will have significantly broader signals.[38]

Very sharp signals were present when observing the proton NMR of **A** in deuterated methanol (Figure 25). The characteristic aromatic protons between 7-8 ppm were present. Additionally, the signal below zero was the result of the protons held in the

center of the aromatic ring displaying a chemical shift consistent with a diamagnetic ring current. When contrasted with the spectrum in Figure 26, which was taken in deuterium oxide, a significant difference was present. No distinct signals were present and there appeared to be little compound in solution. What was most striking was that Figure 25 and Figure 26 were the same concentrations. In fact the spectrum of **A** in deuterium oxide was taken at a higher temperature (60°C) in an attempt to increase the tumbling of the molecules. No difference in the ^{1}H NMR spectrum of **A** was seen at different temperatures (up to 60°C) or concentrations. This substantial difference in the NMR spectra of **A** between methanol and water indicated significant intermolecular interactions which inhibited molecular tumbling.

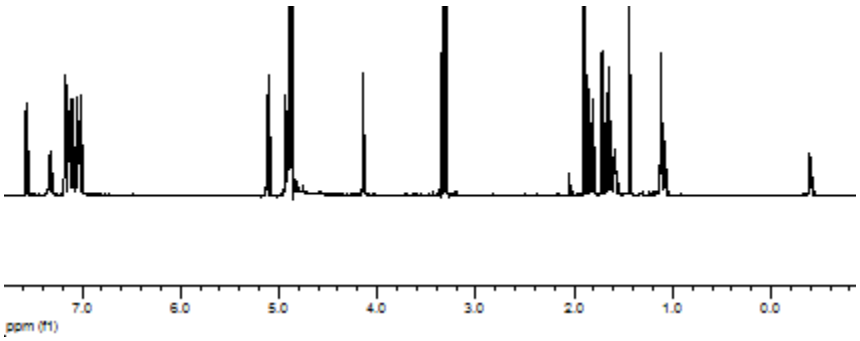

Figure 25. ^{1}H NMR of **A** in CD_3OD, 11 mM solution (21ºC)

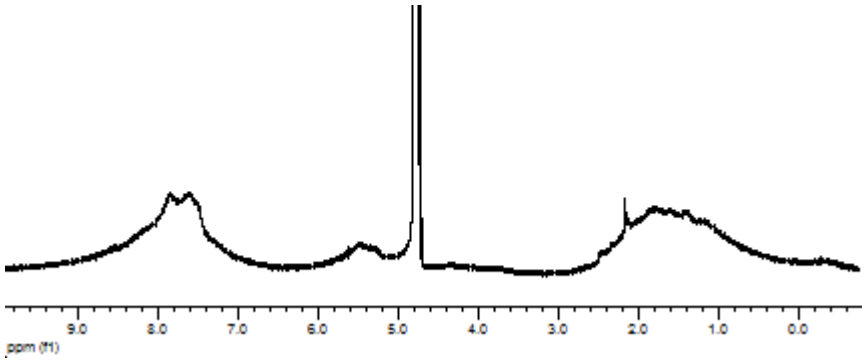

Figure 26. ^{1}H NMR of **A** in D_2O, 11 mM solution (60ºC)

Conductivity

The free ions in aqueous solution can be measured by looking at the conductivity. In surfactant solutions it is possible to explore aggregation based on the conductivity. The plotting of conductivity against surfactant concentration for a traditional amphiphile results in a graph similar to the one in Figure 27. At lower concentrations there is a linear increase in the conductivity as concentration increases; however, at a certain point there is a break and the slope is no longer as steep. The break in the conductivity verses concentration point indicates the CMC of the solution. When an ionic surfactant forms a micelle, there are significant ionic repulsions between the head groups. To minimize these repulsions 63% of the counter ions in solution will bind to the micelle surface.[39] This binding is illustrated through the change in the slope of the plot. It will be possible to probe assembly and the ionic surface of the aggregates by examining conductivity versus concentration for **A**.

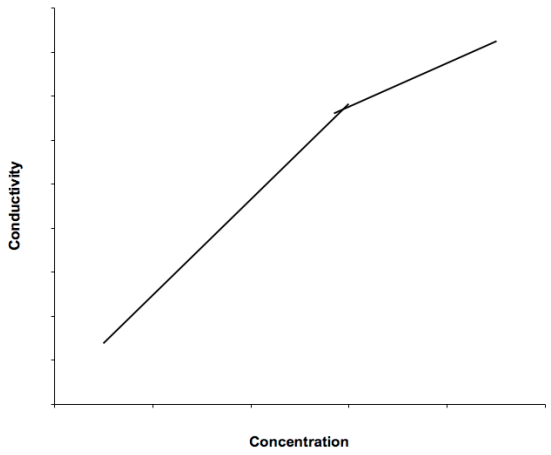

Figure 27. A plot of conductivity vs. concentration

In Figure 28 SDS displayed the characteristic break at a concentration of 8 mM, indicating the CMC. However, for **A** there was simply a linear progression of increasing conductivity with increasing concentration. This was consistent with the surface tension data: There was no apparent CMC for **A** and any possible aggregates formed did so non-cooperatively. Also, the data confirmed that the aggregates of rigid amphiphilic structure (**A**) did not have a traditional anionic surface necessitating counter-ion binding to counteract the charge repulsion.[39]

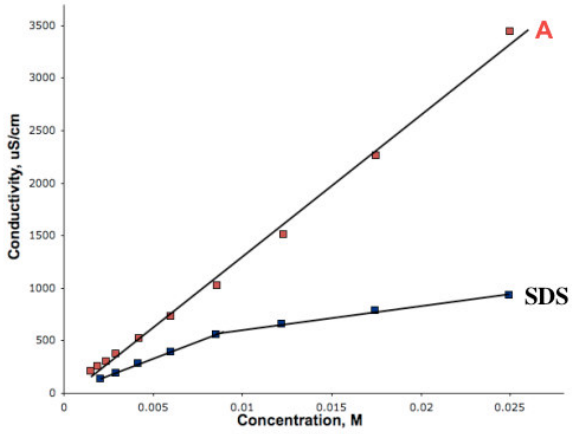

Figure 28. Conductivity vs. concentration for compound **A** as well as SDS

Viscosity

The viscosity of a solution is an indication of the intermolecular interactions in solution. A highly viscous solution can indicate strong intermolecular interactions. To determine the viscosity of a solution, many different techniques are available. One method is microrheology, which looks at the movement of particles in solution as a function of time to determine the viscosity.[40,41] This is accomplished through the use of a fundamental mathematical equation known as the Stokes-Einstein Relation (Equation 2).

$$D = \frac{k_B T}{6\pi\eta r}$$

Equation 2

This equation indicates that diffusion is equal to Boltzmann's constant multiplied by the temperature and then divided by the sum of six pi times the viscosity times the radius of a tracer particle. It is also possible to relate the mean squared displacement of a tracer particle to the diffusion times the lag time shown in Equation 3. Therefore, if the radius of the tracer particle is known then the displacement as it relates to the lag time can yield the viscosity of a solution.

$$dx^2 = 2Ddt$$

Equation 3

Microrheology was used to determine the viscosity of a freshly prepared 40.1 mM solution of **A** (Figure 29). As a point of reference the viscosity of water is 1 mPa·sec.

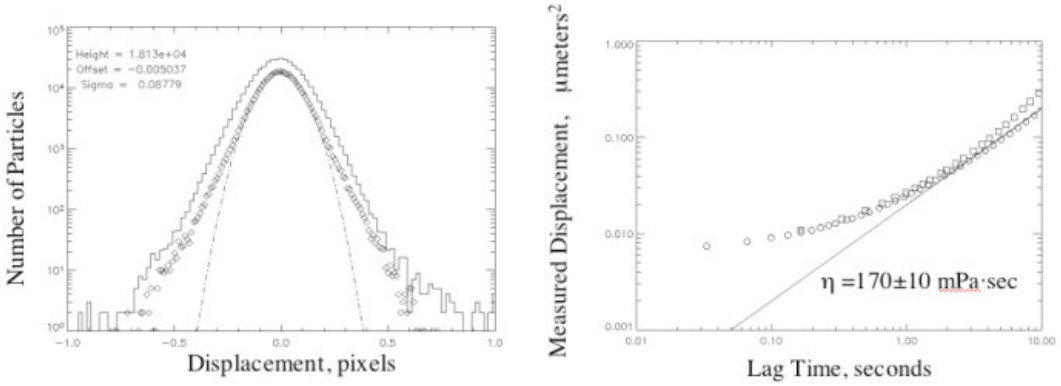

Figure 29. Microrheology data obtained from a freshly prepared sample of **A**

On the left the graph indicates the number of particles plotted against the displacement. This illustrates that the appropriate Gaussian distribution was obtained where a majority of the particles moved very little, while fewer particles moved very far. From this the viscosity of the solution was calculated by plotting the mean squared displacement versus the lag time to obtain a viscosity of 170±10 mPa·sec.

When this experiment was duplicated six days later an interesting result was obtained. As indicated in Figure 30 the Gaussian distribution of the same sample was significantly narrower and the resulting viscosity was much higher, 1100±100 mPa·sec. These data in combination suggested two very important pieces of information. The fact that the solution was viscous indicates that some sort of aggregation was occurring. Additionally, the increase in viscosity over 6 days illustrated that the aggregation was not instantaneous as found in traditional amphiphiles. The aggregates were still forming over time!

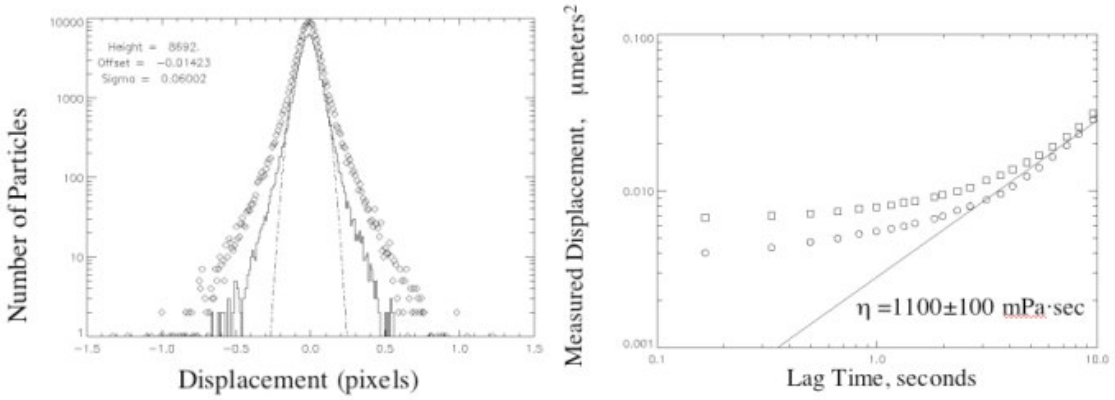

Figure 30. Microrheology data of a 40.1 mM 6-day aged sample of **A**

Cryo-High Resolution Scanning Electron Microscopy (HRSEM)

Cryo-HRSEM is a technique which allows examination of the solution state structure through frozen samples. This technique is accomplished by plunge freezing a solution in liquid ethane to obtain vitreous-non crystalline ice.[42] Doing so prevents the formation of ice crystals which would alter the bulk solution. The surface of the sample is fractured, etched under high vacuum, and coated with a thin layer of chromium. The fractured surface is subjected to HRSEM, which allows an image of aggregates and bound water with the bulk water removed.

A noticeable difference between day 0 and day 6 solutions could be seen. At day 0 (Figure 31 upper) less defined structures and thinner walled aggregates were apparent. Upon aging for 6 days (Figure 31 lower) thicker walled aggregates were evident as well as more defined aggregate structures. These images in addition to the viscosity data supported the assertion that aggregates formed in solution. However, it is important to remember that this data may not directly correspond to the solution state.

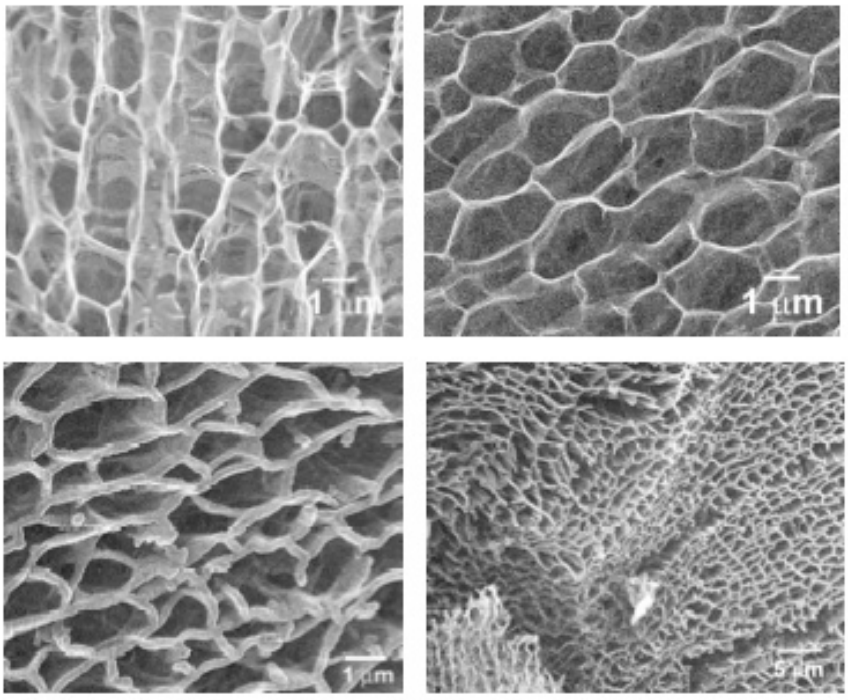

Figure 31. Cryo-HRSEM images of A, the upper two are freshly prepared samples, while the lower two are 6 day aged samples

Birefringence

Optical properties of surfactants are often used to assist in the characterization of the structure of the aggregates. As mentioned in the introduction, many different types of aggregates are possible in surfactant systems. Viewing a sample through cross polarizers presents an opportunity to examine the homogeneity of a solution on the macroscopic level.

Light is a wave that is scattered in many directions.[43] However, when light passes through a polarizer (Figure 32), the wave is oriented in a single direction. If the light wave meets a light polarizer in the perpendicular direction it will not pass through. When looking through perpendicular polarizers pointed at a light source, no light can be

detected. When polarized light meets a sample (crystalline solid, or an ordered liquid for example) the wave may change directions. Thus, this will allow light to be observed through perpendicular polarizers.

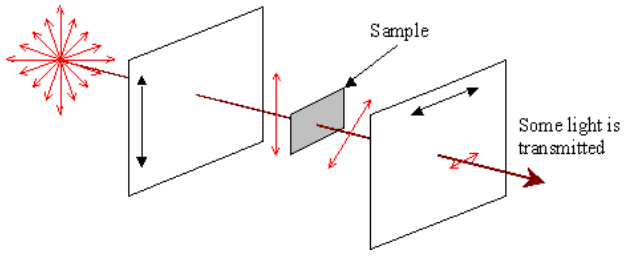

Figure 32. Illustration of light passing through cross polarizers[44]

When observing a traditional spherical micellar solution through cross polarizers, no light is seen indicating an isotropic solution. Isotropic micellar solutions are macroscopically the same in all directions. If a surfactant solution is viewed through cross polarizers and light is apparent, an anisotropic solution is indicated.[45] Anisotropy is when a solution presents order that is not equivalent in all directions. An example of this is a lamellar phase more commonly known as a bilayer.[46]

The examining of a 40.1 mM, 6-day aged sample of **A** through cross polarizers showed birefringence, or light passing through the perpendicular polarizers (Figure 33). This anisotropy provides evidence of an aggregate formation that in not equivalent in all directions, which is different from a standard micellar solution of SDS, which is isotropic.

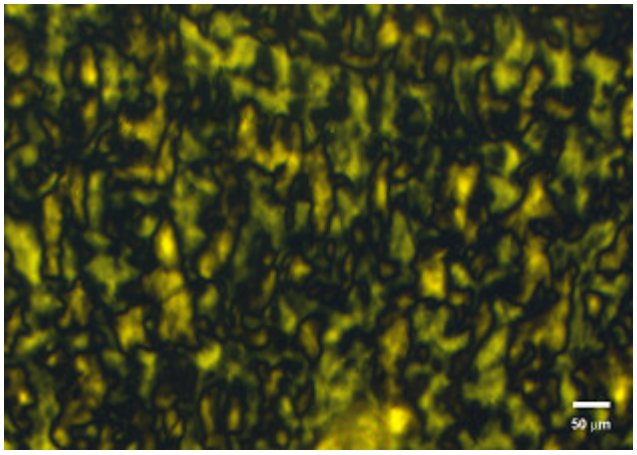

Figure 33. 40.1 mM 6-day aged sample of A as viewed through cross polarizers

Conclusion

Aggregation and amphiphilic behavior of **A** was characterized extensively by a number of techniques. The water insolubility of **B** indicated that for large rigid hydrophobic structures facial amphipilicity was important for solubility. The rigid facial amphiphile, **A**, did not form aggregates in a cooperative manner, as illustrated by the surface tension data. The lack of a break in the conductivity data supports this assertion. However, this does not mean that aggregates did not form. The viscosity of the solution indicated that there were intermolecular interactions. An examination of the viscosity of a freshly prepared sample vs. a 6-day aged sample indicated aggregates formed over time and not instantaneously. The observed birefringence as well as the cryo-HRSEM data supported a large aggregate network, which increased solution viscosity. All this suggestions that molecule **A**, is a unique addition to the growing research on new facial amphiphiles.

Experimental

Procedures

Solvents used in the synthesis were reagent grade and dried over 4 Å molecular sieves. Reagents were purchased from Aldrich, Fluka, or VWR and used without further purification. Float-A-Lyzers, molecular weight 500, dialysis tubes were purchased from SPECRTA/POR®. The Biorad AG 50W-X8 resin (Na^+ form, 200-400 mesh) was purchased from Bio-Rad Laboratories, Inc.

Methods ^1H and ^{13}C NMR spectra were obtained either on a Varian INOVA 400 MHz (100 MHz for ^{13}C) or a Varian INOVA 600 MHz (150 MHz for ^{13}C) instrument. Mass spectra were collected at Emory University Mass Spectrometry Center. Atlantic Microlabs in Norcross, GA performed all elemental analyses. A Fischer Surface Tensiomat® using the Du Noüy ring method was used to obtain surface tension measurements. Conductivity was performed using a Fischer Scientific Traceable™ Conductivity Meter. All light microscope images were taken using a Nokia Diaphot TMD with a Retiga 1300i camera. The microrheology data were collected using a Leica DMIRB inverted microscope equipped with a fluorescent lamp at 40x magnification. Data analysis to obtain the viscosity values was completed using Interactive Data Language (IDL) software. The cryo-HRSEM picture was acquired using the Topcon DS-130F Schottky Field Emission Scanning Electron Microscope. Crystal structures were obtained and solved by the X-ray Crystallography Center at Emory University.

Conductivity All experiments were conducted at room temperature (22°C) using a sample volume of 10 mL. A Fischer Scientific Traceable™ Conductivity Meter was used

and calibrated using a 1000 uS/cm standard purchased from Fischer.

Tensiometry (Surface Tension). All tensiometry experiments were performed at room temperature (22°C) using a sample volume of 25 mL. Each concentration was measured 10 times and the obtained values were averaged. Between each concentration measurement the platinum ring was rinsed with copious amounts of water and flame dried.

Microrheology All microrheology experiments were performed at room temperature (20°C). A 40.01 mM solution of syn trimer disulfate (29 mg) in water (1.0 mL) was prepared. To the amphiphile solution (112 μL) carboxylate modified polystyrene beads with a fluorescent tag (0.5 μm diameter) were added (2 μL). The sample was examined under a fluorescence microscope with a 20x objective. At least 50-100 particles were in the field of view. 1500 images were collected at a frame rate of 0.165 seconds. The viscosity was found to be 170±10 mPa·sec. The viscosity was calculated by tracking the particles, obtaining the time-dependent mean-squared displacement, and then using the Stokes-Einstein relationship. Six days later the same initial syn trimer disulfate solution was used to examine the viscosity. 300 μL of the syn trimer disulfate solution with 2 μL of the fluorescent beads were combined. At least 50-100 particles were in the field of view. 1500 images were collected at a frame rate of 0.165 seconds. The viscosity was found to be 1100±100 mPa·sec.

CRYO HRSEM 2 μL of a 32mM syn trimer disulfate solution (aged 6 days) was frozen to –105°C to create non-crystalline ice. The sample was then etched for 9 minutes under high vacuum (2 X 10^{-7} Torr) to sublime off the bulk water from the colloid. The sample is then coated with 1-2 nm of chromium and images were obtained.

Birefringent Images 1 μL of 32 mM syn trimer disulfate solution (aged 7 days) was placed on a microscope slide and a cover slip set on top. The sample was placed between cross-polarizers and images were obtained with the light microscope.

Synthesis

Procedure for the synthesis of Methyl 9-Anthracenecarboxylate (**1**): 9-Anthracene-carboxylic acid (10.0 g, 44.96 mmol, 1 equiv) and trifluoroacetic anhydride (25.0 g, 119.0 mmol, 2.6 equiv) were placed in an Erlenmeyer flask and stirred for 45 minutes in toluene (100 mL). Methanol (5.0 mL, 123 mmol, 2.7 equiv) was added to the reaction and stirred for an additional 3 hours. The solution was then extracted with (150 mL X 3) portions of saturated $NaHCO_3$ solution. The yellow organic layer was dried over magnesium sulfate, gravity filtered and evaporated to dryness. This resulted in 8.26 g (78%) of a yellow crystalline product.

Methyl 9-Anthracenecarboxylate (**1**): IR (neat) 2945, 1726, 1448, 1434, 1204, 1020. ^{1}H NMR [400 MHz, $CDCl_3$]: δ 8.55 (s, 1H), 8.04 (d, *J* =8.0 Hz, 4H), 7.53 (m, 4H), 4.20 (s, 3H). ^{13}C NMR [100 MHz, $CDCl_3$]: δ 170.05, 131.06, 129.58, 128.74, 128.61, 127.13, 125.57, 125.12, 52.72. HRMS: (ESI) Calcd for $C_{16}H_{13}O_2$ ($[M+H]^+$): 237.09108. Found: 237.09101.

Procedure for Norbornadiene Trimer (**2**): 2,5-Norbornadiene (50.0 mL, 491.6 mmol, 135 equiv) of was added dioxane (50 mL) along with bis-cycloctadiene nickel catalyst (1.0 g, 3.64 mmol, 1 equiv) in a controlled atmosphere glove bag. This was stirred at room temperature for about 20 hours. To the reaction solution additional 2,5-norbornadiene

(50.0 mL, 491.6 mmol, 135 equiv) was added and the temperature was raised to 53°C. Two days later (48 hours) the temperature was lowered to 40°C and stirred for an additional 24 hours. The dioxane was removed through evaporation. Purification was accomplished through fractional sublimation. The dimer product was sublimed under vacuum at 60°C. Once all the dimer product was sublimed from the mixture the trimer product was sublimed under vacuum at 127°C. The white solid resulted in 14.57 g (16.1%).

Dimer: ^{1}H NMR [400 MHz $CDCl_3$]: δ 6.04 (s, 4H), 2.65 (s, 4H), 1.72 (d, *J*=8.4 Hz, 2H), 1.37 (s, 4H), 1.25 (d, *J*=8.8 Hz , 2H).^{13}C NMR [100 MHz $CDCl_3$]: δ 136.39, 44.42, 42.44, 40.01. HRMS (EI): calcd. For $C_{14}H_{16}$ ([M^+]), 184.12520. Found, 184.12478.

Trimer (**2**): ^{1}H NMR [400 MHz, $CDCl_3$]: δ 5.95 (s, 4H), 2.61 (s, 4H), 1.91 (s, 2H), 1.76 (d, *J*=12.8 Hz, 2H), 1.55 (s, 2H), 1.39 (s, 4H), 1.32 (s, 4H), 1.16 (d, *J*=9.2 Hz, 2H). ^{13}C NMR [100 MHz, $CDCl_3$]: δ 135.66, 44.39, 42.04, 41.81, 41.75, 40.83, 29.13. HRMS (ESI): Calcd for $C_{21}H_{25}$ ([M+H]): 277.19521. Found: 277.19508.

Procedure for the Diels-Alder Reaction (**3** and **4**): 2,5-Norbornadiene trimer (2.00 g, 7.2 mmol) was added to methyl 9-anthracenecarboxylate (4.0 g, 16.9 mmol), in toluene (14 mL). The reaction mixture was split into two-8.0 mL microwave reactor pressure tubes. The reaction was heated at 200°C for 48 hours. Following reaction, the solution was evaporated and the products were purified using silica gel column chromatography (75/25 benzene/hexane) yielding white powders of separated syn trimer diester (R_f=0.04)

and anti trimer diester (R_f=0.26). A 62.2% (3.35 g) total yield was obtained with 37.3% (1.25 g) resulting in anti trimer diester and 62.7% (2.10 g) resulting in syn trimer diester. The syn trimer diester was crystallized in benzene and submitted for x-ray analysis.

Syn Trimer Diester (**3**): IR (neat) 2921, 1733, 1457, 1246, 1034. ^{1}H NMR [400 MHz, $CDCl_3$]: δ 7.46 (m, 2H), 7.27-6.98 (m, 14H), 4.17 (d, *J*=2.4 Hz, 2H), 4.05 (s, 6H), 2.02 (d, *J* =8.8 Hz, 2H), 1.91 (s, 2H), 1.73-1.62 (m, 8H), 1.53 (d, *J*=5.6 Hz, 2H), 1.43 (d, *J* =6 Hz, 2H), 1.08 (bs, 6H), -0.61 (d, *J* =11.2 Hz, 2H). ^{13}C NMR [100 MHz, $CDCl_3$]: δ 172.99, 143.92, 142.99, 142.06, 139.35, 126.72, 126.45, 126.28, 125.75, 124.60, 124.28, 123.29, 122.09, 59.07, 52.12, 49.65, 48.91, 48.66, 47.33, 47.25, 42.88, 42.56, 42.79, 41.57, 41.40, 29.23, 27.85. HRMS (FAB/LSIMS): Calcd for $C_{53}H_{48}O_4Li$ ($[M+Li]^+$): 755.3713. Found: 755.3744.

Anti Trimer Diester (**4**): IR (neat) 2923, 1730, 1456, 1246, 1034. ^{1}H NMR [400 MHz, $CDCl_3$]: δ 7.36 (m, 2H), 7.15-6.95 (m, 12H), 6.87 (d, *J*=6.8 Hz, 2H), 4.07 (d, *J*=2.4 Hz, 2H), 3.95 (s, 6H), 1.92 (d, *J*=8.4 Hz, 2H), 1.80 (s, 2H), 1.64-1.56 (m, 8H), 1.42 (d, *J* =5.6 Hz, 2H), 1. 33 (d, *J* =5.6 Hz, 2H), 0.98 (bm, 6H), -0.71 (d, *J*=11.6 Hz, 2H).^{13}C NMR [100 MHz, $CDCl_3$]: δ 172.73, 143.67, 142.72, 141.82, 139.09, 128.31, 126.48, 126.21, 126.02, 125.49, 124.36, 124.01, 123.06, 121.82, 58.81, 51.84, 49.41, 48.63, 48.38, 47.06, 47.01, 42.60, 42.28, 41.55, 41.23, 28.98, 27.59. HRMS (FAB/LSIMS): calcd. For $C_{53}H_{48}O_4Li$ ([M+Li]+), 755.3713. Found, 755.3702.

General Procedure for the Lithium Aluminum Hydride Reduction (**5** and **6**): Lithium aluminum hydride (0.274 g, 7.20 mmol, 3 equiv) was suspended in dry THF (10 mL) and stirred in an ice bath for 20 minutes. The syn trimer diester (1.80 g, 2.40 mmol, 1 equiv) was dissolved in THF (200 mL) and added to the reaction mixture. The solution was then refluxed for 18 hours. Following reflux, the solution was cooled to room temperature and dumped into 300 ml ice cold 1M H_3PO_4. The phosphoric acid solution was then extracted with ethyl ether (3 x 200 mL). The organic layers were then combined and subsequently extracted with saturated $NaHCO_3$ (3 x 200 mL) and brine (1 x 400 mL). The organic layer was dried with Na_2SO_4 and evaporated to dryness. Resulting products were used without further purification.

Syn Trimer Diol (**5**): (87% yield) ^{1}H NMR [400 MHz, $CDCl_3$]: δ 7.47 (d, 7.2 *J*, 2H), 7.27-7.06 (m, 12H), 4.83 (d, *J*=15.2 Hz, 2H), 4.62 (d, *J*=10.8 Hz, 2H), 4.16 (brs, 2H), 1.81-1.57 (m, 12H), 1.42 (brd, 13.6 *J*, 4H), 1.08 (brs, 6H), -0.46 (d, *J*=10.8 Hz, 2H). ^{13}C NMR [100 MHz, $CDCl_3$]: δ 145.74, 143.90, 143.26, 126.16, 125.78, 125.68, 124.59, 123.44, 122.29, 121.97, 68.21, 62.82, 49.09, 48.78, 47.34, 47.20, 42.71, 42.51, 42.47, 39.69, 28.36, 25.84. HRMS (FAB/LSIMS): Calcd for $C_{51}H_{47}O_2$+Li ($[M+Li]^+$): 699.3809. Found: 699.3924.

Anti Trimer Diol (**6**): (87% yield) ^{1}H NMR [400 MHz, $CDCl_3$]: δ 7.47 (d, *J*=7.2 Hz, 2H), 7.25-7.05 (m, 14H), 4.83 (d, *J*=11.2 Hz, 2H), 4.16 (d, *J*=2.4 Hz, 2H), 2.20 (impurity), 1.79-1.56 (m, 12H), 1.40 (brd, 4H), 1.25 (impurity), 1.08 (brs, 6H), -0.47 (d, *J*=11.6 Hz, 2H). ^{13}C NMR [100 MHz, $CDCl_3$]: δ 126.15, 125.68, 124.83, 124.60, 123.45, 122.61,

121.94, 48.77, 47.98, 47.31, 47.19, 42.44, 41.95, 41.45, 40.67, 39.68. HRMS (ESI): Calcd for $C_{51}H_{47}O_2$ ([M-H]$^-$): 691.35670. Found: 691.35706.

General Procedure for the Sulfonation: Syn Trimer diol (1.74 g, 2.41 mmol, 1 equiv.) was combined with sulfur trioxide pyridine complex (1.15 g, 7.24 mmol, 3 equiv) in 50 mL of pyridine. The solution was refluxed overnight and then cooled to room temperature. The precipitate was then filtered and rinsed with copious amounts of hexanes. The solid was dissolved in methanol and 10 g of Dowex (sodium form) ion exchange resin (AG 50W-X8, 200-400 mesh) was added. The solution was stirred for 10 minutes and then filtered. The methanol was flashed down and the solid was dissolved in 300 mL of 0.1 M NaOH. The solution was then loaded into MW 500 dialysis tubes (10 mL volume) and stirred in 4.0 L of water. The 4 L of water was changed 3 times over the course of 24 hours and the sample was removed from the dialysis tubes. When the water was removed by lyopholization, pure product was obtained.

Syn Trimer Disulfate Sodium salt (**A**): (32% yield) ^{1}H NMR [600 MHz, CD_3OD]: δ 7.54 (d, *J*=7.2 Hz, 2H), 7.30 (d, *J*=6.8 Hz, 2H), 7.15-6.97 (m, 12H), 5.08 (d, *J*=10 Hz, 2H), 4.91 (d, *J*=10 Hz, 2H), 4.12 (d, *J*=2.4 Hz, 2H), 1.88 (s, 2H), 1.81 (d, *J*=17.6 Hz, 4H), 1.69 (s, 2H), 1.64-1.55 (m, 6H), 1.42 (s, 4H), 1.09-1.04 (m, 6H), -0.43 (d, *J*=11.2 Hz, 2H). ^{13}C NMR [150 MHz, CD_3OD]: δ 146.47, 145.26, 144.20, 142.94, 126.90, 126.35, 123.62, 50.26, 49.88, 49.44, 49.29, 49.01, 49.01, 48.86, 48.72, 48.59, 47.57, 43.92, 40.8, 28.82. HRMS (ESI$^+$): Calcd for $C_{51}H_{47}O_8Na_2S_2$ ([M+H]): 897.24997. Found: 897.24967.

Anti Trimer Disulfate Pyridine salt (**B**)**:** (crude isolation yield is 115%) ^{1}H NMR [600 MHz, DMSO]: δ 8.88 (d, *J*=5.2 Hz, 4H), 8.48 (t, *J*=7.6 Hz, 2H), 7.97 (t, *J*=7.0 Hz, 4H), 7.49 (m, 2H), 7.29 (d, *J*=6 Hz, 2H), 7 19-7.00 (m, 12H), 4.79 (d, *J*=10.4 Hz, 2H), 4.59 (d, *J*=9.6 Hz, 2H), 4.18 (d, *J*=2.4 Hz, 2H), 1.71 (d, *J*=12.8 Hz, 4H), 1.62 (s, 2H), 1.57 (d, *J*=8.8 Hz, 1H), 1.38 (m, 4H), 1.06 (s, 3H), 1.09 (d, *J*=10.4 Hz, 2H), -0.53 (d, *J*=10.4 Hz, 2H). ^{13}C NMR [150 MHz, CD_3OD]: δ 147.21, 146.62, 145.33, 144.32, 143.81, 142.98, 128.47, 127.10, 127.04, 126.59, 126.44, 125.35, 123.91, 123.75, 68.52, 50.43, 49.99, 49.90, 48.51, 48.56, 43.98, 43.93, 43.87, 42.64, 40.93, 29.95, 28.95, HRMS (ESI$^-$): calcd. For $C_{51}H_{47}O_8S_2$ ([M-2Pyr$^+$+1H$^+$]), 851.27007. Found, 851.27069.

Crystal data and structure refinement for Syn Trimer Diester (**3**)

Identification code	jstris	
Empirical formula	C53 H48 O4	
Formula weight	748.91	
Temperature	173(2) K	
Wavelength	1.54178 Å	
Crystal system	Monoclinic	
Space group	C2/c	
Unit cell dimensions	a = 33.299(5) Å	α= 90°.
	b = 8.7863(10) Å	β= 113.836(6)°.
	c = 35.011(4) Å	γ= 90°.
Volume	9370(2) $Å^3$	
Z	8	
Density (calculated)	1.062 Mg/m^3	
Absorption coefficient	0.513 mm^{-1}	
F(000)	3184	
Crystal size	0.39 x 0.23 x 0.18 mm^3	
Theta range for data collection	8.24 to 59.13°.	
Index ranges	-35<=h<=29, -8<=k<=9, -38<=l<=37	
Reflections collected	19152	
Independent reflections	6338 [R(int) = 0.0988]	
Completeness to theta = 59.13°	93.5 %	
Absorption correction	Semi-empirical from equivalents	
Max. and min. transmission	0.9133 and 0.8249	
Refinement method	Full-matrix least-squares on F^2	
Data / restraints / parameters	6338 / 5 / 511	
Goodness-of-fit on F^2	1.010	
Final R indices [I>2sigma(I)]	R1 = 0.1076, wR2 = 0.2706	
R indices (all data)	R1 = 0.1992, wR2 = 0.3034	
Extinction coefficient	0.00123(16)	
Largest diff. peak and hole	0.360 and -0.273 $e.Å^{-3}$	

Table 2. Atomic coordinates (x 10^4) and equivalent isotropic displacement parameters ($Å^2$x 10^3) for Compound **3**. U(eq) is defined as one third of the trace of the orthogonalized U^{ij} tensor.

	x	y	z	U(eq)
C(1)	5725(3)	-1647(8)	-1755(2)	66(2)
C(2)	6114(3)	-1148(7)	-1780(2)	60(2)
C(3)	6500(3)	-1623(7)	-1481(2)	53(2)
C(4)	6527(3)	-2582(7)	-1152(2)	52(2)
C(5)	6138(3)	-3012(7)	-1123(2)	66(2)
C(6)	5738(2)	-2604(7)	-1434(2)	58(2)
C(7)	6957(2)	-1300(7)	-1476(2)	51(2)
C(8)	6982(2)	-2998(7)	-856(2)	59(2)
C(9)	7174(2)	-2823(7)	-1456(2)	54(2)
C(10)	7188(2)	-3733(7)	-1127(2)	51(2)
C(11)	7380(2)	-5106(8)	-1063(2)	62(2)
C(12)	7580(3)	-5654(8)	-1320(2)	76(2)
C(13)	7563(3)	-4764(9)	-1641(2)	76(2)
C(14)	7364(2)	-3338(8)	-1718(2)	69(2)
C(15)	6910(2)	-221(9)	-1834(2)	63(2)
C(16)	6659(3)	64(8)	-2558(2)	95(3)
C(17)	7218(2)	-481(7)	-1045(2)	49(2)
C(18)	7236(2)	-1485(6)	-670(2)	53(2)
C(19)	7708(2)	-120(7)	-925(2)	59(2)
C(20)	7948(2)	-1592(7)	-703(2)	55(2)
C(21)	7726(2)	-1580(6)	-392(2)	49(2)
C(22)	7842(2)	1030(7)	-553(2)	63(2)
C(23)	7852(2)	1(7)	-181(2)	52(2)
C(24)	8323(2)	1370(7)	-339(2)	57(2)
C(25)	8352(2)	361(6)	40(2)	48(2)
C(26)	8455(2)	2935(7)	-142(2)	61(2)
C(27)	8283(2)	2967(7)	199(2)	61(2)

C(28)	8519(2)	1498(6)	411(2)	51(2)
C(29)	8955(2)	2846(7)	118(2)	57(2)
C(30)	8986(2)	1796(7)	497(2)	50(2)
C(31)	9185(2)	4162(7)	410(2)	55(2)
C(32)	9232(2)	3107(6)	802(2)	52(2)
C(33)	9659(2)	4507(7)	489(2)	53(2)
C(34)	9888(2)	2957(7)	677(2)	59(2)
C(35)	9731(2)	2980(7)	1032(2)	50(2)
C(36)	9827(2)	5585(7)	864(2)	60(2)
C(37)	9892(2)	4495(6)	1248(2)	46(2)
C(38)	10257(3)	6542(7)	950(2)	66(2)
C(39)	10379(2)	4674(7)	1567(2)	59(2)
C(40)	10630(3)	5399(7)	1038(2)	62(2)
C(41)	10689(2)	4421(7)	1356(2)	46(2)
C(42)	10999(3)	3285(8)	1459(2)	65(2)
C(43)	11257(3)	3155(8)	1223(2)	73(2)
C(44)	11183(2)	4121(8)	899(2)	71(2)
C(45)	10885(3)	5258(8)	797(2)	76(2)
C(46)	10348(2)	7371(7)	1379(2)	53(2)
C(47)	10417(2)	6308(7)	1697(2)	53(2)
C(48)	10487(2)	6922(8)	2087(2)	60(2)
C(49)	10501(2)	8419(8)	2156(2)	67(2)
C(50)	10430(2)	9438(8)	1833(2)	72(2)
C(51)	10353(2)	8868(8)	1432(2)	65(2)
C(52A)	10251(6)	7799(19)	644(5)	63(3)
C(53A)	10593(4)	9875(12)	456(3)	54(3)
O(3A)	9917(3)	8115(10)	367(3)	61(2)
O(4A)	10629(3)	8553(9)	713(3)	52(2)
C(52B)	10114(6)	7550(20)	587(5)	63(3)
C(53B)	9545(4)	8799(13)	-3(3)	54(3)
O(3B)	10367(3)	8230(10)	493(3)	61(2)
O(4B)	9675(3)	7761(9)	352(2)	52(2)
O(1)	6756(2)	-935(5)	-2199(1)	67(2)
O(2)	6993(2)	1109(6)	-1789(1)	87(2)

Table 3. Bond lengths [Å] and angles [°] for Compound **3**.

C(1)-C(6)	1.392(8)
C(1)-C(2)	1.402(9)
C(1)-H(1)	0.9500
C(2)-C(3)	1.356(8)
C(2)-H(2)	0.9500
C(3)-C(4)	1.401(8)
C(3)-C(7)	1.540(9)
C(4)-C(5)	1.394(9)
C(4)-C(8)	1.493(9)
C(5)-C(6)	1.384(9)
C(5)-H(5)	0.9500
C(6)-H(6)	0.9500
C(7)-C(9)	1.508(8)
C(7)-C(15)	1.528(8)
C(7)-C(17)	1.578(7)
C(8)-C(10)	1.521(8)
C(8)-C(18)	1.569(8)
C(8)-H(8)	1.0000
C(9)-C(14)	1.384(8)
C(9)-C(10)	1.387(8)
C(10)-C(11)	1.341(8)
C(11)-C(12)	1.403(9)
C(11)-H(11)	0.9500
C(12)-C(13)	1.353(9)
C(12)-H(12)	0.9500
C(13)-C(14)	1.393(9)
C(13)-H(13)	0.9500
C(14)-H(14)	0.9500
C(15)-O(2)	1.196(7)
C(15)-O(1)	1.327(7)
C(16)-O(1)	1.457(7)
C(16)-H(16A)	0.9800

C(16)-H(16B)	0.9800
C(16)-H(16C)	0.9800
C(17)-C(19)	1.546(8)
C(17)-C(18)	1.563(7)
C(17)-H(17)	1.0000
C(18)-C(21)	1.529(8)
C(18)-H(18)	1.0000
C(19)-C(20)	1.554(8)
C(19)-C(22)	1.564(8)
C(19)-H(19)	1.0000
C(20)-C(21)	1.544(8)
C(20)-H(20A)	0.9900
C(20)-H(20B)	0.9900
C(21)-C(23)	1.549(7)
C(21)-H(21)	1.0000
C(22)-C(24)	1.500(8)
C(22)-C(23)	1.576(8)
C(22)-H(22)	1.0000
C(23)-C(25)	1.558(8)
C(23)-H(23)	1.0000
C(24)-C(26)	1.521(8)
C(24)-C(25)	1.564(7)
C(24)-H(24)	1.0000
C(25)-C(28)	1.554(7)
C(25)-H(25)	1.0000
C(26)-C(27)	1.518(8)
C(26)-C(29)	1.542(8)
C(26)-H(26)	1.0000
C(27)-C(28)	1.538(7)
C(27)-H(27A)	0.9900
C(27)-H(27B)	0.9900
C(28)-C(30)	1.483(8)
C(28)-H(28)	1.0000
C(29)-C(31)	1.529(8)

C(29)-C(30)	1.583(7)
C(29)-H(29)	1.0000
C(30)-C(32)	1.561(7)
C(30)-H(30)	1.0000
C(31)-C(33)	1.517(8)
C(31)-C(32)	1.612(7)
C(31)-H(31)	1.0000
C(32)-C(35)	1.529(8)
C(32)-H(32)	1.0000
C(33)-C(36)	1.528(7)
C(33)-C(34)	1.569(7)
C(33)-H(33)	1.0000
C(34)-C(35)	1.531(8)
C(34)-H(34A)	0.9900
C(34)-H(34B)	0.9900
C(35)-C(37)	1.517(7)
C(35)-H(35)	1.0000
C(36)-C(38)	1.583(9)
C(36)-C(37)	1.592(7)
C(36)-H(36)	1.0000
C(37)-C(39)	1.560(8)
C(37)-H(37)	1.0000
C(38)-C(52B)	1.460(14)
C(38)-C(40)	1.527(9)
C(38)-C(52A)	1.532(15)
C(38)-C(46)	1.585(8)
C(39)-C(47)	1.495(8)
C(39)-C(41)	1.512(9)
C(39)-H(39)	1.0000
C(40)-C(41)	1.356(8)
C(40)-C(45)	1.425(9)
C(41)-C(42)	1.376(8)
C(42)-C(43)	1.417(9)
C(42)-H(42)	0.9500

C(43)-C(44)	1.355(9)
C(43)-H(43)	0.9500
C(44)-C(45)	1.350(9)
C(44)-H(44)	0.9500
C(45)-H(45)	0.9500
C(46)-C(51)	1.328(8)
C(46)-C(47)	1.400(8)
C(47)-C(48)	1.397(7)
C(48)-C(49)	1.335(8)
C(48)-H(48)	0.9500
C(49)-C(50)	1.385(8)
C(49)-H(49)	0.9500
C(50)-C(51)	1.412(8)
C(50)-H(50)	0.9500
C(51)-H(51)	0.9500
C(52A)-O(3A)	1.175(17)
C(52A)-O(4A)	1.355(18)
C(53A)-O(4A)	1.444(11)
C(53A)-H(53A)	0.9800
C(53A)-H(53B)	0.9800
C(53A)-H(53C)	0.9800
C(52B)-O(3B)	1.184(16)
C(52B)-O(4B)	1.370(18)
C(53B)-O(4B)	1.461(11)
C(53B)-H(53D)	0.9800
C(53B)-H(53E)	0.9800
C(53B)-H(53F)	0.9800

C(6)-C(1)-C(2)	120.8(6)
C(6)-C(1)-H(1)	119.6
C(2)-C(1)-H(1)	119.6
C(3)-C(2)-C(1)	117.9(7)
C(3)-C(2)-H(2)	121.1
C(1)-C(2)-H(2)	121.1

C(2)-C(3)-C(4)	123.1(8)
C(2)-C(3)-C(7)	125.2(7)
C(4)-C(3)-C(7)	111.5(6)
C(5)-C(4)-C(3)	118.1(6)
C(5)-C(4)-C(8)	126.6(6)
C(3)-C(4)-C(8)	115.3(7)
C(6)-C(5)-C(4)	120.1(7)
C(6)-C(5)-H(5)	120.0
C(4)-C(5)-H(5)	120.0
C(5)-C(6)-C(1)	119.8(7)
C(5)-C(6)-H(6)	120.1
C(1)-C(6)-H(6)	120.1
C(9)-C(7)-C(15)	118.5(6)
C(9)-C(7)-C(3)	106.8(5)
C(15)-C(7)-C(3)	109.4(6)
C(9)-C(7)-C(17)	106.9(5)
C(15)-C(7)-C(17)	109.6(5)
C(3)-C(7)-C(17)	104.7(5)
C(4)-C(8)-C(10)	105.0(5)
C(4)-C(8)-C(18)	107.8(5)
C(10)-C(8)-C(18)	108.4(6)
C(4)-C(8)-H(8)	111.8
C(10)-C(8)-H(8)	111.8
C(18)-C(8)-H(8)	111.8
C(14)-C(9)-C(10)	119.4(6)
C(14)-C(9)-C(7)	126.7(6)
C(10)-C(9)-C(7)	113.9(6)
C(11)-C(10)-C(9)	120.8(7)
C(11)-C(10)-C(8)	125.6(6)
C(9)-C(10)-C(8)	113.6(6)
C(10)-C(11)-C(12)	121.2(7)
C(10)-C(11)-H(11)	119.4
C(12)-C(11)-H(11)	119.4
C(13)-C(12)-C(11)	117.7(7)

C(13)-C(12)-H(12)	121.1
C(11)-C(12)-H(12)	121.1
C(12)-C(13)-C(14)	122.4(8)
C(12)-C(13)-H(13)	118.8
C(14)-C(13)-H(13)	118.8
C(9)-C(14)-C(13)	118.5(7)
C(9)-C(14)-H(14)	120.8
C(13)-C(14)-H(14)	120.8
O(2)-C(15)-O(1)	124.5(6)
O(2)-C(15)-C(7)	123.8(6)
O(1)-C(15)-C(7)	111.6(6)
O(1)-C(16)-H(16A)	109.5
O(1)-C(16)-H(16B)	109.5
H(16A)-C(16)-H(16B)	109.5
O(1)-C(16)-H(16C)	109.5
H(16A)-C(16)-H(16C)	109.5
H(16B)-C(16)-H(16C)	109.5
C(19)-C(17)-C(18)	102.1(5)
C(19)-C(17)-C(7)	117.8(5)
C(18)-C(17)-C(7)	111.4(5)
C(19)-C(17)-H(17)	108.4
C(18)-C(17)-H(17)	108.4
C(7)-C(17)-H(17)	108.4
C(21)-C(18)-C(17)	103.6(5)
C(21)-C(18)-C(8)	118.4(5)
C(17)-C(18)-C(8)	107.4(4)
C(21)-C(18)-H(18)	109.0
C(17)-C(18)-H(18)	109.0
C(8)-C(18)-H(18)	109.0
C(17)-C(19)-C(20)	103.8(5)
C(17)-C(19)-C(22)	105.8(5)
C(20)-C(19)-C(22)	101.9(4)
C(17)-C(19)-H(19)	114.6
C(20)-C(19)-H(19)	114.6

C(22)-C(19)-H(19)	114.6
C(21)-C(20)-C(19)	92.9(5)
C(21)-C(20)-H(20A)	113.1
C(19)-C(20)-H(20A)	113.1
C(21)-C(20)-H(20B)	113.1
C(19)-C(20)-H(20B)	113.1
H(20A)-C(20)-H(20B)	110.5
C(18)-C(21)-C(20)	104.1(5)
C(18)-C(21)-C(23)	105.6(5)
C(20)-C(21)-C(23)	103.2(5)
C(18)-C(21)-H(21)	114.2
C(20)-C(21)-H(21)	114.2
C(23)-C(21)-H(21)	114.2
C(24)-C(22)-C(19)	115.6(6)
C(24)-C(22)-C(23)	92.2(4)
C(19)-C(22)-C(23)	102.8(5)
C(24)-C(22)-H(22)	114.5
C(19)-C(22)-H(22)	114.5
C(23)-C(22)-H(22)	114.5
C(21)-C(23)-C(25)	116.6(5)
C(21)-C(23)-C(22)	102.0(4)
C(25)-C(23)-C(22)	87.5(5)
C(21)-C(23)-H(23)	115.5
C(25)-C(23)-H(23)	115.5
C(22)-C(23)-H(23)	115.5
C(22)-C(24)-C(26)	117.5(6)
C(22)-C(24)-C(25)	90.0(5)
C(26)-C(24)-C(25)	102.7(4)
C(22)-C(24)-H(24)	114.5
C(26)-C(24)-H(24)	114.5
C(25)-C(24)-H(24)	114.5
C(28)-C(25)-C(23)	119.7(5)
C(28)-C(25)-C(24)	102.9(4)
C(23)-C(25)-C(24)	90.4(4)

C(28)-C(25)-H(25)	113.6
C(23)-C(25)-H(25)	113.6
C(24)-C(25)-H(25)	113.6
C(27)-C(26)-C(24)	104.0(5)
C(27)-C(26)-C(29)	101.4(5)
C(24)-C(26)-C(29)	105.5(5)
C(27)-C(26)-H(26)	114.8
C(24)-C(26)-H(26)	114.8
C(29)-C(26)-H(26)	114.8
C(26)-C(27)-C(28)	94.7(5)
C(26)-C(27)-H(27A)	112.8
C(28)-C(27)-H(27A)	112.8
C(26)-C(27)-H(27B)	112.8
C(28)-C(27)-H(27B)	112.8
H(27A)-C(27)-H(27B)	110.2
C(30)-C(28)-C(27)	103.9(5)
C(30)-C(28)-C(25)	105.9(5)
C(27)-C(28)-C(25)	101.3(4)
C(30)-C(28)-H(28)	114.8
C(27)-C(28)-H(28)	114.8
C(25)-C(28)-H(28)	114.8
C(31)-C(29)-C(26)	119.1(5)
C(31)-C(29)-C(30)	92.1(4)
C(26)-C(29)-C(30)	102.4(5)
C(31)-C(29)-H(29)	113.5
C(26)-C(29)-H(29)	113.5
C(30)-C(29)-H(29)	113.5
C(28)-C(30)-C(32)	119.0(5)
C(28)-C(30)-C(29)	103.0(5)
C(32)-C(30)-C(29)	89.0(4)
C(28)-C(30)-H(30)	114.1
C(32)-C(30)-H(30)	114.1
C(29)-C(30)-H(30)	114.1
C(33)-C(31)-C(29)	118.5(6)

C(33)-C(31)-C(32)	102.9(5)
C(29)-C(31)-C(32)	89.1(4)
C(33)-C(31)-H(31)	114.3
C(29)-C(31)-H(31)	114.3
C(32)-C(31)-H(31)	114.3
C(35)-C(32)-C(30)	117.7(5)
C(35)-C(32)-C(31)	101.6(5)
C(30)-C(32)-C(31)	89.8(4)
C(35)-C(32)-H(32)	114.7
C(30)-C(32)-H(32)	114.7
C(31)-C(32)-H(32)	114.7
C(31)-C(33)-C(36)	105.9(5)
C(31)-C(33)-C(34)	101.3(5)
C(36)-C(33)-C(34)	103.4(4)
C(31)-C(33)-H(33)	114.9
C(36)-C(33)-H(33)	114.9
C(34)-C(33)-H(33)	114.9
C(35)-C(34)-C(33)	93.5(5)
C(35)-C(34)-H(34A)	113.0
C(33)-C(34)-H(34A)	113.0
C(35)-C(34)-H(34B)	113.0
C(33)-C(34)-H(34B)	113.0
H(34A)-C(34)-H(34B)	110.4
C(37)-C(35)-C(32)	106.7(5)
C(37)-C(35)-C(34)	104.3(5)
C(32)-C(35)-C(34)	103.1(5)
C(37)-C(35)-H(35)	113.9
C(32)-C(35)-H(35)	113.9
C(34)-C(35)-H(35)	113.9
C(33)-C(36)-C(38)	118.8(6)
C(33)-C(36)-C(37)	103.2(5)
C(38)-C(36)-C(37)	110.7(5)
C(33)-C(36)-H(36)	107.9
C(38)-C(36)-H(36)	107.9

C(37)-C(36)-H(36)	107.9
C(35)-C(37)-C(39)	120.1(5)
C(35)-C(37)-C(36)	102.0(4)
C(39)-C(37)-C(36)	107.1(5)
C(35)-C(37)-H(37)	109.0
C(39)-C(37)-H(37)	109.0
C(36)-C(37)-H(37)	109.0
C(52B)-C(38)-C(40)	121.9(10)
C(52B)-C(38)-C(52A)	17.9(12)
C(40)-C(38)-C(52A)	113.4(10)
C(52B)-C(38)-C(36)	101.7(8)
C(40)-C(38)-C(36)	106.8(5)
C(52A)-C(38)-C(36)	119.6(8)
C(52B)-C(38)-C(46)	114.5(9)
C(40)-C(38)-C(46)	106.4(5)
C(52A)-C(38)-C(46)	105.9(9)
C(36)-C(38)-C(46)	103.7(5)
C(47)-C(39)-C(41)	107.4(5)
C(47)-C(39)-C(37)	104.5(5)
C(41)-C(39)-C(37)	110.4(5)
C(47)-C(39)-H(39)	111.4
C(41)-C(39)-H(39)	111.4
C(37)-C(39)-H(39)	111.4
C(41)-C(40)-C(45)	120.5(7)
C(41)-C(40)-C(38)	114.8(7)
C(45)-C(40)-C(38)	124.6(6)
C(40)-C(41)-C(42)	121.3(7)
C(40)-C(41)-C(39)	114.1(6)
C(42)-C(41)-C(39)	124.6(6)
C(41)-C(42)-C(43)	118.3(7)
C(41)-C(42)-H(42)	120.9
C(43)-C(42)-H(42)	120.9
C(44)-C(43)-C(42)	119.2(7)
C(44)-C(43)-H(43)	120.4

C(42)-C(43)-H(43)	120.4
C(45)-C(44)-C(43)	123.5(8)
C(45)-C(44)-H(44)	118.3
C(43)-C(44)-H(44)	118.3
C(44)-C(45)-C(40)	117.2(7)
C(44)-C(45)-H(45)	121.4
C(40)-C(45)-H(45)	121.4
C(51)-C(46)-C(47)	124.0(6)
C(51)-C(46)-C(38)	125.2(6)
C(47)-C(46)-C(38)	110.8(5)
C(48)-C(47)-C(46)	115.4(6)
C(48)-C(47)-C(39)	128.9(6)
C(46)-C(47)-C(39)	115.7(5)
C(49)-C(48)-C(47)	122.5(6)
C(49)-C(48)-H(48)	118.7
C(47)-C(48)-H(48)	118.7
C(48)-C(49)-C(50)	120.5(6)
C(48)-C(49)-H(49)	119.8
C(50)-C(49)-H(49)	119.8
C(49)-C(50)-C(51)	118.9(6)
C(49)-C(50)-H(50)	120.5
C(51)-C(50)-H(50)	120.5
C(46)-C(51)-C(50)	118.6(6)
C(46)-C(51)-H(51)	120.7
C(50)-C(51)-H(51)	120.7
O(3A)-C(52A)-O(4A)	122.1(13)
O(3A)-C(52A)-C(38)	119.3(14)
O(4A)-C(52A)-C(38)	118.6(12)
C(52A)-O(4A)-C(53A)	116.5(10)
O(3B)-C(52B)-O(4B)	118.1(13)
O(3B)-C(52B)-C(38)	121.9(14)
O(4B)-C(52B)-C(38)	119.9(13)
O(4B)-C(53B)-H(53D)	109.5
O(4B)-C(53B)-H(53E)	109.5

H(53D)-C(53B)-H(53E)	109.5
O(4B)-C(53B)-H(53F)	109.5
H(53D)-C(53B)-H(53F)	109.5
H(53E)-C(53B)-H(53F)	109.5
C(52B)-O(4B)-C(53B)	118.3(10)
C(15)-O(1)-C(16)	114.2(5)

Symmetry transformations used to generate equivalent atoms:

Table 4. Anisotropic displacement parameters ($Å^2 x\ 10^3$) for Compound **3**. The anisotropic displacement factor exponent takes the form: $-2\pi^2[\ h^2\ a^{*2}U^{11} + ... + 2\ h\ k\ a^*\ b^*\ U^{12}\ ]$

	U^{11}	U^{22}	U^{33}	U^{23}	U^{13}	U^{12}
C(1)	70(6)	72(5)	33(4)	-21(4)	-3(4)	22(5)
C(2)	70(6)	54(5)	41(4)	-5(3)	7(4)	10(4)
C(3)	70(6)	40(4)	33(4)	-10(3)	4(4)	8(4)
C(4)	52(5)	56(5)	33(4)	-1(3)	2(4)	-1(4)
C(5)	90(7)	58(5)	31(4)	-6(3)	7(4)	7(5)
C(6)	57(5)	64(5)	44(4)	-7(4)	12(4)	5(4)
C(7)	70(6)	39(4)	31(4)	-7(3)	6(3)	3(4)
C(8)	94(6)	44(4)	22(3)	-7(3)	6(4)	1(4)
C(9)	67(5)	52(5)	29(4)	-5(4)	4(4)	2(4)
C(10)	79(5)	29(4)	26(4)	3(3)	2(3)	10(4)
C(11)	73(6)	52(5)	45(4)	4(4)	6(4)	-3(4)
C(12)	94(6)	59(5)	50(5)	-12(4)	4(4)	22(4)
C(13)	99(7)	70(6)	48(5)	-11(4)	17(4)	-1(5)
C(14)	88(6)	58(5)	49(5)	-16(4)	14(4)	6(4)
C(15)	81(6)	59(5)	33(4)	3(4)	6(4)	-2(4)
C(16)	144(8)	82(6)	37(4)	-4(4)	14(5)	-7(5)
C(17)	59(5)	49(4)	25(3)	-7(3)	1(3)	-2(3)
C(18)	70(5)	38(4)	37(4)	0(3)	7(3)	10(3)
C(19)	66(5)	62(5)	36(4)	4(4)	7(3)	6(4)
C(20)	76(5)	48(4)	27(4)	-2(3)	9(3)	0(4)
C(21)	63(5)	41(4)	26(3)	9(3)	0(3)	7(3)
C(22)	74(5)	56(4)	29(4)	-8(3)	-10(3)	10(4)
C(23)	66(5)	51(4)	20(3)	-3(3)	-4(3)	16(3)
C(24)	66(5)	61(5)	19(3)	-9(3)	-8(3)	4(4)
C(25)	74(5)	38(4)	17(3)	-3(3)	3(3)	8(3)
C(26)	72(5)	55(5)	30(4)	7(3)	-7(4)	11(4)
C(27)	74(5)	63(5)	29(4)	-8(3)	2(4)	1(4)
C(28)	62(5)	43(4)	35(4)	13(3)	6(3)	19(4)
C(29)	84(6)	46(4)	25(3)	-1(3)	6(4)	7(4)

C(30)	58(5)	48(4)	28(3)	-6(3)	2(3)	12(4)
C(31)	69(5)	56(4)	31(4)	17(3)	10(3)	21(4)
C(32)	65(5)	49(4)	31(4)	-1(3)	8(3)	20(4)
C(33)	64(5)	60(5)	20(3)	0(3)	1(3)	16(4)
C(34)	83(6)	51(4)	34(4)	-4(3)	14(4)	17(4)
C(35)	64(5)	49(4)	22(3)	6(3)	2(3)	20(4)
C(36)	76(6)	52(5)	42(4)	2(4)	12(4)	5(4)
C(37)	67(5)	35(4)	22(3)	3(3)	4(3)	13(3)
C(38)	113(7)	49(4)	25(4)	27(3)	17(4)	23(5)
C(39)	96(6)	37(4)	27(4)	15(3)	7(4)	8(4)
C(40)	87(6)	41(4)	53(4)	10(4)	24(4)	24(4)
C(41)	57(5)	32(4)	40(4)	12(3)	10(3)	9(3)
C(42)	88(6)	52(5)	37(4)	0(4)	7(4)	-7(4)
C(43)	98(7)	44(5)	61(5)	-1(4)	16(5)	5(4)
C(44)	92(6)	45(5)	65(5)	5(4)	21(4)	13(4)
C(45)	107(7)	49(5)	64(5)	4(4)	25(5)	20(5)
C(46)	84(6)	28(4)	40(4)	-6(3)	17(4)	9(3)
C(47)	73(5)	43(4)	31(4)	-3(3)	10(3)	8(3)
C(48)	72(5)	51(5)	40(4)	-5(4)	6(4)	0(4)
C(49)	97(6)	56(5)	34(4)	-13(4)	11(4)	-15(4)
C(50)	101(6)	53(5)	58(5)	-10(4)	30(4)	4(4)
C(51)	94(6)	57(5)	33(4)	-3(4)	15(4)	5(4)
O(1)	99(4)	59(3)	25(2)	3(2)	6(2)	5(3)
O(2)	128(5)	66(4)	37(3)	1(3)	2(3)	-14(3)

Table 5. Hydrogen coordinates (x 10^4) and isotropic displacement parameters ($Å^2$x 10^3) for Compound **3**.

	x	y	z	U(eq)
H(1)	5450	-1328	-1960	79
H(2)	6106	-498	-2000	72
H(5)	6147	-3586	-889	79
H(6)	5473	-2976	-1427	69
H(8)	6981	-3703	-632	71
H(11)	7381	-5719	-839	75
H(12)	7721	-6617	-1270	91
H(13)	7693	-5125	-1821	91
H(14)	7358	-2733	-1945	83
H(16A)	6525	1005	-2516	143
H(16B)	6456	-448	-2811	143
H(16C)	6932	306	-2588	143
H(17)	7063	490	-1041	59
H(18)	7084	-937	-516	64
H(19)	7780	220	-1163	71
H(20A)	7870	-2494	-888	65
H(20B)	8271	-1473	-566	65
H(21)	7810	-2455	-193	59
H(22)	7647	1943	-608	76
H(23)	7669	366	-33	63
H(24)	8502	993	-490	68
H(25)	8544	-555	83	58
H(26)	8357	3805	-342	73
H(27A)	7959	2878	88	74
H(27B)	8383	3871	382	74
H(28)	8465	1178	660	62
H(29)	9121	2444	-42	68
H(30)	9166	855	528	60

H(31)	8998	5085	375	66
H(32)	9079	3504	976	62
H(33)	9705	4869	239	64
H(34A)	9768	2088	483	71
H(34B)	10211	2999	776	71
H(35)	9831	2082	1223	60
H(36)	9585	6316	833	72
H(37)	9693	4833	1381	55
H(39)	10447	3979	1812	71
H(42)	11040	2607	1683	78
H(43)	11479	2399	1290	88
H(44)	11349	3990	736	85
H(45)	10848	5935	574	91
H(48)	10525	6249	2311	72
H(49)	10562	8789	2429	80
H(50)	10432	10503	1880	86
H(51)	10305	9541	1206	78
H(53A)	10454	9586	161	81
H(53B)	10887	10283	518	81
H(53C)	10415	10652	515	81
H(53D)	9685	9790	90	81
H(53E)	9225	8922	-124	81
H(53F)	9637	8380	-215	81

Part II

Diketopiperazine Based Surfactants

Preface

This dissertation focused on the development of new amphiphilic systems to probe the relationship between structure and function. Moving beyond the traditional hydrophobic and hydrophilic characteristics which drive surfactant assembly, we were interested in how symmetrical hydrogen bonding could affect self-assembly. This led to the preparation of the structures illustrated in Figure 34. The core structure was a diketopiperazine composed of two serine moieties. Additionally, the affect of chirality was examined by preparing two diastereomers. In one set of molecules the hydrophobic and hydrophilic moieties were positioned on the same face of the ring (**C**, **D**, and **E**). However, the other molecules had the sulfate and long alkyl chain on opposite faces (**F** and **G**). Using diketopiperazines in materials assemblies is not novel. The cyclic(serine-serine) core structure (as well as other naturally occurring amino acid diketopiperazines) have been used in the preparation of polymers.[47] Also, hydrophobic amino acid derived diketopiperazines have been used as organogelators (evidence for significant ordering in the solution state).[48,49] Our molecules were designed to examine intermolecular associations through the diketopiperazine rings. Bilayer or cylindrical micelles were envisioned as a result of the diketopiperazine directed ordering. These molecules enabled us to further probe the structure function relationship in surfactant aggregation.

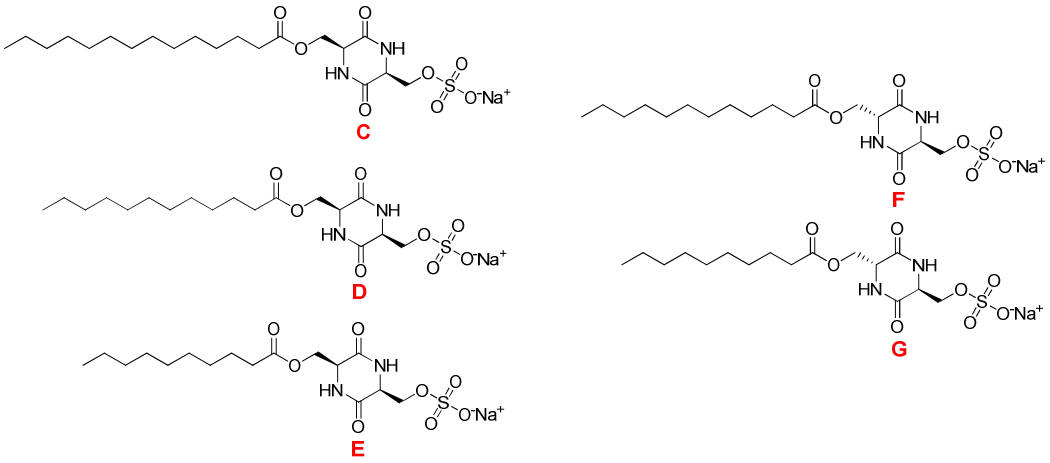

Figure 34. Cyclic dipeptide molecules

Synthesis

The syntheses of **C**, **D**, **E**, **F**, and **G** were completed using the multistep sequences outlined in Scheme 2 and Scheme 3. A four step sequence was employed to prepare final products of **C**, **D**, and **E** while a seven step sequence was used to prepare **F** and **G**. The reaction yields were not fully optimized. Upon isolation the products were analyzed using ^{1}H and ^{13}C NMR, HRMS, and/or elemental analysis.

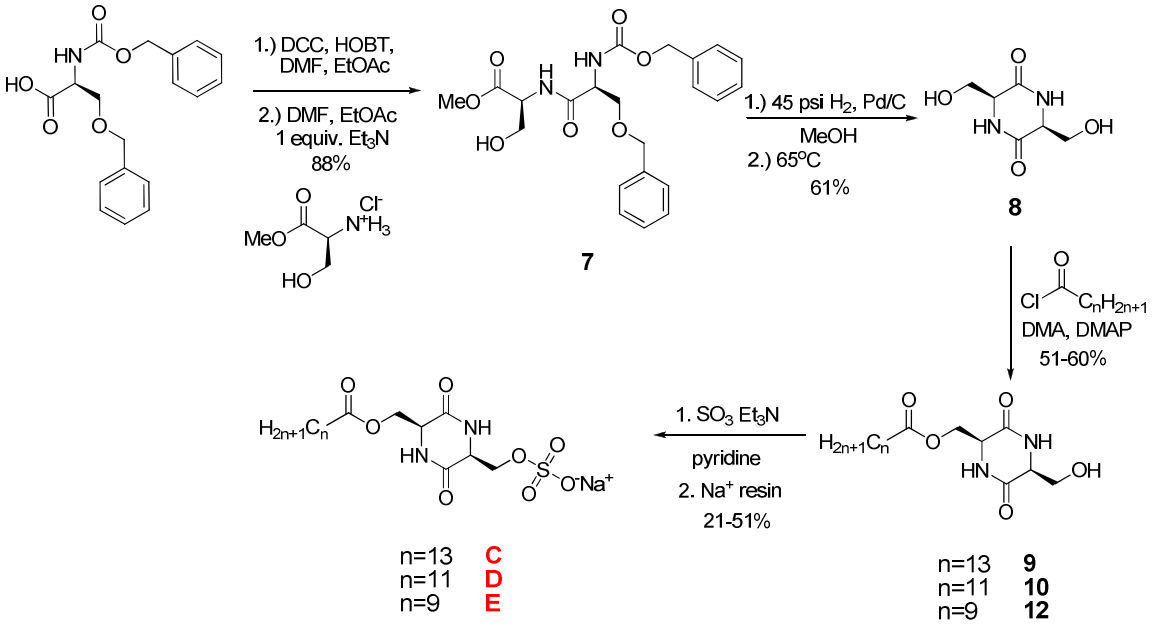

Scheme 2. Synthesis of (S,S)-cyclo(serine-serine) surfactants

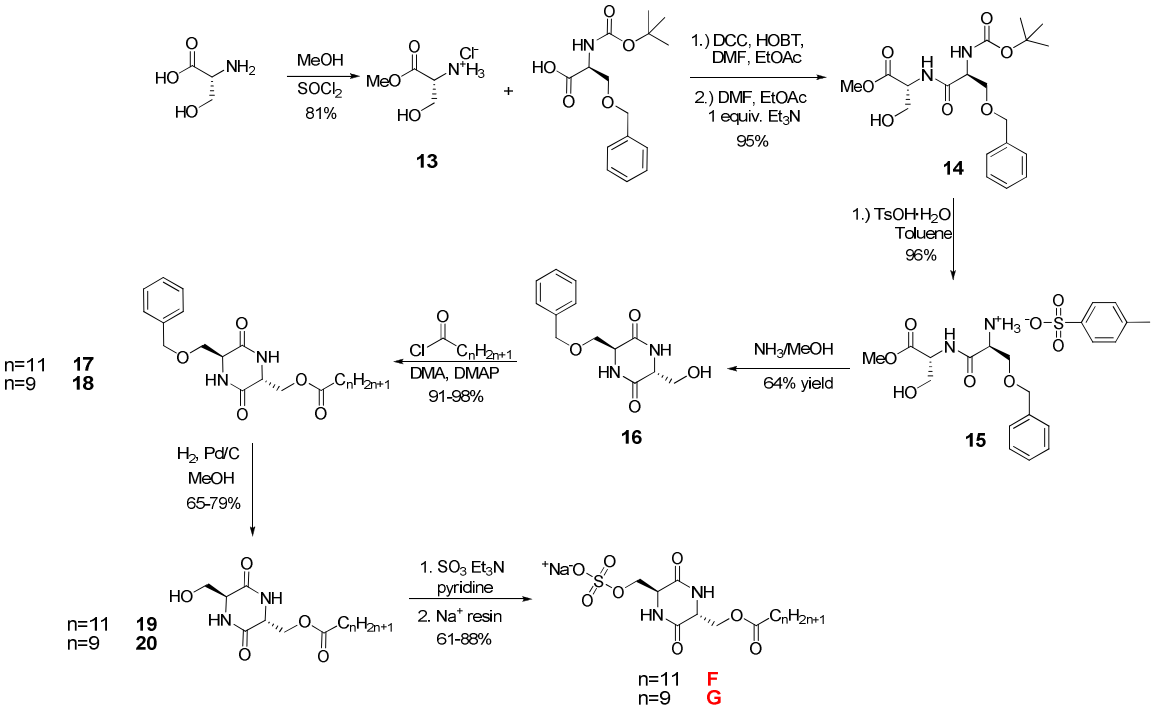

Scheme 3. Synthesis of (R,S)-cyclo(serine-serine) surfactants

Discussion

The synthesis of **C**, **D**, and **E** (S, S) all utilized the same 4 step sequence coming from a common intermediate **8**. Although the cyclo(ser-ser) core structure was commercially available, it was advantageous to synthesize due to the high cost ($200/gram) and the practical knowledge obtained to allow for the synthesis of the non-commercially available diastereomer. There are several literature methods for the preparation of **7** and/or **8**;[50,51] however none worked effectively for the formation of desired product.

We instead turned to a traditional peptide coupling procedure using dicyclohexylcarbodiimide/1-hydroxybenzotriazole (DCC/HOBt) to obtain the protected dipeptide (**7**).[52] A global deprotection under forcing conditions with activated palladium on carbon (Pd/C) in the presence of hydrogen yielded **8**. The product was isolated by crystallization from methanol. A crystal structure was obtained to verify the structure of our product and was consistent with the previously reported structure (Figure 35).[53] The absolute structure parameter is a measure of the statistical probability of the absolute configuration. The absolute structure parameter of compound **8** was 0.4(4), which indicated a low level of confidence in the absolute configuration of the molecule. The poor statistics are possibly the result of rotational isomers in the crystalline state. However, the x-ray data clearly indicated the configuration of the ring substituents was syn. Additionally, the optical rotation was in reasonable agreement with the literature value[53] leading us to propose that we had our desired enantiomer.

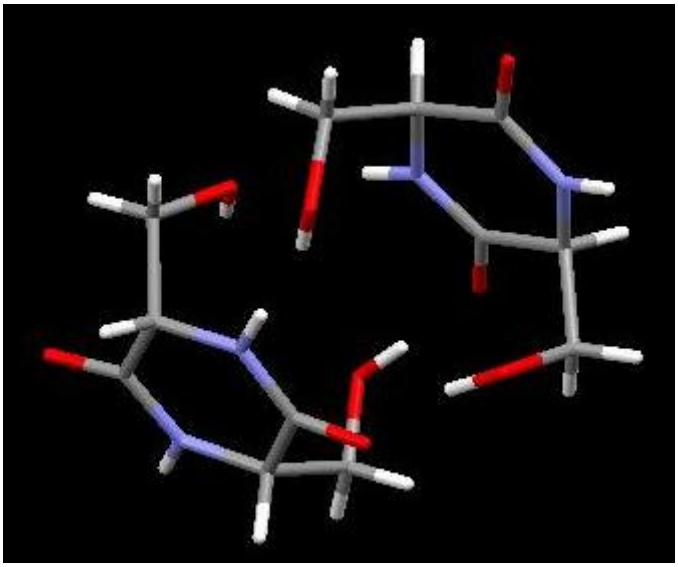

Figure 35. Crystal structure of (3*S*,6*S*)-3,6-bis(hydroxymethyl)piperazine-2,5-dione (**8**)

The completion of the synthesis utilized monoesterification of **8** to form the long chain alcohol. This was accomplished using an acid chloride and dimethylaminopyridine (DMAP). The resulting alcohol was then stirred at room temperature with an excess of sulfur trioxide triethylamine complex in pyridine. This led to complete conversion of product. Isolation and purification of this product was perhaps one of the most challenging aspects of this synthesis. Although the crude NMR indicated complete conversion, isolation and purification was plagued by the presence of starting alcohol. When the pyridine solvent was removed under reduced pressure water was added. The solution then became acidic due to the excess sulfur trioxide triethylamine complex present. It was ultimately realized that the product underwent hydrolysis of the sulfonate through neighboring group assistance by the amide carbonyl under acidic conditions.[54] Successful isolation and purification was eventually accomplished by keeping a few milliliters of pyridine in solution which acted as a buffer to maintain a neutral pH. Ion-

exchange resin (sodium form) was used to introduce the sodium counter ion. Size exclusion chromatography (Sephadex LH20) with water as the mobile phase purified the product. Fractions containing the product were identified using mass spectrometry and were isolated by lyopholization.

The syntheses of **F** and **G** (R, S) were accomplished using a similar synthetic sequence. Methyl ester serine was prepared using thionyl chloride in methanol.[55] The starting protect serine utilized a tert-butoxycarbonyl (BOC) protecting group on the amine as opposed to the carbobenzyloxy (CBZ) group used in the preparation of **C**, **D**, and **E**. The same procedure was used for the formation of the protected peptide (**14**) and the product was isolated in excellent yields. Selective removal of the BOC protecting group was completed using para-toluenesulfonic acid monohydrate in toluene. The amino salt was isolated (**15**) and cyclized using ammonia in methanol to produce the mono-protected cyclo(ser-ser) (**16**). This compound was crystallized from methanol to verify the structure of our molecule (Figure 36). Due to the poor quality of the crystal, verification of the absolute stereochemistry was not possible (absolute structure parameter was 2(2)). However, the x-ray data clearly indicated that the relative stereochemistry of the ring substituents were anti in confirmation. Additionally, since we obtained an optical rotation of +10.3°, a 50/50 mixture of enantiomers was not present. Further experiments are in progress to further verify the absolute configuration of the molecule. Esterification was also accomplished using the acid chloride and DMAP. Removal of the benzyl protecting group was completed under a hydrogen atmosphere with activated Pd/C in methanol/THF. Preparation and isolation of the sulfate was accomplished as previously discussed.

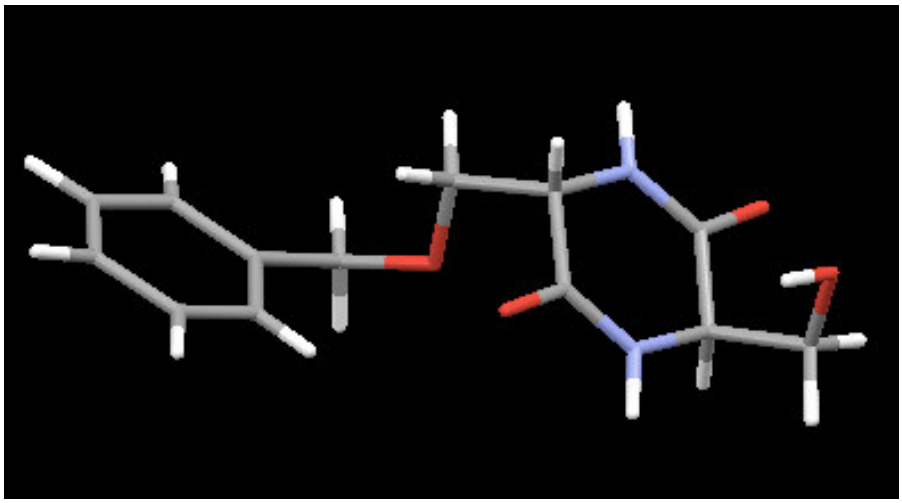

Figure 36. Crystal structure of (3S,6R)-3-(benzyloxymethyl)-6-(hydroxymethyl) piperazine-2,5-dione (**16**)

Characterization

Physical Characteristics

Initial examination indicated that **C**, **D**, and **F** were all virtually insoluble at room temperature. Compounds **E** and **G** (both 10-carbon chain derivatives) formed clear non-viscous, isotropic solutions at 22°C. All of the compounds displayed strong solid state interactions, indicated by not melting and low temperatures. All of the compounds were found to decompose at temperatures above 230ºC. Amino acid based surfactants with only a single amide have melting points near 100ºC.[29] The presence of a diketopiperazine moiety must have a strong effect on the associations in the solid state and therefore prevent melting.

Table 1. Decomposition temperatures of **C**-**G**

Compound	Decomposition Point(^{o}C)
C	228-230
D	246-248
E	255-257
F	231-233
G	239-240

Crystal Structure

Information about the ordering in the solid state can be extrapolated from the crystal structure. Although the primary interest is in the solution state assembly, the crystal structure provides important information about the ideal intermolecular interactions. There are significant intermolecular associations via the diketopiperazine ring (Figure 37). The crystal structure indicates that the symmetrical amide bonds are a major organizational force in the crystalline state. There is a perfect alignment of the central diketopiperazine rings. Each associates to the next via the amide bonds creating a continuous array. The substituent benzyl groups do not interact and are aligned in a staggered arrangement (Figure 37). This crystal structure verifies the ordering potential of the diketopiperazines; however, it is important to note that ordering in the solid state cannot be directly related to the aqueous solution state.

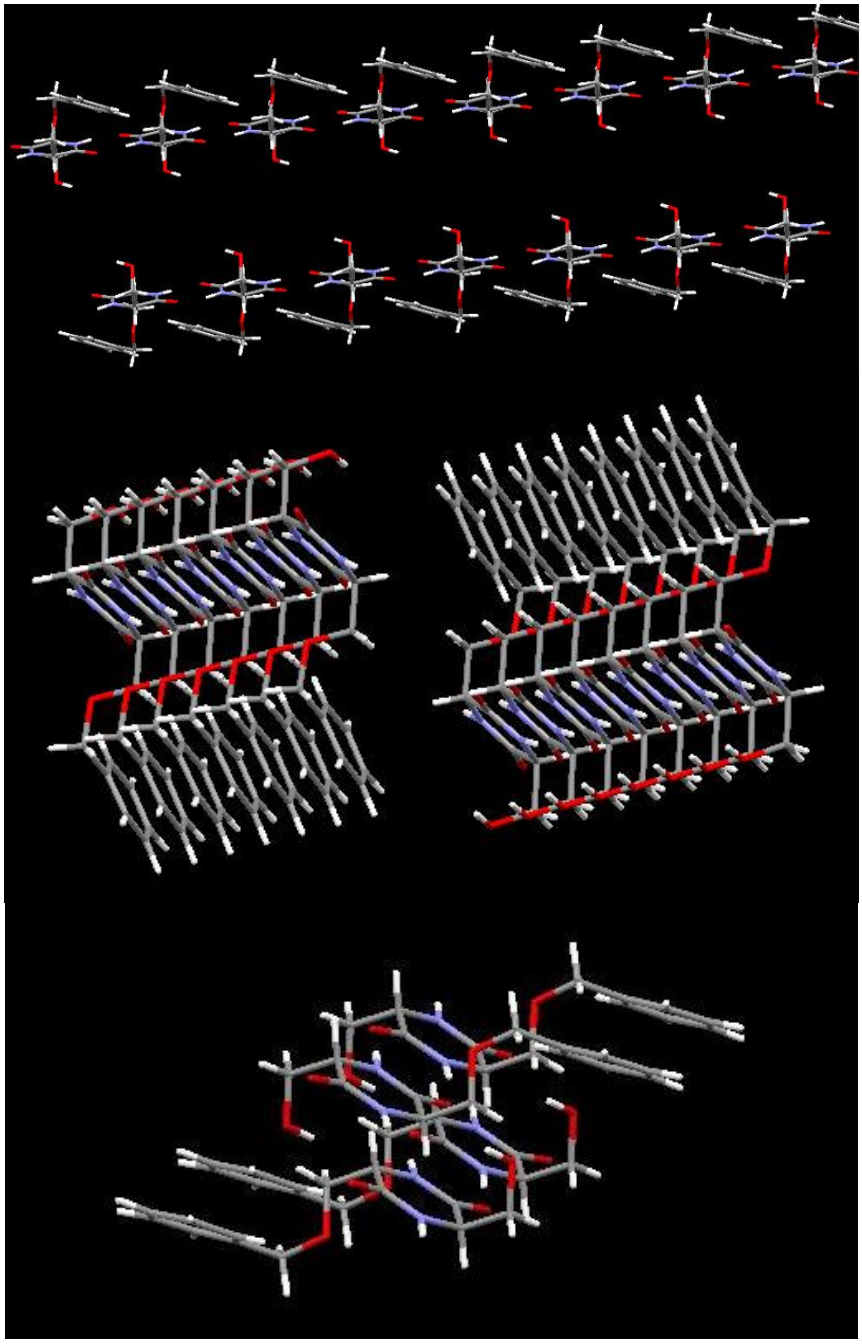

Figure 37. Crystal structure packing of the benzyl protected diketopiperazine

Solubility

Solubility is characterized in qualitative terms: A compound visually appears to either have dissolved or not. However, this is the apparent solubility and not the thermodynamic solubility.[56] The apparent solubility was often a meta-stable state which will eventually lead to the formation of a precipitate. The desire for precise solubility values led to High Pressure Liquid Chromatography (HPLC) experiments. Precise solubility values are determined by examining detector response at a given concentration.[20]

For these experiments, a Shimadzu HPLC system was employed and attached to an Evaporative Light Scattering Detector (ELSD). A more traditional detector such as Ultraviolet/Visible wavelength detection (UV/Vis) was not useful since the compounds do not absorb appreciably in the 220-780 nm range. A more universal detector such as an ELSD allows for the detection of most non-volatile analytes (Figure 38).[57] In this system the liquid flows from the HPLC to the detector where it is combined with a constant stream of gas. The flow is passed through a nebulizer which vaporizes the sample. The vaporized particles pass though a beam of light and the light scattering is viewed at 45°.[58]

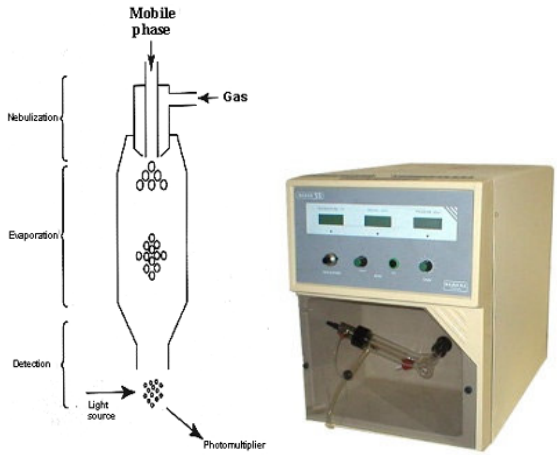

Figure 38. Evaporative light scattering detection system[59,60]

In UV/Vis spectroscopy, Beer's law is often employed to determine the concentration of a compound in solution.[43] With ELSD a calibration curve is employed to examine the detector response with respect to concentration. Dilute solutions (~1 mM) solutions of **E** and **G** were prepared (22ºC) and the detector response was measured. The two solutions were diluted 3 times to obtain the plot illustrated in Figure 39. A saturated solution (heterogeneous) was prepared and stirred at room temperature (22°C) for 24 hours. The solutions were filtered; a known volume was removed; and then the solution was diluted. The detector response was evaluated and the concentration was determined. The concentrations for **C** and **D** were estimated based on the calibration curve of **E** while the concentration for **F** was estimated from the calibration curve of **G** (Figure 39).

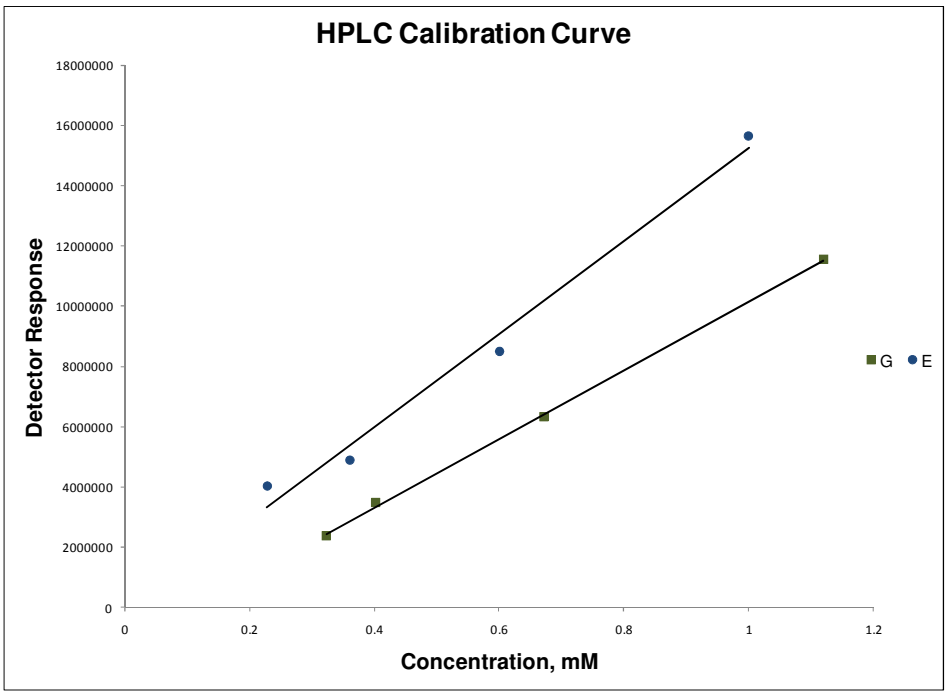

Figure 39. Calibration curve used to determine solubility

The apparent insolubility of **C**, **D**, and **F** was unusual for 12 and 14 alkyl chain surfactants. From the solubility experiments, the compounds were not completely insoluble, but had very low solubility at room temperature (Table 2). Additionally, compounds **E** and **G** both had relatively low solubility for 10 carbon alkyl chain surfactants. This data emphasized the profound effect of the diketopiperazine on solubility. The interactions of the molecules in the solid state were more favorable than the solute-solvent interactions. Additionally, the molecules all followed the expected trend of increasing chain length leads to decreasing solubility. This interplay of intermolecular forces and structure leads to compounds with low solubility at room temperature (22^{o}C).

Table 2. Thermodynamic solubility at 22ºC

Compound	Solubility (mM)
C	0.0
D	0.4
E	8.25
F	0.94
G	12.5

Krafft Temperature

The presence of both hydrophobic and hydrophilic functionalities can impart unique solubility issues in surfactant molecules. The low solubility encourages exploration of a potential Krafft phenomenon in these molecules. When a surfactant molecule is below the Krafft temperature, micelles cannot form.[1,61] The solid state of the molecule is more favorable and there is not enough energy in the system to disrupt the solid state forces and allow for micelles to form. Typical Krafft temperatures for long chain sulfates (10 and 12 carbons) are usually below room temperature.[62]

The Krafft temperature of surfactants **D**, **E**, **F**, and **G** were determined using conductivity and supported through qualitative observations. The Krafft temperature is where a significant increase in the solubility is observed. It is possible to do this qualitatively, however conductivity may also be employed. The conductance of a solution is directly proportional to the concentration of an ionic solute in solution. Previously it has been demonstrated that a sharp rise in the conductivity of a saturated surfactant solution that was slowly heated shows a break where the Krafft temperature occurs.[63,64]

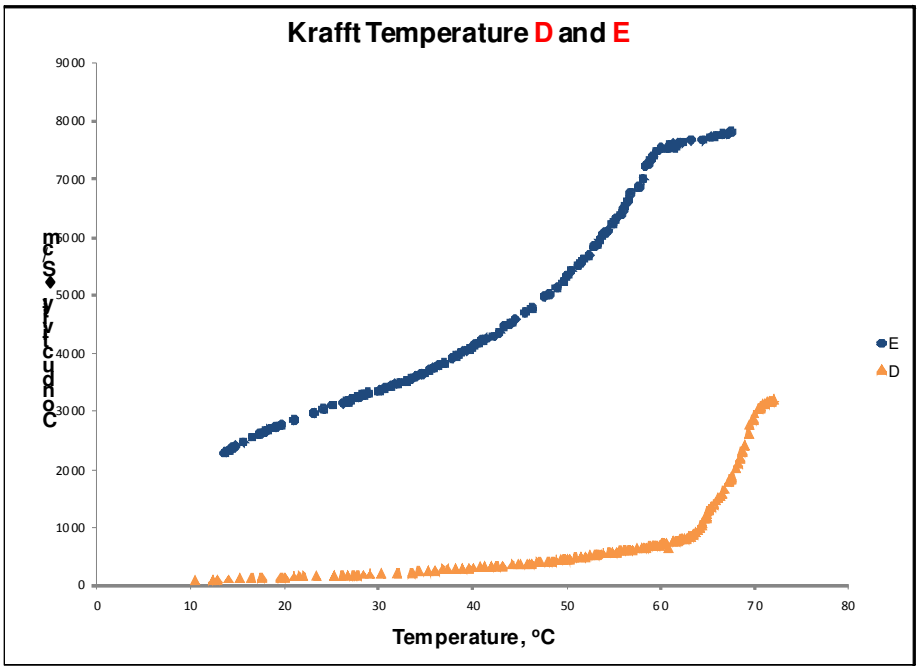

Figure 40. The Krafft temperature as determined by conductivity for **D** and **E**

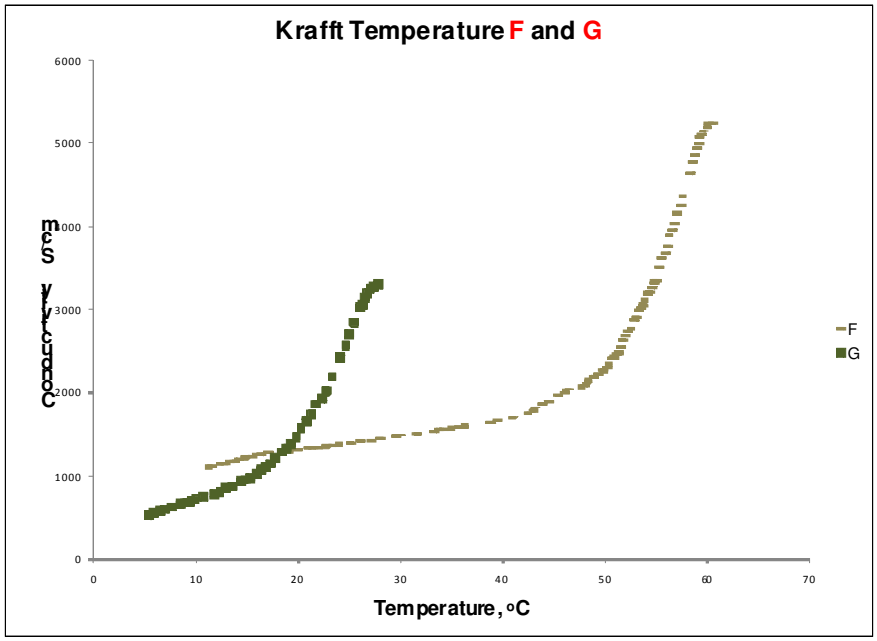

Figure 41. Krafft temperatures determined by conductivity for **F** and **G**

As illustrated in Figure 40, compound **D** showed a substantial increase in conductivity over the temperature range of 65-69ºC. The break at 69ºC also corresponded to clarity of the solution displaying additional evidence for the Krafft temperature. In the conductivity vs. temperature plot of compound **E** a less rapid increase in the temperature was observed. The break occurred at a temperature of 59°C and clarity of the solution was observed indicating a Krafft temperature. As expected **D** had a higher Krafft temperature than **E** due to the longer alkyl chain. A longer alkyl chain led to increased hydrophobicity of the surfactant and therefore a higher Krafft temperature.

Compounds **F** and **G** both displayed smaller breaks after a sharp increase in the conductivity vs. temperature plot (Figure 41). Compound **F** had a Krafft temperature near 59°C, while **G** had a lower Krafft temperature around 27°C (both temperatures were obtained from a slight break in the plot as well as clarification of the solution at that temperature). The higher Krafft temperature of **F** than **G** was due to the longer alkyl chain and increased hydrophobicity.

Comparing the Krafft temperatures based on stereochemistry, there was only a 10ºC difference in the Krafft temperatures of **D** and **F** (both 12 carbon derivatives). However the differences in Krafft temperature of **E** and **G** are more substantial with a 20ºC difference. In both cases the homochiral (SS) derivatives had the higher Krafft temperatures indicating more energy was required to disrupt the solid state forces and allow for micelles to form in solution. The very high Krafft temperatures of **D**, **E**, and **F** made full characterization of aggregation somewhat prohibitive. However, a Krafft

temperature of 27°C for **G** allowed for a more thorough characterization of aggregation in solution.

Conductivity

As previously discussed in Part I the conductivity of a solution can be used to determine the aggregation of an ionic surfactant in solution. Briefly, when there is free monomer amphiphile in solution the conductivity vs. concentration shows a linear relationship. However, when aggregates form there is an abrupt change in slope due to the binding of counter ions to the surface of the micelle.[35]

At room temperature (22°C), conductivity vs. concentration of **E** and **G** were examined in comparison to SDS (Figure 42). Neither **E** nor **G** displayed a break characteristic of micellization. The break for SDS was apparent at 8 mM indicating the CMC. The linear relationship of conductivity and concentration with no CMC supported the surface tension data which also didn't indicate a micellization concentration. Additionally the Krafft temperature data suggested that room temperature was below the possible micellization temperature for these two systems.

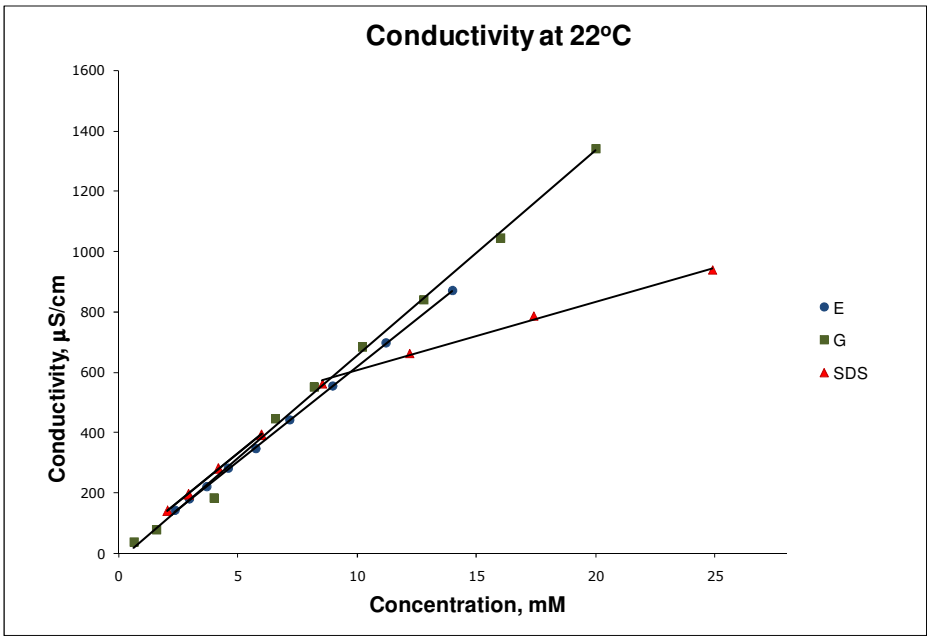

Figure 42. Conductivity obtained at 22°C

When conductivity vs. concentration was examined for **G** above the Krafft temperature (33°C) a CMC was evident (Figure 43). Additionally, this indicated that the aggregate formed had a traditional ionic micelle surface which required counterion binding to stabilize the charge repulsions of the head groups.[35] The 16.2 mM CMC of **G** was higher than SDS (8 mM), but lower than the 33 mM for sodium decyl sulfate (SdeS).[65] If the entire amide-ring structure is considered to be a part of the head group, the hydrocarbon tail was the same length as sodium decyl sulfate. The significant decrease in the CMC of **G** vs. sodium decyl sulfate may be due to favorable intermolecular interactions of the amide bonding head groups. These may stabilize the micelle state leading to a lower CMC.

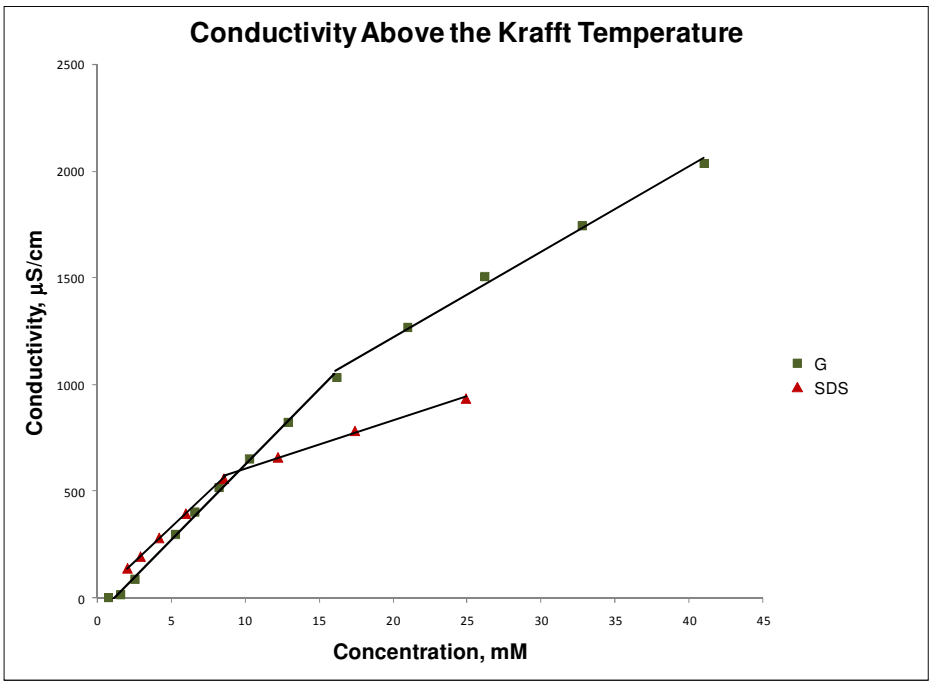

Figure 43. Conductivity obtained above the Krafft temperature (**G** at 33ºC and SDS at 22ºC.

Surface Tension

As discussed previously in Part I, evaluation of the surface tension of a surfactant solution provides imperative information about the adsorption of the amphiphile at the air-water interface. Briefly, a surfactant in aqueous solution adsorbs at the air-water interface to minimize the unfavorable interactions between the hydrophobic tails and the bulk aqueous solution.

The Gibbs equation describes the relationship between surface tension and concentration. By measuring the surface tension of an amphiphilic solution and plotting it versus the log of concentration the CMC can be determined. Additionally the area per molecule can be calculated by examining the saturated surface of an amphiphilic solution, indicated by the sharp slope in the plot of surface tension vs. the logarithm of

concentration. The Gibbs equation relates the Gibbs Free Energy (Γ) of a solution to the surface tension(γ) and concentration (Equation 4). [66,67] The Gibbs Free Energy of the solution can then be used to obtain the area per molecule (Equation 5). With the area per molecule, the packing of a molecule at the air-water interface can be examined.

$$\Gamma = \frac{-1}{RT}\frac{d\gamma}{d\ln c}$$

Equation 4

$$A = \frac{10^{16}}{6.02X10^{23}\cdot\Gamma}$$

Equation 5

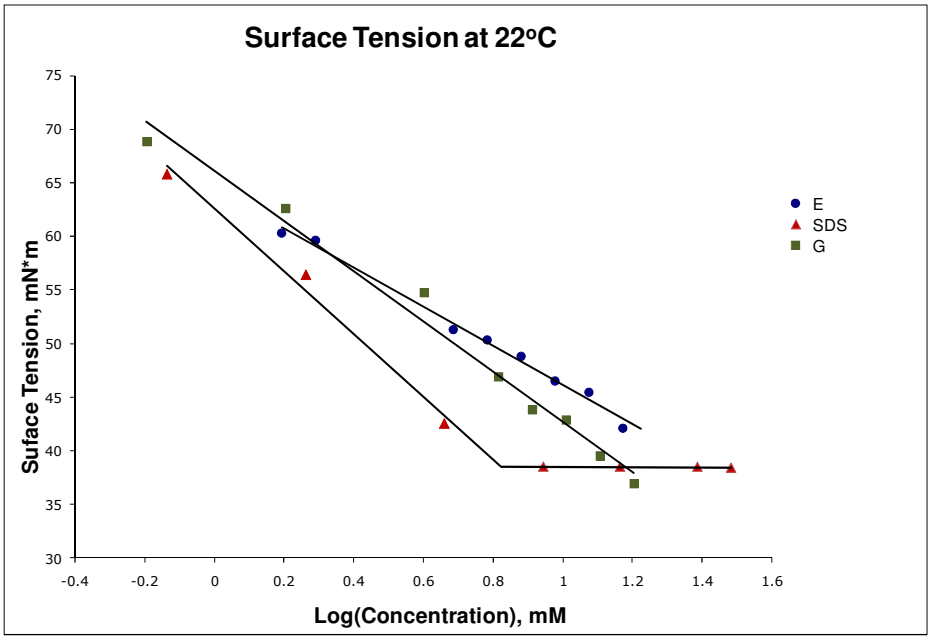

Figure 44. Surface tension obtained at 22°C

The surface tension for **E** and **G** was obtained at 22°C, which was below the Krafft temperature. No distinct break in the surface tension plot was observed for either **E** or **G** unlike SDS, where a break was observed at 8 mM. This supports the assertion

that both compounds are below the Krafft temperature and are unable to form micelles in a cooperative fashion. As amphiphilic compounds the molecules lowered the surface tension and adsorbed at the air/water interface. Interestingly, **E** and **G** both contain alkyl chains with 10 carbons, while SDS has a 12 carbon alkyl chain. However all three compounds lowered the surface tension of water to around 40 mN·m. This suggests similar efficiency of packing at the interface and possible favorable interactions of the amide bonds at the air-water interface. The surface tension of adsorption allowed the area per molecule to be calculated (Table 3).

Table 3. Calculated Area Per Molecule

Compound	Area per molecule(Å^2)
E	51.5
G	40.5
SDS	41[68,69]

It is interesting to note that at room temperature SDS and **G** had almost the same area per molecule (41 and 40.5 respectively) whereas **E** had a larger area per molecule. The value for SDS is in agreement with literature values.[68,69] Comparing **E** and **G**, the difference in area per molecule is probably due to differences in the conformation of the head groups. In **E**, both substituents are on the same face of the central ring, whereas in **G** they are on opposite faces of the ring. Examining Figure 45, it is possible to see how the differences in stereochemistry between **E** and **G** may lead to a slightly different packing density at the air-water interface. Compound **E** has more of a bowl shape and therefore may take up more space at the interface. The more open confirmation of **G** could allow for denser packing on the surface.

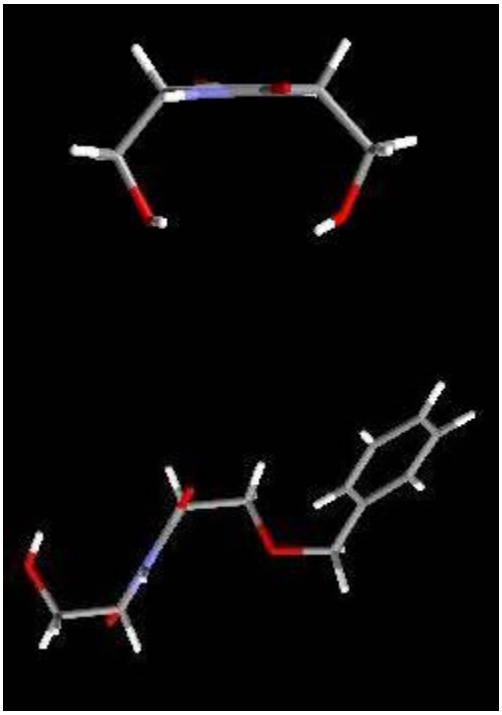

Figure 45. Differences stereochemistry between **E** and **G** looking at the orientations of the substituents around the diketopiperazine ring

However, the similarity in the area per molecule of SDS and **E** is unusual considering the large head group of **E**. There are two factors which may account for the similarity in numbers. One is that with such large head group, there must be significant ordering at the air-water interface. The sulfates will be submerged in the water and the diketopiperazine and the hydrophobic tail oriented towards the air. Drawing from what was learned in the crystal structure packing an array of amide bonding can be envisioned (Figure 46). Another issue is illustrated in Figure 47. Traditionally, the adsorption of surfactants to the air-water interface is drawn with the tails sticking straight out into the air in perfect alignment. Most likely that is not the case, with the hydrophobic tails

folding back on themselves and taking up additional space at the air-water interface. The interface although saturated is probably more disordered than traditionally depicted. This adsorption of SDS in addition to the tight packing of **E** at the air-water interface probably is partially responsible for the similar area per molecule.

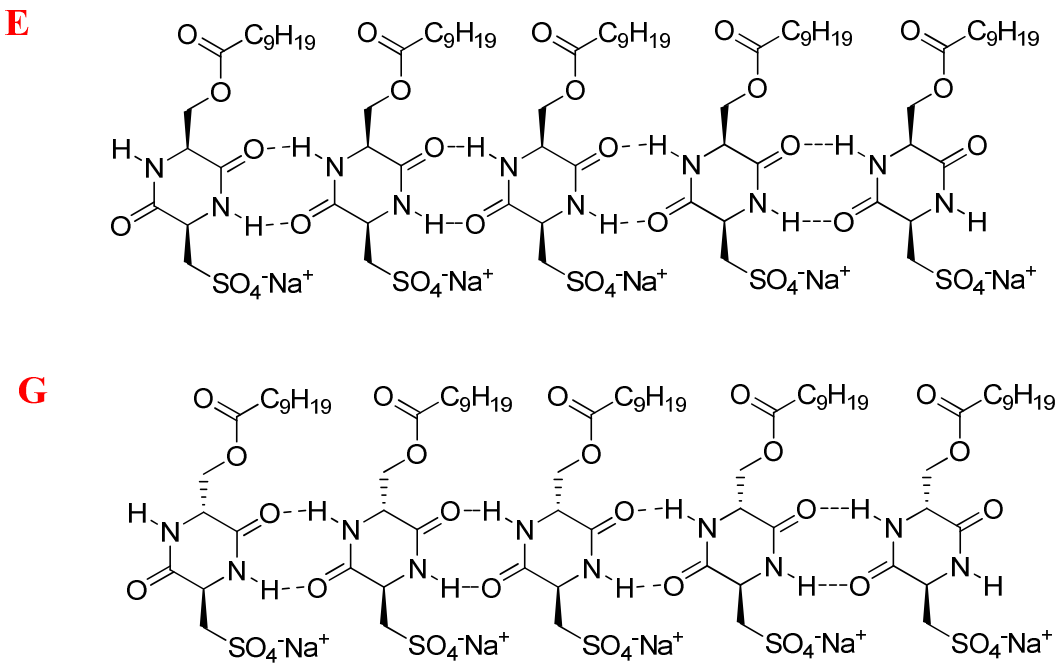

Figure 46. Amide bonding arrays of **E** and **G**

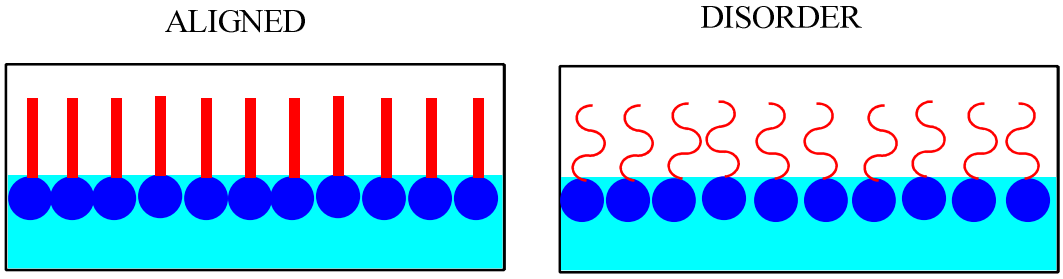

Figure 47. Depiction of amphiphile packing at the air-water interface

Measurement of the surface tension of **G** at 33°C was accomplished using a Nima Tech DST 9005 controlled temperature surface tensiometer (Figure 48).

Figure 48. Nima Tech DST 9005 controlled temperature surface tensiometer

The surface tension vs. the log of concentration was plotted in Figure 49. A break in the surface tension plot for **G** was noticed near 16.2 mM; however, an increase in the surface tension was observed after the break as opposed to a leveling off of the surface tension. This differs from SDS where a break is observed at 8.0 mM with no rise in the surface tension above the CMC. The increase in the surface tension of **G** after the CMC is traditionally observed when a surface active contaminant is present.[70] ^{1}H NMR of the compound used in the elevated temperature surface tension experiment did not indicate the presence of decyl acid, the most likely contaminant since it was the product of ester hydrolysis. Extended heating displayed slow ester hydrolysis (60ºC for 12 hours resulting in ~25% hydrolysis) in aqueous solution presumably assisted by the amide nitrogen 5 atoms away.[71] To put a number on this possible impurity, a sample of **G** was doped with 0.5% and 1% decyl acid. There is ≤0.5% decyl acid in the sample following the surface tension experiment (Figure 50). Surface tension plots of technical grade SDS

also showed this magnitude of an increase in the surface tension after a minimum had been reached.[70] Technical grade SDS can have as much as 10% dodecanol impurity when purchased from Fluka. However, extensive examination of this has shown that in this case the CMC was not at the minimum in the surface tension plot, but at a higher concentration.[70] This was determined based on the comparison of surface tension and conductivity data. The data presented here illustrates that the conductivity and the surface tension both showed the CMC at the minimum point on the surface tension plot. If trace amounts of the impurity were present, there was no noticeable effect on the CMC value.

The CMC of 16.2 mM indicated by the conductivity and the ^{1}H NMR after the experiment lends doubt that an impurity could cause such a massive increase in the surface tension after the minimum at 16.2 mM. However, if an impurity didn't cause the increase after the break, then there must be another explanation. One possibility is the apparent cloudiness of the samples.

A slight cloudiness was present above the Krafft temperature (33ºC) of **G** and at temperatures approaching the CMC as well as beyond the CMC (Figure 51). The clouding of the samples remained constant (at 33ºC) and was not a precipitate. This phenomenon may have had a deleterious impact on the surface tension of the liquid. Since the clouding was most apparent above the CMC this may be responsible for the increase in the surface tension after the break. If the solid particles deposited on the platinum ring, this may have caused a rise in the surface tension.

The appearance of the solutions was more reminiscent of clouding observed in nonionic surfactants.[20] In the case of nonionic surfactants the clouding has been usually

attributed to the decrease in hydration of the head groups with increasing temperature leading to a decrease in solubility of the micelle.[15] The presence of a diketopiperazine moiety in the head group may display association and dehydration behavior similar to nonionic surfactants. Clouding of the samples is evidence for aggregates that flirt with insolubility. The solutions of **G** above the CMC at 33ºC are not birefringent when viewed through cross polarizers. Therefore bilayer structures are probably not formed. In traditional micellar systems above the Krafft temperature, surfactants display very high solubility and often aggregates grow in size and/or shape. For **G** there appeared to be significantly improved solubility above the Krafft temperature; however, these aggregates may be limited in size and solubility.

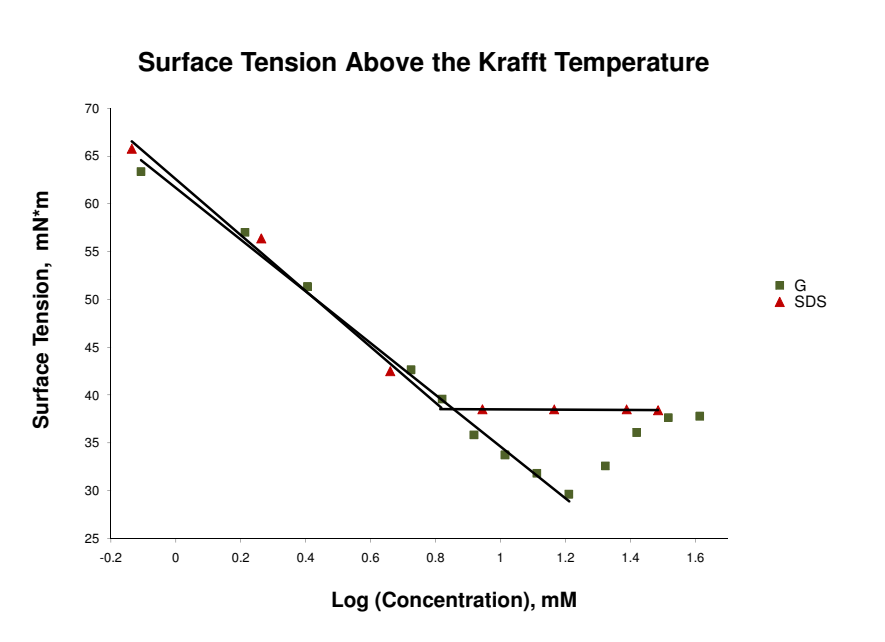

Figure 49. Surface tension obtained above the Krafft temperature

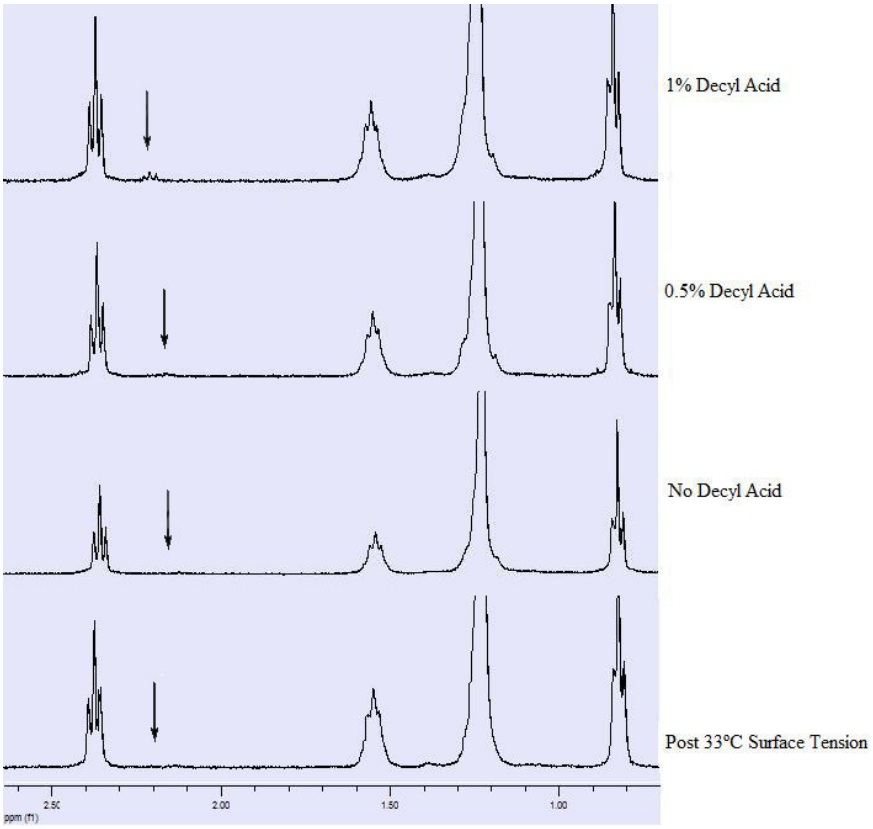

Figure 50. ^{1}H NMR of alkyl chain region of G doped with decyl acid (trace triplet observed near 2.2 ppm)

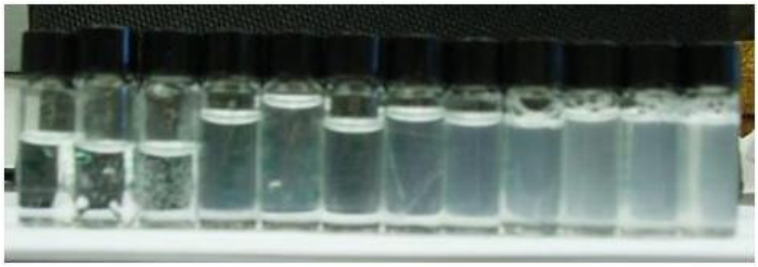

Figure 51. Increasing concentrations of **G** at 33ºC (From L to R: 0.78, 1.63, 2.54, 5.6, 8.27, 10.3, 12.9, 16.2, 21.0, 26.2, 32.8, and 41 mM)

NMR Experiments

Line Broadening

Evidence for spherical micelles at 33ºC of **G** came from diffusion NMR (discussed later) as well as line broadening experiments.[15,38,72] Examining the line widths of ^{1}H NMR spectra across several concentrations indicate the potential shape of the aggregates in solution. No noticeable change in the line widths was observed across the concentrations above and below the CMC for **G** (Figure 52). The line widths of SDS (21°C) also did not increase with increasing concentration (Figure 52). This data in addition to the lack of an increase in the viscosity of the system indicated a traditional spherical micelle as opposed to larger elongated micelles. Larger and elongated micelles are characterized by significant line broadening in the ^{1}H NMR spectra which was not apparent for SDS or **G**.[15,38,72]

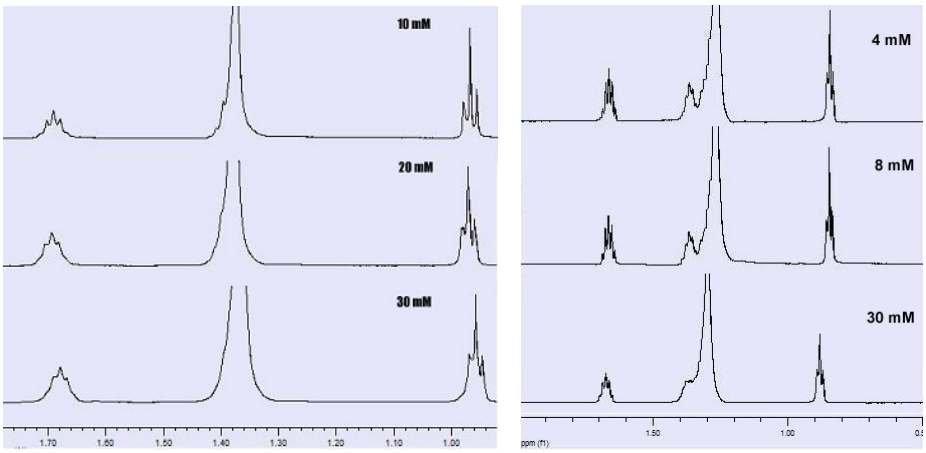

Figure 52. ^{1}H NMR spectra of **G** (left) and SDS (right) do not show significant line broadening above and below the CMC in the alkyl chain region.

Diffusion

The diffusion of molecules in a system can aid in the determination of the size of aggregates as well as the shape of the aggregate. The effect on diffusion can be explored by looking at a variety of concentrations above and below the CMC. When there are free molecules in a system they will diffuse faster than when molecules are aggregated into a large clump. The theory of how this technique works is rooted in the Stokes-Einstein Equation (Equation 2).[73,74]

$$D = \frac{k_B T}{6\pi\eta r}$$

Equation 2.

This technique has been applied to a number of unusual aggregation systems and has been found to be in good agreement for the aggregation shape and size obtained from other methods.

The diffusion data is obtained from the reduction in signal strength of the echo peaks by obtaining a linear fit to the Stejstal-Tanner Equation (Equation 6).[73,74]

$$Ln(\frac{I}{I_o}) = -(\gamma G\delta)^2 D(\Delta - \delta/3)$$

Equation 6

In this equation, I is the signal intensity and I_o is the initial signal intensity without the gradient. The magnetogyric ratio of the protons is γ, G is the Gradient, and δ is the width of the pulsed field gradient (PG). The delay between the PG is Δ. The diffusion can be obtained by setting fixed values of the delay between the PG, the width of the PG, and linearly increasing the gradient strength.

Examining the diffusion of a surfactant in solution is representative of two possible states, a monomer in solution as well as a micelle in solution. Below the CMC it can be assumed that only monomers are present. Above the CMC, micelles are considered hard spheres and the observed diffusion is a weighted average illustrated in Equation 7.[1] Below the CMC the observed diffusion is the diffusion of a monomer in solution. However, above the CMC the observed diffusion considers the relative amounts of monomer as well as aggregate in solution.

$$D_{obs} = \frac{c_{mono}}{c} D_{mono} + \frac{c_{agg}}{c} D_{agg}$$

Equation 7

The diffusion values of SDS (Figure 53) are in agreement with previous literature reports[75] and indicated cooperative micellization above the CMC (8.0 mM). When compared to the diffusion of **G** (showing a CMC of 17.9 mM), a similar trend was noted (Figure 54). In the case of **G** the break at the CMC is more apparent and abrupt than for SDS. Perhaps the amide bonds assist in the micellization process explaining the more abrupt break. This supports cooperative aggregation for **G** also observed in the surface tension and conductivity data.

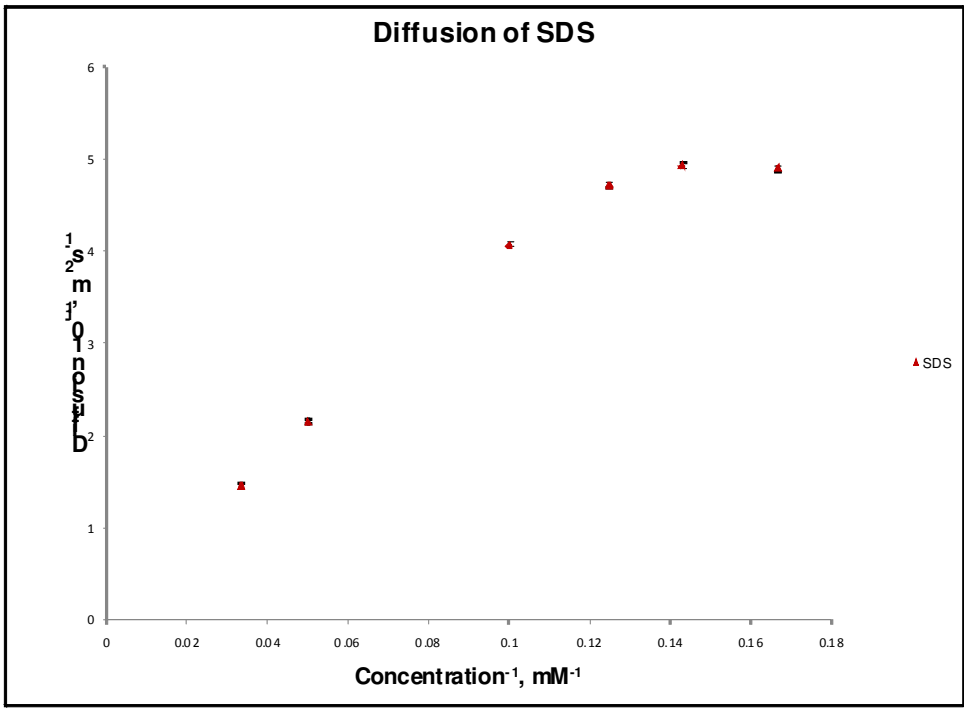

Figure 53. Diffusion of SDS above and below the CMC at 25°C

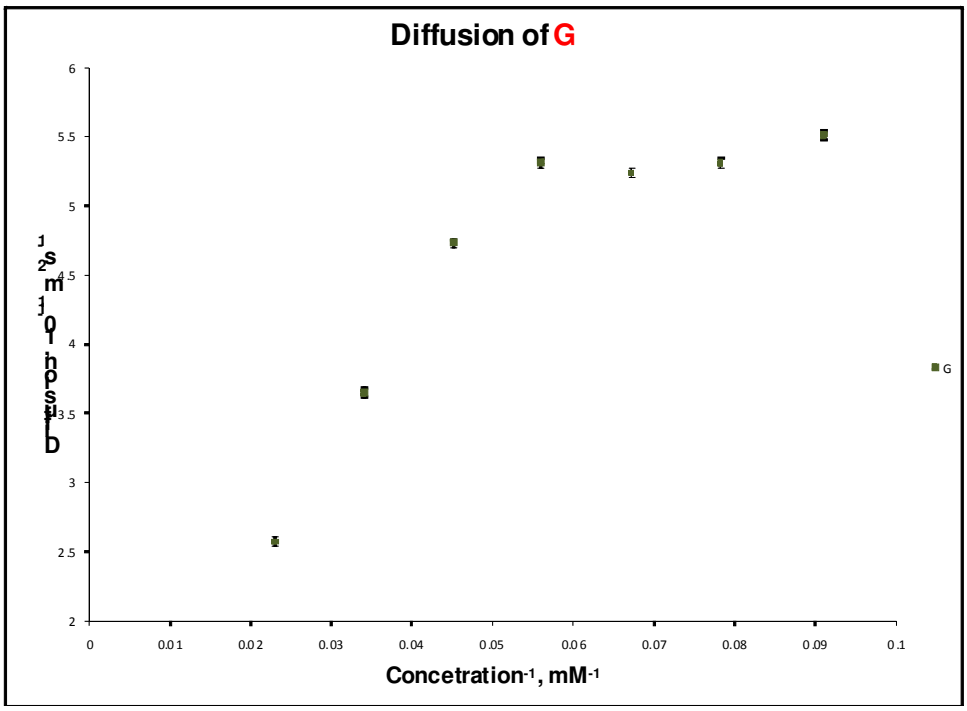

Figure 54. Concentration dependent diffusion NMR G at 33°C

Further examination of the diffusion data to obtain the potential size of the micelles invokes the Stokes-Einstein equation (Equation 2). The hydrodynamic radius of the micelle can be obtained using the viscosity of D_2O at the appropriate temperature (33ºC or 25ºC) and the diffusion constant obtained from the extrapolation of the diffusion where concentration^{-1} equals zero (an exclusively micellar solution). Comparison of SDS to **G** indicated micelles that were similar in size. The hydrodynamic radius of SDS is 2.45 nm (at 25ºC), while the hydrodynamic radius of **G** was 3.29 nm (at 33ºC). The larger hydrodynamic radius of **G** was consistent with expectation considering the extended confirmation of **G** including the head group is longer than that of SDS. Additionally, the presence of the extra hydrophilic functionalities (two amides, an ester and a sulfate) can bind more water than SDS, thereby leading to a larger hydrodynamic radius for **G**.

Conclusion

The incorporation of a diketopiperazine moiety into the head group of a surfactant leads to an increase in the Krafft temperature. Length of the hydrophobic region was extremely important for the solubility of the molecule. The associative interactions between the amides favored the solid state rather than the solution state at room temperature (22ºC). Conductivity and surface tension at 22ºC both indicated that no micellization was occurring for **E** or **G**. Although a difference in the packing at the air-water interface was observed for **E** and **G**, this was most likely due to the differences in chirality and therefore molecular orientation of the head groups.

The presence of micelles and a CMC for **G** was indicated through surface tension, conductivity, and diffusion NMR experiments at 33ºC (Table 4). The CMC values of **G**

when compared with traditional long chain alkyl sulfates appeared to be in between those of SDS (12-carbon chain sulfate) and SdeS (10-carbon chain sulfate). The 10 carbon alkyl chain of **G** indicated the CMC should be closer to 33mM like SdeS. However the large diketopiperazine head group appeared to lower the CMC probably due to the increased length of the surfactant. The lack of line broadening with increasing concentration in ^{1}H NMR as well as a lack of viscosity supported a traditional spherical micellar system rather than elongated micelles. Thus the driving force for micellization was hydrophobic associations of the tail rather than associations of the amides. Associations of the amide head groups may lead to insolubility based on the higher Krafft temperatures of **D**, **E**, **F**, and **G**. Presumably the high Krafft temperatures are due to the diketopiperazine interactions in the solid state. Thus clouding of the solutions and the presence of only spherical micelles indicated that the formation of larger aggregates may not be soluble. The diffusion NMR experiments of **G** showed diffusion similar to that of SDS further supporting a spherical micelle with a CMC closer to 17.9 mM rather than 16.2 mM.

Table 4. CMC values given in mM

Method	SDS	**G**	SdeS
Surface Tension	8.0 (22ºC)[68,69]	16.2 (33ºC)	33 (25ºC)[65]
Conductivity	8.0 (22ºC)[76]	16.2 (33ºC)	31 (25ºC)[76]
Diffusion	8.7 (25ºC)	17.9 (33ºC)	

This research further supports what was found by Menger and Zhang,[20] that the length of the hydrophobic region severely impacts solubility. Elevating the temperature increased the solubility. When the molecules are subjected to high temperatures (60ºC) for extended periods of time (overnight), significant (~25%) hydrolysis was observed.

Therefore, further exploration of these molecules for high temperature applications will require structural changes to the molecules. However, exploration of diketopiperazine surfactants could provide a whole new class of amphiphiles for higher temperature applications.

Experimental

Procedures

Solvents used in the synthesis were reagent grade and dried over 4 Å molecular sieves. Reagents were purchased from Aldrich, BaChem, or VWR and used without further purification. Sephadex LH20 was purchased from GE Healthcare. The BioRad AG 50W-X8 resin (Na^+ form, 200-400 mesh) was purchased from Bio-Rad Laboratories, Inc and rinsed with copious amounts of water before use.

Methods ^1H and ^{13}C NMR spectra were obtained either on a Varian INOVA 400 MHz (100 MHz for ^{13}C) or a Varian INOVA 600 MHz (150 MHz for ^{13}C) instrument. Mass spectra were collected at the Emory University Mass Spectrometry Center. Atlantic Microlabs in Norcross, GA performed all elemental analyses. Crystal structures were done by Emory University's X-Ray Crystallography Laboratory. A Fischer Surface Tensiomat® using the Du Noüy ring method was used to obtain surface tension measurements at room temperature. The Du Noüy Ring method using a Nima Tech DST 9005 was used for the elevated temperature surface tension experiments. Conductivity was performed using a Fischer Scientific Traceable™. Conductivity Meter for the elevated temperature experiments.

Conductivity (22°C) All experiments were conducted at room temperature using a sample volume of 10 mL. A Fischer Scientific Traceable™ Conductivity Meter was used and calibrated using a three point calibration of 100uS/cm, 1000 uS/cm, and 10,000 uS/cm standards purchased from Fischer.

Conductivity (33°C) All experiments were conducted at elevated temperature (33°C) by

equilibrating the samples in a controlled temperature water bath. The accuracy of the temperature was verified using an external thermometer. The sample volume was 5 mL and a Vernier Conductivity Probe connected to a "Go! Logger Lite" interface was used. 20 measurements were obtained the value was averaged.

Tensiometry (22^{o}C) All tensiometry experiments were performed at room temperature (22°C) or controlled using a circulating water bath at 33^{o}C. The sample volume was 25 mL and was prepared using a volumetric flask. Each concentration was measured 10 times and the obtained values were averaged. Between each concentration measurement the platinum ring was rinsed with copious amounts of water and flame dried.

Tensiometry (33^{o}C) All tensiometry experiments were performed using a Nima Tech DST 9005 equiped with a controlled temperature circulating water bath. The sample volume was 25 mL and was prepared using a volumetric flask. Each concentration was measured 5 times and the obtained values were averaged. Between each concentration measurement the platinum ring was rinsed with copious amounts of water and flame dried.

Krafft Temperature Experiments All experiments were conducted using a temperature controlled oil bath. A saturated solution was prepared by heating until a clear solution formed. The solution was then placed in the refrigerator (5ºC) for 24 hours. The precipitated solution was slowly heated and the temperature of the solution was monitored using a Thermocouple (VWR). The conductivity was monitored with a Fischer Scientific Traceable™ Conductivity Meter. Both the conductivity probe and the thermocouple were in the surfactant solution. Before each experiment the conductivity meter was calibrated using a three point calibration of 100uS/cm, 1000 uS/cm, and

10,000 uS/cm standards purchased from Fischer.

HPLC All HPLC experiments were accomplished on a low pressure gradient pump (Shimadzu LC-10AT *vp*). The column was an Alltech Surfactant/R column packed with a polydivinylbeneze resin of 7 µm. An Evaporative Light Scattering detection system Sedex-55 (ELSD) was used. The detector was set to 30°C and had a continuous 2.2 bar flow of nitrogen gas. A Rheodyne injection system 7725i was employed with a 20 µL loop. The mobile phase was isocratic with 90% methanol and 10% water. For determining the solubility of **C**, **D**, **E**, **F**, and **G** a 1 mL/min flow rate was employed. For compounds **E** and **G** a calibration curve was prepared. This was accomplished by preparing a stock solution of **E** (or **G**) and diluting. Each concentration was run on the HPLC and the detector response was recorded. The detector response was plotted against concentration. To determine the thermodynamic solubility: a saturated solution was prepared by placing excess solid into water. The solution was heated twice, sonicated twice, and allowed to stir at room temperature for 24 hours. This solution was filtered, diluted, and injected on the HPLC. The detector response was measured and the solution concentration was calculated.

Diffusion NMR All experiments were performed using a 600 MHz NMR. The solutions were all prepared by dilution of a stock solution. Each sample was placed into the NMR for at least 15 min to reach 33°C before the spectra were obtained. The diffusion experiments were completed using a Hahn-echo pulse sequence with intervening pulse field gradient (PG). The pulse sequence was 90°-PG-180° -PG with the delays between the PG (Δ) fixed to 140ms. The width (δ) of PG was set to 7 ms and the strength was increased linearly from 0.01 to 0.6 T/m in 16 steps. The strength of the gradient was

calibrated with trace H_2O in D_2O at 33°C where Diffusion =2.36X10^{-9}m^{2}s^{-1}. Also, the gradient amplifier was verified to be linear using PEG with a known Diffusion.

Synthesis

Procedure for the synthesis of (*S*)-methyl 2-((*S*)-3-(benzyloxy)-2-(benzyl –oxycarbonyl-amino)propanamido)-3-hydroxypropanoate (**7**) :

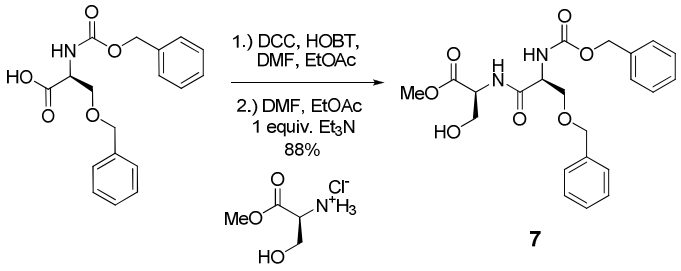

To a dry-3-neck 500 mL round bottom flask, (S)-3-(benzyloxy)-2-(tert-butoxycarbonylamino)propanoic acid (6.01 g, 18.2 mmol, 1 equiv.) and 1-hydroxybenztriazole (HOBT) (3.69 g, 27.3 mmol, 1.5 equiv.) were combined with dimethylformamide (DMF) (18 mL) under nitrogen. Once dissolved, dicyclohexylcarbodiimide (DCC) (3.76 g, 18.2 mmol, 1 equiv.) and dry ethyl acetate (EtOAc) (100 mL) were added to the solution. The reaction was stirred under nitrogen for ~1 hour. In a separate dry flask, 3.69 g (23.7 mmol, 1.3 equiv.) of (S)-serine methyl ester hydrochloride was dissolved in 18 mL of DMF. To this solution 3.30 mL (23.7 mmol, 1.3 equiv.) of dry triethylamine was added and the solution was diluted with 100 mL of EtOAc. The (S)-serine methyl ester solution was then cannulated into the reaction mixture and stirred overnight under nitrogen. The reaction mixture was filtered and then extracted 4 times with saturated sodium bicarbonate solution (100 mL). The organic layer was then extracted twice with a 3% hydrochloric acid solution followed by extraction with brine. The resulting organic layer was dried over sodium sulfate and then

concentrated in vacuo. The resulting white solid (6.89 g, 88% crude yield) contained a slight impurity of dicyclohexylurea. The product was used without further purification.

(*S*)-methyl 2-((*S*)-3-(benzyloxy)-2-(benzyl-oxycarbonylamino) propanamido)-3-hydroxy-propanoate (**7**) ^{1}H NMR [600 MHz, $CDCl_3$]: δ 7.60-7.30 (broad m, 10H), 5.75 (s, 1H), 5.12 (m, 2H), 4.65 (m, 1H), 4.56 (broad s, 2H), 4.23 (broad s, 1H), 3.93 (broad s, 3H), 3.76 (s, 3H), 3.63 (broad s, 1H), 2.70 (broad s, 1H). ^{13}C NMR [150 MHz, $CDCl_3$]: δ 170.69, 170.45, 156.38, 137.36, 136.17, 128.77, 128.73, 128.47, 128.35, 128.24, 128.10, 73.78, 69.95, 67.49, 63.03, 55.18, 54.71, 52.97. Melting Point, 108-110°C. $[\alpha]^{20}_{589}$ +33° (c=1 g/100mL, $CHCl_3$). HRMS (ESI+) calcd. For $C_{22}H_{27}O_7N_2$ ([M+H]), 431.18128. Found, 431.18056.

Procedure for the synthesis of (3*S*,6*S*)-3,6-bis(hydroxymethyl)piperazine-2,5-dione (**8**):

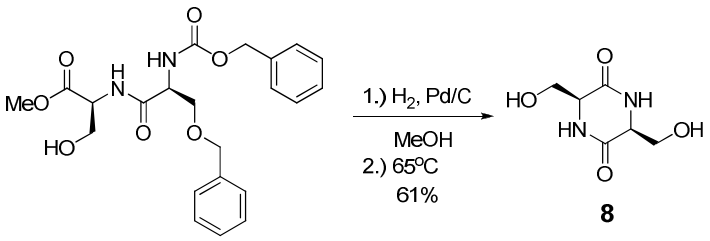

7 **8**

To a thick-walled hydrogenator flask, (*S*)-methyl 2-((*S*)-3-(benzyloxy)-2-(benzyl-oxycarbonylamino)propanamido)-3-hydroxypropanoate (3.0 g, 6.97 mmol, 1 equiv.) was dissolved in methanol (150 mL). Activated 5% palladium on carbon (Degussa type E101 NO/W) was added to the flask (20%, 2.96 g). The reaction was then placed in a Parr

Shaker apparatus, pressurized to 45 psi and shaken for 24 hours. Upon completion of the reaction the solution was filtered through a bed of celite and followed by filtration through fine filter paper. The methanol solution was concentrated under boiling conditions to 100 mL. The solution was then capped until crystal formation (~10 hours). The crystals were collected and an x-ray structure was obtained (data provided at the end of the experimental section). The reaction yield was 742 mg (61%).

(3*S*,6*S*)-3,6-bis(hydroxymethyl)piperazine-2,5-dione (**8**) ^{1}H NMR [600 MHz, DMSO]: δ 8.02 (s, 2H), 5.01 (t, *J*=5.4 Hz, 2H), 3.76 (s, 2H), 3.66 (dd, *J*= 4.8 Hz, *J*=10.2 Hz, 2H), 3.57 (dd, *J*=4.8 Hz, *J*=10.8 Hz, 2H). ^{13}C NMR [150 MHz, DMSO]: δ 165.94, 63.43, 57.17. Melting Point, >260°C. $[\alpha]^{20}_{589}$ -78° (c=.094 g/100mL, DMF). HRMS (ESI$^-$) calcd. For $C_6H_9O_4N_2$ ([M-H]), 173.05836. Found, 173. 05673.

General Procedure for the monoesterification of (3*S*,6*S*)-3,6-bis(hydroxymethyl)piperazine-2,5-dione (**9**, **10**, **11**):

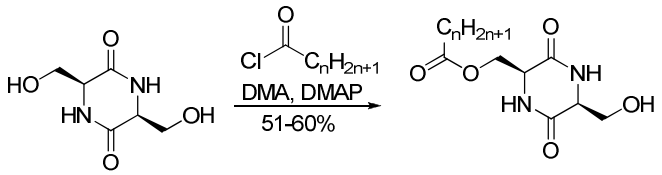

8

n=13 **9**
n=11 **10**
n=9 **12**

(3*S*,6*S*)-3,6-bis(hydroxymethyl)piperazine-2,5-dione (1 equivalent) was combined with dry dimethylacetamide (DMA) (200 mL) under nitrogen. The solution was heated to 60°C until completely dissolved. When the solution cooled to room temperature, 0.25

equivalents of 4-dimethylaminopyridine (DMAP) were added followed by 1 equivalent of the corresponding acid chloride. The solution was stirred under nitrogen overnight. Isolation of the product consisted of pouring the reaction mixture into 600 mL of distilled water. Once the solution cooled to room temperature it was filtered through a medium frit. For **8** and **9**, the isolated white solid was triturated with tetrahydrofuran and filtered. The resulting white solid yielded pure product. For **10**, the resulting solid was stirred with methanol and filtered. The product was then isolated from the methanol solution. The resulting (white solid) pure product was isolated in good yield.

((2S,5S)-5-(hydroxymethyl)-3,6-dioxopiperazin-2-yl)methyl tetradecanoate (**9**): (52% yield); IR (neat) 3195, 2914, 2848, 1742, 1681, 1447, 1338, 1157. ^{1}H NMR [600 MHz, DMSO]: δ 8.30 (s, 1H), 8.14 (s, 1H), 5.14 (t, *J*=5.4 Hz, 1H), 4.28 (dd, *J*=3.6 Hz, *J*=11.4 Hz, 2H), 4.19 (dd, *J*=6 Hz, *J*=10.8 Hz, 2H), 4.06 (broad, 1H), 3.77 (broad s, 1H), 3.68 (m, 1H), 3.55 (m, 1H), 2.30 (t, *J*=7.2 Hz, 2H), 1.50, (broad, 2H), 1.23 (broad, 20H), 0.85 (t, *J*=6.6 Hz, 3H). ^{13}C NMR [100 MHz, DMSO]: δ 172.87, 166.11, 164.82, 65.71, 62.68, 57.13, 53.82, 33.30, 31.36, 29.08, 28.99, 28.79, 28.54, 24.28, 22.16, 14.04. Melting Point, 186-188^{o}C. FTMS+ (APCI): calcd. 385.26970 For $C_{20}H_{37}O_5N_2$. Found, 385.26980.

((2S,5S)-5-(hydroxymethyl)-3,6-dioxopiperazin-2-yl)methyl dodecanoate (**10**): (60% yield); IR (neat) 3194, 2915, 2849, 1747, 1679, 1443, 1337, 1158. ^{1}H NMR [400 MHz, DMSO]: δ 8.31 (s, 1H), 8.16 (s, 1H), 5.16 (t, *J*=5.2 Hz, 1H), 4.28 (dd, *J*=3.6 Hz, *J*=11.2 Hz, 1H), 4.20 (dd, *J*=6.0 Hz, *J*=11.2 Hz, 1H), 4.07 (broad , 1H), 3.77 (broad s, 1H), 3.66 (m, 1H), 3.55 (m, 1H), 2.30 (t, *J*=7.6 Hz, 2H), 1.50, (broad, 2H), 1.24 (broad, 16H), 0.85

(t, *J*=6.8 Hz, 3H). ^{13}C NMR [100 MHz, DMSO]: δ 172.87, 166.12, 164.83, 65.71, 62.67, 57.13, 53.82, 33.30, 31.35, 29.07, 28.96, 28.78, 28.53, 24.27, 22.16, 14.04. Melting Point, 184-187°C. $[\alpha]^{20}_{589}$ -40° (c=.09 g/100mL, DMSO). FTMS+ (APCI): calcd. 357.23840 For $C_{18}H_{33}O_5N_2$. Found, 357.23830.

((2S,5S)-5-(hydroxymethyl)-3,6-dioxopiperazin-2-yl)methyl decanoate (**11**): (51% yield); IR (neat) 3195, 2916, 2849, 1741, 1680, 1447, 1337, 1157. ^{1}H NMR [600 MHz, DMSO]: δ 8.29 (s, 1H), 8.14 (s, 1H), 5.14 (t, *J*=4.8 Hz, 1H), 4.28 (dd, *J*=3 Hz, *J*=10.8 Hz, 1H), 4.20 (dd, *J*=6.6 Hz, *J*=10.8 Hz, 1H), 4.06 (broad s, 1H), 3.78 (broad s, 1H), 3.68 (m, 1H), 3.55 (m, 1H), 2.30 (t, *J*=7.2 Hz, 2H), 1.51, (broad, 2H), 1.24 (broad, 12H), 0.86 (t, *J*=6.6 Hz, 3H). ^{13}C NMR [150 MHz, DMSO]: δ 172.79, 166.05, 164.76, 65.63, 62.65, 57.08, 53.78, 33.26, 31.27, 28.85, 28.72, 28.65, 28.48, 24.22, 22.09, 13.96. Melting Point, 196-197°C. $[\alpha]^{20}_{589}$ -47° (c=.09 g/100mL, DMA). FTMS+ (APCI): calcd. 329.20710 For $C_{16}H_{29}O_5N_2$. Found, 329.20757.

General Procedure for the Sulfonation of **9**, **10**, **11**:

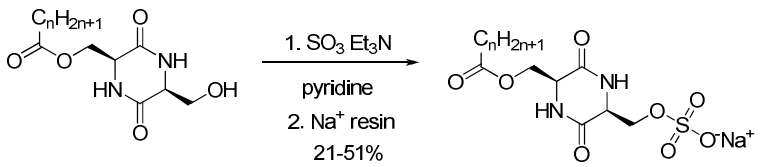

n=13 **9**
n=11 **10**
n=9 **12**

n=13 **C**
n=11 **D**
n=9 **E**

To a flame dried round bottom flask, 1 equivalent of alcohol was combined with 5 equivalents of sulfur trioxide triethylamine complex under nitrogen. Pyridine was

canulated into the flask and the reaction was stirred overnight. After at least 12 hours, a small amount (0.5 mL) of reaction solution was removed and dried under reduced pressure. A crude ^{1}H NMR was obtained to insure no starting alcohol remained. The reaction solution was concentrated to 20 mL and 100 mL of distilled water was added. The pH of the solution was checked to insure neutrality. If the pH indicates any acidity, additional pyridine is added until pH 7 is obtained.

Purification for (**C** and **D**): Excess saturated $NaHCO_3$ solution was added until the solution was basic. A precipitate immediately formed and the solution was filtered through a medium frit as soon as possible. The yellow-white solid was rinsed with hexanes and air dried. The solid was then stirred with methanol (~100mL MeOH per 0.5 g of material) and filtered through a medium frit to obtain pure product.

Purification for (**E**): The solution was stirred with ion exchange resin (sodium form) for 10 minutes (~10 g of resin per 0.5 g of starting alcohol). The resin was filtered off and the liquid was run on a Sephadex LH-20 size exclusion column. The mobile phase was 100% water and 20 mL fractions were collected. As fractions were collected the pH was checked to insure neutrality. If a fraction was found to be acidic 1-2 mL of pyridine was added to achieve neutral pH. The fractions were then checked with mass spectrometry looking for the desired product. Fractions with an ionization signal > E^5 were pooled and lyophilyzed to remove the water. This resulted in two separate lyophilyzed samples (due to size limitations on the lyophilyzer). These two samples were kept separate and checked by NMR for purity and complete ion exchange. If the presence of any triethylamine was detected the sample was stirred with ion exchange resin (sodium form) and purified again on the Sephadex LH-20 column. If signals in the aromatic region are

detected, this indicated the presence of impurities and a Sephadex LH-20 column is run again. Each reaction needed at least 3 total columns to purify all the material, however most needed 5 total columns to fully purify the reaction.

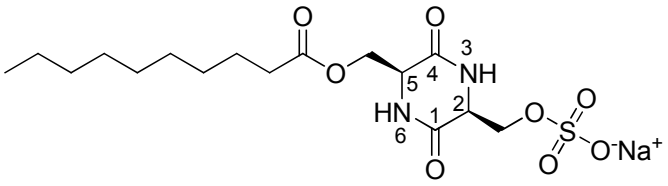

Sodium ((2S,5S)-3,6-dioxo-5-(tetradecanoyloxymethyl)piperazin-2-yl)methyl sulfate (**C**): (21% yield) ^{1}H NMR [600 MHz, DMSO]: δ 8.34 (s, 1H), 8.18 (s, 1H), 4.33 (dd, *J*=3 Hz, *J*=7.2 Hz, 1H), 4.17 (dd, *J*=6.6 Hz, *J*=11.4 Hz, 1H), 4.53 (br, 1H), 3.99 (br, 1H), 3.94 (brd, *J*=4.2 Hz, 2H), 2.33 (t, *J*=7.2 Hz, 2H), 1.49 (m, 2H), 1.23 (s, 20H), 0.851 (t, *J*=6 Hz, 3H). ^{13}C NMR (150 MHz, DMSO): δ 172.86, 165.21, 164.64, 67.18, 65.29, 33.21, 31.31, 29.07, 29.03, 28.93, 28.78, 28.73, 28.47, 24.29, 22.11, 13.97. Decomposition Point, 228-230^{o}C. $[\alpha]^{20}_{589}$ $^{+}28^{\circ}$ (c=.09 g/100mL, DMSO). HRMS (ESI^{-}) calcd. For $C_{20}H_{35}O_8N_2SNa$([M-Na]), 463.21086. Found, 463.21226.

Sodium ((2S,5S)-5-(dodecanoyloxymethyl)-3,6-dioxopiperazin-2-yl)methyl sulfate (**D**): (27% yield) ^{1}H NMR [600 MHz, DMSO]: δ 8.34, 8.18, 4.33 (dd, *J*=3 Hz, *J*=10.8 Hz, 2H), 4.18 (dd, *J*=6 Hz, *J*=10.2 Hz, 2H), 4.06 (br, 1H0, 3.99 (br, 1H), 3.45 (s, 2H), 2.33 (t, *J*=7.2 Hz, 2H), 1.49 (br, 2H), 1.24 (br, 16H), 0.851 (t, *J*=6.6 Hz, 3H). ^{13}C NMR (150 MHz, DMSO): δ 172.86, 165.21, 164.65, 67.19, 65.29, 54.80, 53.75, 33.21, 31.31, 29.03, 28.93, 28.93, 28.78, 28.73, 28.47, 24.29, 22.11, 13.97. Decomposition Point, 246-248^{o}C

$[\alpha]^{20}_{589}$ -30.3° (c=.09 g/100mL, DMSO). HRMS (ESI-) calcd. For $C_{18}H_{31}O_8N_2SNa$ ([M-Na]), 435.17956. Found, 435.18076. Elemental Anal. Calc. for $C_{18}H_{31}O_8N_2SNa$ (458.5): C 47.15, H 6.81, N 6.11, O 27.92, S 6.99; found C 47.08, H 6.81, N 6.14, O 28.05, S 6.93.

Sodium ((2S,5S)-5-(decanoyloxymethyl)-3,6-dioxopiperazin-2-yl)methyl sulfate (**E**): (51% yield) ^{1}H NMR [400 MHz, D_2O]: δ 4.40 (m, 4H) 4.31 (dd, *J*=5.2 Hz, *J*=10.4 Hz, 1H), 4.23 (dd, *J*=2.4 Hz, *J*=10.4 Hz, 1H), 2.42 (t, *J*=7.6 Hz, 2H), 1.56 (m, 2H), 1.23 (brd, 12 H), 0.82 (t, *J*=6.8 Hz, 3H). ^{13}C NMR [150 MHz, D_2O]: δ 166.29, 156.78, 156.28, 58.10, 54.40, 43.99, 43.59, 23.18, 18.13, 17.98, 17.89, 17.68, 13.97, 11.64, 3.02. Decomposition Point, 255-257°C. $[\alpha]^{20}_{589}$ -21° (c=.13 g/100mL, H_2O). HRMS (ESI-) calcd. For $C_{16}H_{27}O_8N_2SNa$ ([M-Na]), 407.14826. Found, 407.14932. Elemental Anal. Calc. for $C_{16}H_{27}O_8N_2SNa$ (430.45): C 44.64, H 6.32, N 6.51, O 29.74, S 7.45; found C 44.91, H 6.56, N 6.67, O 29.67, S 7.91.

Procedure for the synthesis of (R)-serine-methylester hydrochloride (**13**):

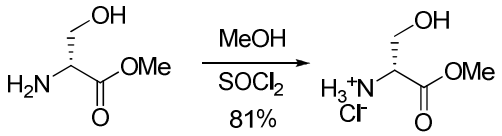

13

(R)-Serine (25.0 g, 238 mmol) was suspended dry methanol (200 mL) and stirred at 0°C under argon for 45 minutes. Thionyl chloride (33.96 g, 285 mmol, 1.2 equiv.) was added and the reaction was stirred overnight under argon. The solvent was removed under reduced pressure. The product was redissolved in methanol, and the solvent was

evaporated. The resulting white solid was dissolved in methanol and precipitated using diethyl ether. The product was filtered through a Hirsch funnel and dried under reduced pressure. 29.8 g (81% yield) was obtained of white solid. Data was in agreement with literature values for (S)-serine-methylester hydrochloride (opposite sign obtained for the optical rotation).[77]

(R)-serine-methylester hydrochloride (**13**): ^{1}H NMR [400 MHz, CD_3OD]: δ 4.03 (m, 1H), 3.90 (dd, *J*=6.6 Hz, *J*=18.6 Hz, 1H), 3.82 (dd, *J*=4.8 Hz, *J*=17.4 Hz, 1H), 3.81 (s, 3H). ^{13}C NMR [100 MHz, DMSO]: δ 168.62, 59.54, 54.49, 52.89. $[\alpha]^{20}_{589}$ -5.23° (c=.4 g/100mL, MeOH). HRMS (ESI^+) calcd. For $C_4H_{10}O_3N$ ([M+H]) 120.06552. Found, 120.06548.

Literature values for (S)-serine-methylester hydrochloride: $[\alpha]^{25}_{589}$ = +3.4 (*c* 0.2, MeOH); ^{1}H NMR (250 MHz, CD_3OD) δ 3.85 (s, 3H), 3.93 (dd, *J* = 11.8 Hz, *J* = 3.6 Hz, 1H), 4.01 (dd, *J*= 11.8 Hz, *J* = 4.4 Hz, 1H), 4.14 (m, 1H); ^{13}C NMR (63 MHz, CD_3OD) δ 53.9, 56.3, 60.9, 169.6.

Procedure for the synthesis of (R)-methyl 2-((S)-3-(benzyloxy)-2-(tert-butoxycarbonyl amino)propanamido)-3-hydroxypropanoate (14):

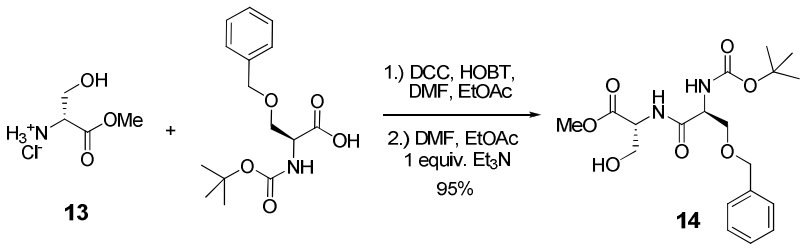

To a dry-3-neck 500 mL round bottom flask, (S)-3-(benzyloxy)-2-(tert-butoxycarbonylamino)propanoic acid (5.00 g, 16.9 mmol, 1 equiv.) and HOBT (3.43 g, 25.4 mmol, 1.5 equiv.) was added and were combined with DMF (18 mL) under nitrogen. Once dissolved, DCC (3.49 g, 16.9 mmol, 1 equiv) was added to the reaction along with dry EtOAc (100 mL). The solution was stirred under nitrogen for ~1 hour. In a separate dry flask, R-serine methyl ester hydrochloride (3.42 g, 22.0 mmol, 1.3 equiv.) was dissolved in DMF (18 mL). To this solution dry triethylamine (3.06 mL, 22.0 mmol, 1.3 equiv.) was added and the solution was diluted with EtOAc (100 mL). The (R)-serine methyl ester solution was cannulated into the reaction mixture and stirred overnight under nitrogen. The reaction mixture was filtered and then extracted 4 times with 100 mL portions of saturated sodium bicarbonate solution. The organic layer was then extracted twice with a 3% hydrochloric acid solution followed by extraction with brine. The resulting organic layer was dried over sodium sulfate and then concentrated in vacuo. The resulting yellow sticky oil (6.37 g, 95% crude yield) had a slight impurity of dicyclohexyl urea. The product was used without further purification.

(R)-methyl-2-((S)-3-(benzyloxy)-2-(tert-butoxycarbonylamino)propanamido)-3-hydroxy-propanoate (**14**): ^{1}H NMR [600 MHz, $CHCl_3$]: δ 7.31 (m, 5H), 5.51 (s, 1H), 4.64 (brd, 1H), 4.57 (d, *J*=12 Hz, 1H), 4.51 (d, *J*=19.8 Hz, 1H), 4.33 (brd, 1H), 3.90 (brd, 3H), 3.75 (s, 3H), 3.63 (m, 1H), 3.08 (brd, 1H), 1.44 (s, 9H). ^{13}C NMR [150 MHz, $CHCl_3$]: δ 170.84, 170.45, 156.20, 137.46, 128.75, 128.26, 128.08, 80.95, 73.67, 69.59, 62.74, 55.08, 54.95, 52.92, 28.41. $[\alpha]^{20}_{589}$ $^{-}15^{\circ}$ (c=.23 g/100mL, $CHCl_3$). HRMS (APCI) calcd. For $C_{19}H_{29}O_7N_2$ ([M+H]) 397.19693,. Found, 397.19679.

Procedure for the synthesis of (S)-3-(benzyloxy)-1-((R)-3-hydroxy-1-methoxy-1-oxopropan-2-ylamino)-1-oxopropan-2-aminium 4-methylbenzenesulfonate (**15**):

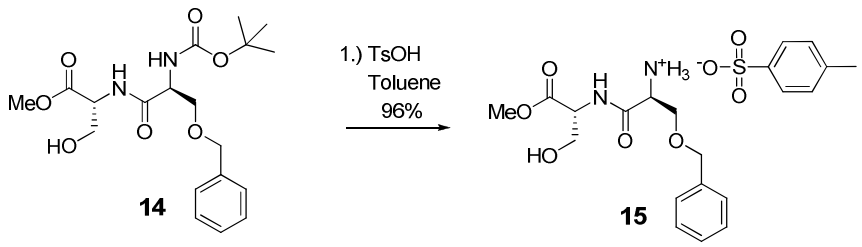

(R)-methyl-2-((S)-3-(benzyloxy)-2-(tert-butoxycarbonylamino)propanamido)-3-hydroxypropanoate (**14**) was placed in a 500mL round bottom flask (6.24 g, 15.7 mmol, 1 equiv.) and dissolved in toluene (200mL) with slight heating (50^{o}C). The solution was cooled to room temperature and para-toluene sulfonic acid monohydrate (p-TSA) (3.89 g, 20.4 mmol, 1.3 equiv.) was added in one portion. The solution was stirred at room temperature overnight and a precipitate formed. Filtration through a coarse frit rinsing with hexanes resulted in a white solid which was placed under reduced pressure to dry. The crude product was isolated in 7.13 g (96% yield). The product was used immediately without further purification.

(S)-3-(benzyloxy)-1-((R)-3-hydroxy-1-methoxy-1-oxopropan-2-ylamino)-1-oxopropan-2-aminium 4-methylbenzenesulfonate (**15**): ^{1}H NMR [600 MHz, DMSO]: δ 8.87 (d, *J*=7.8 Hz, 1H), 8.23 (brd, 3H), 7.47 (dd, *J*=1.8 Hz, *J*=8.4 Hz, 2H) 7.34 (m, 5H), 7.11 (d, *J*=7.2 Hz, 2H), 5.20 (brd, 1H), 4.56 (d, *J*=12 Hz, 1H), 4.50 (d, *J*=12 Hz, 1H), 4.23 (m, 1H), 4.15 (brd, 3H), 3.65 (s, 3H), 3.58 (brd, 1H), 2.29 (s, 3H). ^{13}C NMR [150 MHz, DMSO]: δ 170.55, 166.67, 145.78, 137.58, 128.30, 128.05, 127.69, 127.61, 125.50, 72.35,

68.53, 61.18, 54.74, 52.31, 52.10, 20.79. Melting Point, 150-152°C. $[\alpha]^{20}_{589}$ +17° (c=.17 g/100mL, H_2O). HRMS (ESI^+) calcd. For $C_{14}H_{21}O_5N_2$ ([M+H]), 297.14450. Found, 297.14470.

Procedure for the synthesis of (3S,6R)-3-(benzyloxymethyl)-6-(hydroxymethyl) piperazine-2,5-dione (**16**):

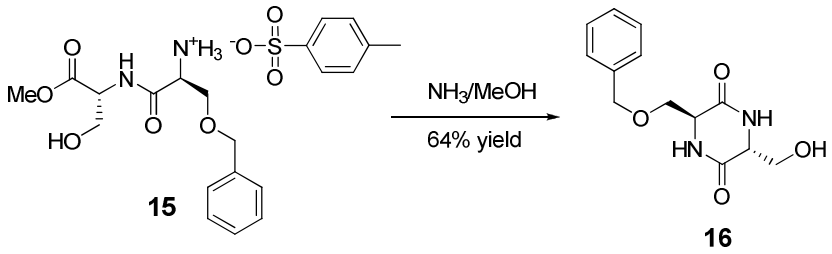

15 **16**

In a 250 mL round bottom flask (**15**) (4.50 g, 9.60 mmol, 1 equiv) was dissolved in methanol (175 mL). Once dissolved, 7M NH_3 in methanol (19 mL, 134 mmol, 14 equiv.) was added. The solution was stirred for six hours and a precipitate formed. The resulting white solid was filtered and dried under reduced pressure. A crystal structure was obtained upon crystallization from methanol. The product was obtained in 64% yield (3.06 g).

(3S,6R)-3-(benzyloxymethyl)-6-(hydroxymethyl) piperazine-2,5-dione (**16**): ^{1}H NMR [600 MHz, DMSO]: δ 8.11 (s, 1H), 7.98 (s, 1H), 7.34 (m, 2H), 7.29 (m, 3H), 5.02 (s, 1H), 4.49 (s, 2H), 3.93 (s, 1H), 3.80 (dd, *J*=3 Hz, *J*=9.6 Hz, 1H), 3.73 (m, 2H), 3.55 (m, 2H). ^{13}C NMR [150 MHz, DMSO]: δ 167.19, 166.60, 138.22, 128.25, 127.43, 127.26, 72.42, 70.61, 62.54, 56.96, 55.17. Melting Point, 204-205°C. $[\alpha]^{20}_{546}$+10.3° (c=.07 g/100mL, DMSO). HRMS (ESI^-) calcd. For $C_{13}H_{15}O_4N_2$([M-H]), 263.10263. Found, 263.09826.

General procedure for the esterification of (3S,6R)-3-(benzyloxymethyl)-6-(hydroxymethyl) piperazine-2,5-dione (**17** and **18**):

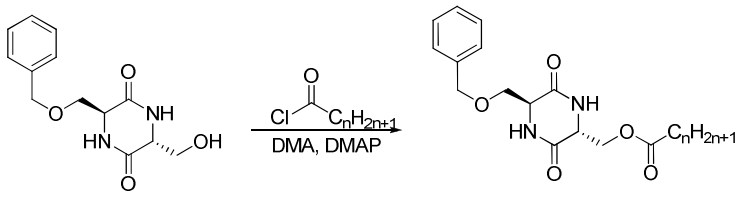

The starting alcohol (**16**) (one equiv.) was dissolved in dry DMA (250 ml) along with DMAP (0.25 equiv) under nitrogen gas. The solution was stirred until dissolved and the appropriate acid chloride was added (1.3 equiv.). Once the reaction was complete, the solution was dumped into 600 mL of distilled water and the resulting precipitate was filtered through a medium frit. The white solid product was triturated with methanol and filtered.

((2R,5S)-5-(benzyloxymethyl)-3,6-dioxopiperazin-2-yl)methyl dodecanoate (**17**): (98% yield); IR (neat) 3201, 2915, 2850, 1743, 1672, 1462, 1338, 12041117. ^{1}H NMR [600 MHz, DMSO]: δ 8.31 (s, 1H), 8.26 (s, 1H), 7.34 (m, 2H), 7.28 (m, 2H), 4.50 (s, 2H), 4.25 (dd, *J*=3 Hz, *J*=10.8 Hz, 1H), 4.21 (dd, *J*=3 Hz, *J*=11.4 Hz, 1H), 4.11 (s, 1H), 3.94 (s, 1H), 3.81 (dd, *J*=2.4 Hz, *J*=9.6 Hz, 1H), 3.56 (dd, *J*=2.4 Hz, *J*=9.6 Hz, 1H), 2.27 (t, *J*=7.2 Hz, 2H), 1.47 (m, 2H), 1.23 (brd, 16H), 0.85 (t, *J*=6.6 Hz, 3H). ^{13}C NMR [150 MHz, DMSO]: δ 172.70, 166.59, 165.78, 138.07, 128.28, 127.46, 127.23, 72.44, 71.09, 63.95, 55.44, 53.48, 33.31, 31.29, 29.00, 28.87, 28.71, 28.37, 24.37, 22.10, 13.96. Melting Point, 171-172°C. $[\alpha]^{20}_{546}$ $^{+}$5.3° (c=.053 g/100mL, DMSO). HRMS (APCI) calcd. For $C_{25}H_{39}O_5N_2$ ([M-H]), 447.28545. Found,447.28476.

((2R,5S)-5-(benzyloxymethyl)-3,6-dioxopiperazin-2-yl)methyl decanoate (**18**): (91% yield); IR (neat) 3199, 2916, 2850, 1743, 1671, 1461, 1338, 1170, 1116. ^{1}H NMR [600 MHz, DMSO]: δ: 8.32 (s, 1H), 8.27 (s, 1H), 7.34 (m, 2H), 7.28 (m, 3H), 4.50 (s, 2H), 4.25 (dd, *J*=3 Hz, *J*=10.8 Hz, 1H), 4.21 (dd, *J*=2.4 Hz, *J*=10.8 Hz, 1H), 4.11 (s, 1H), 3.94 (s, 1H), 3.82 (dd, *J*=3 Hz, *J*=9.6 Hz, 1H), 3.56 (dd, *J*=2.4 Hz, *J*=9.6 Hz, 1H), 2.27 (t, *J*=9.6 Hz, 2H), 1.47 (m, 2H), 1.23 (brd, 12H), 0.85 (t, *J*=6.6 Hz, 3H). ^{13}C NMR [150 MHz, DMSO]: δ 172.72, 166.62, 165.81, 138.09, 128.30, 127.49, 127.35, 72.46, 71.11, 63.96, 55.46, 53.50, 33.32, 31.28, 28.84, 28.72, 28.67, 28.38, 24.38, 22.10, 13.97. Melting Point, 173-174°C. $[\alpha]^{20}_{546}$ $^{+}$4.3° (c=0.047 g/100mL, DMSO). HRMS (APCI) calcd. For $C_{23}H_{35}O_5N_2$ ([M+H]),419.25405. Found,419.25405.

General Procedure of the debenzylation of (**17**) or (**18**):

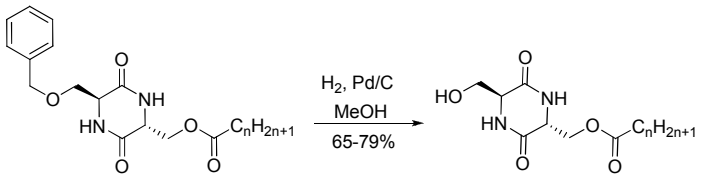

n=11 **17**
n=9 **18**

n=11 **19**
n=9 **20**

1 equiv. of **17** (or **18**) was dissolved in methanol and 30% THF was added. 0.05 equiv of activated Pd/C was added and the solution was stirred under a hydrogen atmosphere. Upon completion, the reaction solution was filtered through a bed of celite and the solvent was removed under reduced pressure. The resulting white solid was triturated with methanol and filtered.

((2R,5S)-5-(hydroxymethyl)-3,6-dioxopiperazin-2-yl)methyl dodecanoate (**19**): (65% yield); IR (neat) 3196, 2916, 2849, 1745, 1674, 1457, 1369, 1167. ^{1}H NMR [600 MHz, DMSO]: δ 8.17 (s, 1H), 8.12 (s, 1H), 5.13 (t, *J*=4.2 Hz, 1H), 4.26 (dd, *J*=3.6 Hz, *J*=11.4 Hz, 1H), 4.20 (d, *J*=10.2 Hz, 1H), 4.12 (s, 1H), 3.74 (m, 2H), 3.53 (d, *J*=10.2 Hz, 1H), 2.67 (t, *J*=7.8 Hz, 2H), 1.48 (m, 2H), 1.23 (brd, 16H), 0.85 (t, *J*=6.6 Hz, 3H). ^{13}C NMR [150 MHz, DMSO]: δ 172.73, 167.24, 165.82, 63.87, 62.95, 57.22, 53.40, 33.33, 32.30, 29.02, 28.88, 28.72, 28.38, 24.38, 22.10, 13.97. Melting Point, 202-203°C. $[\alpha]^{20}_{546}$ $^{+}$5.3° (c=.061 g/100mL, DMSO). FTMS+ (APCI): calcd. 357.23840 For $C_{18}H_{33}O_5N_2$. Found, 357.23861.

((2R,5S)-5-(hydroxymethyl)-3,6-dioxopiperazin-2-yl)methyl decanoate (**20**): (79% yield); IR(neat) 3195, 2916, 2850, 1745, 1673, 1460, 1338, 1165. ^{1}H NMR [600 MHz, DMSO]: δ 8.28 (s, 1H), 8.13 (s, 1H), 5.14, (s, 1H), 4.25 (dd, *J*=3.6 Hz, *J*=11.4 Hz, 1H), 4.21 (dd, *J*=2.4 Hz, *J*=10.8 Hz, 1H), 4.12 (s, 1H), 3.75 (brd, 2H), 3.53 (d, *J*=9.6 Hz, 1H), 2.27 (t, *J*=7.2 Hz, 2H), 1.47 (m, 2H), 1.23 (brd, 12H), 0.83 (t, *J*=6 Hz,3H). ^{13}C NMR [150 MHz, DMSO]: δ 172.83, 166.09, 164.81, 65.66, 62.67, 57.10, 53.81, 33.28, 31.29, 28.87, 28.74, 28.68, 28.50, 24.24, 22.12, 13.99. Melting Point, 202-203°C. $[\alpha]^{20}_{546}$ $^{+}$7.3° (c=.072 g/100mL, DMSO). HRMS (APCI) calcd. For $C_{16}H_{29}O_5N_2$ ([M+H]) 329.20710,. Found, 329.20673.

General Procedure of the sulfonation of (**19**) or (**20**):

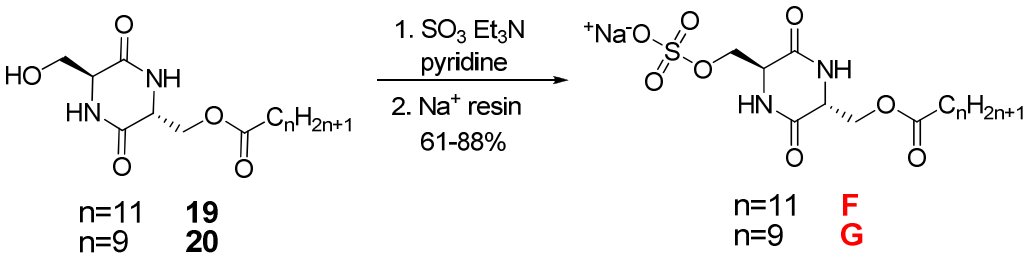

To a flame dried round bottom flask, 1 equivalent of alcohol was combined with 5 equivalents of sulfur trioxide triethylamine complex under nitrogen. Pyridine (100 mL per 0.5 g of starting alcohol) was canulated into the flask and the reaction was stirred overnight. After at least 12 hours, a small amount (0.5 mL) of reaction solution was removed and dried under reduced pressure. A crude ^{1}H NMR was obtained to insure no starting alcohol remained. The reaction solution was concentrated to 20 mL and 100 mL of distilled water was added. The pH of the solution was checked to insure neutrality. If the pH indicated any acidity, additional pyridine was added until pH 7 was obtained.

Purification for (**F**): Excess saturated $NaHCO_3$ solution was added until the solution was basic. A precipitate immediately formed and the solution was filtered through a medium frit as soon as possible. The yellow-white solid was rinsed with hexanes and air dried. The solid was then stirred with methanol (~100mL MeOH per 0.5 g of material) and filtered through a medium frit to obtain pure product.

Purification for (**G**): The solution was stirred with ion exchange resin (sodium form) for 10 minutes (~10 g of resin per 0.5 g of starting alcohol). The resin was filtered off and the liquid was run on a Sephadex LH-20 size exclusion column. The mobile phase was 100% water and 20 mL fractions were collected. As fractions were collected the pH was checked to insure neutrality. If a fraction was found to be acidic 1-2 mL of pyridine was

added to achieve neutral pH. The fractions were then checked with mass spectrometry to identify the desired product. Fractions with an ionization signal > E^5 were pooled and lyophilyzed to remove the water. This resulted in two separate lyophilyzed samples (due to size limitations on the lyophilyzer). These two samples were kept separate and checked by NMR for purity and complete ion exchange. If the presence of any triethylamine was detected the sample was stirred with ion exchange resin (sodium form) and purified again on the Sephadex LH-20 column. If signals in the aromatic region were detected, this indicated the presence of impurities and a Sephadex LH-20 column was run again. Each reaction needed at least 3 total columns to purify all the material, however most needed 5 total columns to fully purify the reaction.

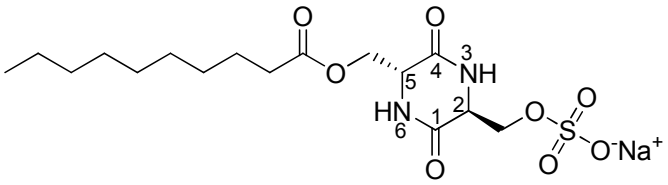

Sodium ((2S,5R)-5-(dodecanoyloxymethyl)-3,6-dioxopiperazin-2-yl)methyl sulfate (**F**) (88% yield) ^{1}H NMR [600 MHz, DMSO]: δ 8.21 (s, 1H), 8.18 (s, 1H), 4.21 (dd, *J*=3 Hz, *J*=8.4 Hz, 1H), 4.16 (d, *J*=11.4 Hz, 1H), 4.08 (s, 1H), 4.97 (m, 1H), 3.89 (m, 3H), 2.43 (t, *J*=7.8 Hz, 2H), 1.44 (m, 2H), 1.20 (brd, 16H), 0.82 (t, *J*=6.6 Hz, 3H). ^{13}C NMR [150 MHz, D_2O]: δ 172.80, 166.38, 165.65, 67.19, 63.79, 55.01, 53.32, 33.33, 31.34, 29.04, 28.92, 28.75, 28.42, 24.41, 22.14, 14.02. Decomposition Point, 231-233°C. $[\alpha]^{20}_{546}$+18.3° (c=.053 g/100mL, DMSO). HRMS (ESI$^-$) calcd. For $C_{18}H_{31}N_2O_8S$ ([M-Na]), 435.17956 Found, 435.18076.

Sodium ((2S,5R)-5-(decanoyloxymethyl)-3,6-dioxopiperazin-2-yl)methyl sulfate (**G**) (61% yield) ^{1}H NMR [400 MHz, D_2O]: δ 4.41 (m, 5H) 4.24 (m, 1H), 2.38 (t, *J*=7.2 Hz, 2H), 1.55 (m, 2H), 1.23 (brd, 12 H), (t, *J*=7.2 Hz, 3H). ^{13}C NMR [150 MHz, D_2O]: δ 176.37, 168.30, 167.81, 68.76, 64.26, 54.94, 54.30, 33.95, 31.46, 28.84, 28.75, 28.63, 28.42, 24.61, 22.33, 13.71. Decomposition Point, 239-240°C. $[\alpha]^{20}_{546}$ $^{+}$21.3° (c=.03 g/100mL, DMSO). HRMS (ESI^{-}) calcd. For $C_{16}H_{27}N_2O_8S$ ([M-Na]) 407.14826, Found, 407.14915. Elemental Anal. Calc. for $C_{16}H_{27}O_8N_2SNa+1/3H_2O$ (430.45): C 44.03, H 6.39, N 6.42, O 30.5, S 7.35; found C 44.02, H 6.53, N 6.63, O 30.09, S 7.16.

Crystal data and structure refinement (3*S*,6*S*)-3,6-bis(hydroxymethyl)piperazine-2,5-dione (**8**)

Identification code	JSser	
Empirical formula	C6 H10 N2 O4	
Formula weight	174.16	
Temperature	173(2) K	
Wavelength	1.54178 Å	
Crystal system	Monoclinic	
Space group	P2(1)	
Unit cell dimensions	a = 8.5121(15) Å	α= 90°.
	b = 7.7427(13) Å	β= 90.134(9)°.
	c = 11.057(2) Å	γ = 90°.
Volume	728.7(2) $Å^3$	
Z	4	
Density (calculated)	1.587 Mg/m^3	
Absorption coefficient	1.157 mm^{-1}	
F(000)	368	
Crystal size	0.34 x 0.06 x 0.05 mm^3	
Theta range for data collection	4.00 to 65.69°.	
Index ranges	-9<=h<=9, -8<=k<=9, -12<=l<=10	
Reflections collected	3341	
Independent reflections	1762 [R(int) = 0.0235]	
Completeness to theta = 65.69°	81.9 %	
Absorption correction	Semi-empirical from equivalents	
Max. and min. transmission	0.9444 and 0.6944	
Refinement method	Full-matrix least-squares on F^2	
Data / restraints / parameters	1762 / 1 / 220	
Goodness-of-fit on F^2	1.220	
Final R indices [I>2sigma(I)]	R1 = 0.0670, wR2 = 0.1751	
R indices (all data)	R1 = 0.0922, wR2 = 0.2446	
Absolute structure parameter	0.4(4)	
Largest diff. peak and hole	1.072 and -0.981 e.$Å^{-3}$	

Table 2. Atomic coordinates (x 10^4) and equivalent isotropic displacement parameters ($Å^2$x 10^3) for **8**. U(eq) is defined as one third of the trace of the orthogonalized U^{ij} tensor.

	x	y	z	U(eq)
C(1)	1145(6)	1539(7)	4159(5)	9(1)
C(2)	2771(6)	2290(7)	4376(6)	10(1)
C(3)	3918(6)	-402(8)	3539(5)	10(1)
C(4)	2294(6)	-1136(8)	3271(5)	11(1)
C(5)	2920(6)	4062(7)	3787(5)	14(1)
C(6)	2150(6)	-1668(8)	1939(6)	14(1)
C(7)	8922(6)	3271(7)	1463(5)	9(1)
C(8)	7276(6)	3952(8)	1715(5)	9(1)
C(9)	6134(6)	1316(7)	853(5)	10(1)
C(10)	7771(6)	564(7)	627(6)	10(1)
C(11)	7151(6)	4516(8)	3051(6)	13(1)
C(12)	7920(6)	-1211(8)	1223(6)	15(1)
N(1)	4053(5)	1157(6)	4001(5)	11(1)
N(2)	1018(5)	22(6)	3614(5)	11(1)
N(3)	6031(5)	2824(6)	1397(4)	13(1)
N(4)	9063(5)	1680(6)	999(5)	12(1)
O(1)	0(4)	2386(6)	4491(4)	17(1)
O(2)	5066(4)	-1321(5)	3297(4)	15(1)
O(3)	3017(4)	3941(7)	2497(4)	19(1)
O(4)	2031(4)	-219(6)	1140(4)	17(1)
O(5)	10058(4)	4184(5)	1695(4)	17(1)
O(6)	5001(5)	465(6)	503(4)	17(1)
O(7)	7047(4)	3060(6)	3851(4)	18(1)
O(8)	8030(4)	-1112(7)	2510(4)	17(1)

Table 3. Bond lengths [Å] and angles [°] for **8**.

C(1)-O(1)	1.232(7)
C(1)-N(2)	1.324(8)
C(1)-C(2)	1.520(7)
C(2)-N(1)	1.460(7)
C(2)-C(5)	1.524(8)
C(2)-H(2)	1.0000
C(3)-O(2)	1.238(7)
C(3)-N(1)	1.315(8)
C(3)-C(4)	1.523(7)
C(4)-N(2)	1.460(7)
C(4)-C(6)	1.534(9)
C(4)-H(4)	1.0000
C(5)-O(3)	1.432(8)
C(5)-H(5A)	0.9900
C(5)-H(5B)	0.9900
C(6)-O(4)	1.431(8)
C(6)-H(6A)	0.9900
C(6)-H(6B)	0.9900
C(7)-O(5)	1.224(7)
C(7)-N(4)	1.341(8)
C(7)-C(8)	1.523(7)
C(8)-N(3)	1.417(7)
C(8)-C(11)	1.544(9)
C(8)-H(8)	1.0000
C(9)-O(6)	1.230(7)
C(9)-N(3)	1.317(8)
C(9)-C(10)	1.531(7)
C(10)-N(4)	1.457(7)
C(10)-C(12)	1.529(8)
C(10)-H(10)	1.0000
C(11)-O(7)	1.436(8)
C(11)-H(11A)	0.9900

C(11)-H(11B)	0.9900
C(12)-O(8)	1.428(8)
C(12)-H(12A)	0.9900
C(12)-H(12B)	0.9900
N(1)-H(1N)	0.8800
N(2)-H(2N)	0.8800
N(3)-H(3N)	0.8800
N(4)-H(4N)	0.8800
O(3)-H(30)	0.8400
O(4)-H(4O)	0.9787
O(7)-H(7O)	0.8400
O(8)-H(8O)	0.8400

O(1)-C(1)-N(2)	122.9(5)
O(1)-C(1)-C(2)	118.1(5)
N(2)-C(1)-C(2)	119.0(5)
N(1)-C(2)-C(1)	113.9(5)
N(1)-C(2)-C(5)	110.9(5)
C(1)-C(2)-C(5)	110.7(4)
N(1)-C(2)-H(2)	107.0
C(1)-C(2)-H(2)	107.0
C(5)-C(2)-H(2)	107.0
O(2)-C(3)-N(1)	122.9(5)
O(2)-C(3)-C(4)	117.3(5)
N(1)-C(3)-C(4)	119.8(5)
N(2)-C(4)-C(3)	113.3(5)
N(2)-C(4)-C(6)	110.9(4)
C(3)-C(4)-C(6)	110.9(4)
N(2)-C(4)-H(4)	107.1
C(3)-C(4)-H(4)	107.1
C(6)-C(4)-H(4)	107.1
O(3)-C(5)-C(2)	111.8(5)
O(3)-C(5)-H(5A)	109.3
C(2)-C(5)-H(5A)	109.3

O(3)-C(5)-H(5B)	109.3
C(2)-C(5)-H(5B)	109.3
H(5A)-C(5)-H(5B)	107.9
O(4)-C(6)-C(4)	112.8(5)
O(4)-C(6)-H(6A)	109.0
C(4)-C(6)-H(6A)	109.0
O(4)-C(6)-H(6B)	109.0
C(4)-C(6)-H(6B)	109.0
H(6A)-C(6)-H(6B)	107.8
O(5)-C(7)-N(4)	122.6(5)
O(5)-C(7)-C(8)	119.2(5)
N(4)-C(7)-C(8)	118.1(5)
N(3)-C(8)-C(7)	115.4(5)
N(3)-C(8)-C(11)	111.0(5)
C(7)-C(8)-C(11)	109.8(4)
N(3)-C(8)-H(8)	106.7
C(7)-C(8)-H(8)	106.7
C(11)-C(8)-H(8)	106.7
O(6)-C(9)-N(3)	124.5(5)
O(6)-C(9)-C(10)	117.3(5)
N(3)-C(9)-C(10)	118.2(5)
N(4)-C(10)-C(12)	110.5(4)
N(4)-C(10)-C(9)	114.6(5)
C(12)-C(10)-C(9)	110.3(5)
N(4)-C(10)-H(10)	107.1
C(12)-C(10)-H(10)	107.1
C(9)-C(10)-H(10)	107.1
O(7)-C(11)-C(8)	111.8(5)
O(7)-C(11)-H(11A)	109.3
C(8)-C(11)-H(11A)	109.3
O(7)-C(11)-H(11B)	109.3
C(8)-C(11)-H(11B)	109.3
H(11A)-C(11)-H(11B)	107.9
O(8)-C(12)-C(10)	112.7(5)

O(8)-C(12)-H(12A)	109.1
C(10)-C(12)-H(12A)	109.1
O(8)-C(12)-H(12B)	109.1
C(10)-C(12)-H(12B)	109.1
H(12A)-C(12)-H(12B)	107.8
C(3)-N(1)-C(2)	126.7(5)
C(3)-N(1)-H(1N)	116.7
C(2)-N(1)-H(1N)	116.7
C(1)-N(2)-C(4)	127.1(4)
C(1)-N(2)-H(2N)	116.5
C(4)-N(2)-H(2N)	116.5
C(9)-N(3)-C(8)	127.5(4)
C(9)-N(3)-H(3N)	116.2
C(8)-N(3)-H(3N)	116.2
C(7)-N(4)-C(10)	125.8(5)
C(7)-N(4)-H(4N)	117.1
C(10)-N(4)-H(4N)	117.1
C(5)-O(3)-H(30)	109.5
C(6)-O(4)-H(4O)	102.1
C(11)-O(7)-H(7O)	109.5
C(12)-O(8)-H(8O)	109.5

Symmetry transformations used to generate equivalent atoms:

Table 4. Anisotropic displacement parameters ($Å^2 x\ 10^3$) for **8**. The anisotropic displacement factor exponent takes the form: $-2\pi^2[\ h^2\ a^{*2}U^{11} + ... + 2\ h\ k\ a^*\ b^*\ U^{12}\ ]$

	U^{11}	U^{22}	U^{33}	U^{23}	U^{13}	U^{12}
C(1)	8(2)	13(3)	7(3)	-1(2)	1(2)	2(2)
C(2)	8(2)	13(3)	9(3)	-1(2)	0(2)	3(2)
C(3)	11(3)	12(2)	8(3)	8(3)	-5(2)	-5(2)
C(4)	14(3)	8(2)	10(3)	-2(2)	-1(2)	2(2)
C(5)	14(2)	10(3)	20(3)	-1(3)	0(2)	3(2)
C(6)	14(3)	12(3)	16(3)	-3(2)	-3(2)	1(2)
C(7)	12(3)	12(2)	3(3)	3(2)	-1(2)	0(2)
C(8)	14(3)	6(2)	8(3)	4(2)	1(2)	1(2)
C(9)	12(2)	14(3)	4(3)	0(2)	-1(2)	-5(2)
C(10)	8(2)	12(2)	8(3)	2(2)	-1(2)	-2(2)
C(11)	17(3)	12(3)	10(3)	-1(2)	6(2)	-2(2)
C(12)	17(3)	11(3)	16(3)	-1(2)	-1(2)	3(2)
N(1)	6(2)	13(2)	14(3)	-2(2)	-3(2)	2(2)
N(2)	4(2)	11(2)	17(3)	-3(2)	3(2)	-2(2)
N(3)	9(2)	18(3)	11(3)	1(2)	-2(2)	6(2)
N(4)	7(2)	14(2)	15(3)	-1(2)	4(2)	3(2)
O(1)	10(2)	23(2)	17(2)	-5(2)	2(2)	2(2)
O(2)	10(2)	17(2)	19(2)	-1(2)	1(2)	4(1)
O(3)	13(2)	26(2)	19(2)	10(2)	1(2)	2(2)
O(4)	12(2)	29(2)	8(2)	3(2)	-1(2)	6(2)
O(5)	11(2)	21(2)	17(2)	-1(2)	0(2)	-5(2)
O(6)	12(2)	20(2)	18(3)	-5(2)	-2(2)	-3(2)
O(7)	14(2)	28(2)	13(2)	1(2)	-1(2)	0(2)
O(8)	9(2)	26(2)	17(2)	11(2)	0(2)	-1(2)

Table 5. Hydrogen coordinates (x 10^4) and isotropic displacement parameters ($Å^2$x 10^3) for **8**.

	x	y	z	U(eq)
H(2)	2883	2464	5268	12
H(4)	2178	-2210	3766	13
H(5A)	1999	4774	4008	17
H(5B)	3873	4645	4101	17
H(6A)	3081	-2363	1713	17
H(6B)	1209	-2406	1838	17
H(8)	7142	5018	1215	11
H(10)	7872	386	-265	11
H(11A)	8085	5214	3268	16
H(11B)	6210	5252	3153	16
H(12A)	6995	-1919	1001	18
H(12B)	8867	-1797	906	18
H(1N)	5013	1558	4093	13
H(2N)	59	-325	3440	13
H(3N)	5078	3171	1586	15
H(4N)	10021	1272	911	14
H(30)	3837	3405	2305	29
H(4O)	3133	99	1026	20
H(7O)	7893	2503	3831	27
H(8O)	7142	-1295	2814	26

Table 6. Torsion angles [°] for **8.**

O(1)-C(1)-C(2)-N(1)	177.3(5)
N(2)-C(1)-C(2)-N(1)	-3.3(8)
O(1)-C(1)-C(2)-C(5)	-56.9(7)
N(2)-C(1)-C(2)-C(5)	122.5(6)
O(2)-C(3)-C(4)-N(2)	178.6(5)
N(1)-C(3)-C(4)-N(2)	-1.9(8)
O(2)-C(3)-C(4)-C(6)	-55.9(7)
N(1)-C(3)-C(4)-C(6)	123.6(5)
N(1)-C(2)-C(5)-O(3)	54.9(6)
C(1)-C(2)-C(5)-O(3)	-72.6(6)
N(2)-C(4)-C(6)-O(4)	53.6(6)
C(3)-C(4)-C(6)-O(4)	-73.3(6)
O(5)-C(7)-C(8)-N(3)	178.8(5)
N(4)-C(7)-C(8)-N(3)	-1.6(7)
O(5)-C(7)-C(8)-C(11)	-54.9(7)
N(4)-C(7)-C(8)-C(11)	124.8(5)
O(6)-C(9)-C(10)-N(4)	176.6(5)
N(3)-C(9)-C(10)-N(4)	-3.0(8)
O(6)-C(9)-C(10)-C(12)	-58.1(7)
N(3)-C(9)-C(10)-C(12)	122.3(6)
N(3)-C(8)-C(11)-O(7)	53.8(6)
C(7)-C(8)-C(11)-O(7)	-75.0(6)
N(4)-C(10)-C(12)-O(8)	55.0(6)
C(9)-C(10)-C(12)-O(8)	-72.6(5)
O(2)-C(3)-N(1)-C(2)	-176.4(6)
C(4)-C(3)-N(1)-C(2)	4.2(8)
C(1)-C(2)-N(1)-C(3)	-1.7(8)
C(5)-C(2)-N(1)-C(3)	-127.3(6)
O(1)-C(1)-N(2)-C(4)	-174.9(6)
C(2)-C(1)-N(2)-C(4)	5.8(9)
C(3)-C(4)-N(2)-C(1)	-3.2(9)
C(6)-C(4)-N(2)-C(1)	-128.7(6)

O(6)-C(9)-N(3)-C(8)	-173.2(6)
C(10)-C(9)-N(3)-C(8)	6.5(9)
C(7)-C(8)-N(3)-C(9)	-4.2(9)
C(11)-C(8)-N(3)-C(9)	-129.9(6)
O(5)-C(7)-N(4)-C(10)	-175.8(6)
C(8)-C(7)-N(4)-C(10)	4.6(8)
C(12)-C(10)-N(4)-C(7)	-127.7(6)
C(9)-C(10)-N(4)-C(7)	-2.5(9)

Symmetry transformations used to generate equivalent atoms:

Table 7. Hydrogen bonds for **8** [Å and °].

D-H...A	d(D-H)	d(H...A)	d(D...A)	<(DHA)
N(1)-H(1N)...O(7)	0.88	2.10	2.949(6)	160.9
N(2)-H(2N)...O(8)#1	0.88	2.10	2.952(6)	163.3
N(3)-H(3N)...O(3)	0.88	2.11	2.970(6)	165.2
N(4)-H(4N)...O(4)#2	0.88	2.08	2.927(6)	161.5
O(3)-H(30)...N(3)	0.84	2.17	2.970(6)	159.5
O(4)-H(4O)...O(6)	0.98	1.72	2.679(6)	167.0
O(7)-H(7O)...O(1)#2	0.84	1.94	2.662(6)	143.9
O(8)-H(8O)...O(2)	0.84	1.85	2.676(5)	168.4

Symmetry transformations used to generate equivalent atoms:
#1 x-1,y,z #2 x+1,y,z

Crystal data and structure refinement for (3S,6R)-3-(benzyloxymethyl)-6(hydroxymethyl) piperazine-2,5-dione (**16**)

Identification code	JS4_180A	
Empirical formula	C13 H16 N2 O4	
Formula weight	264.28	
Temperature	173(2) K	
Wavelength	1.54178 Å	
Crystal system	Orthorhombic	
Space group	P2(1)2(1)2(1)	
Unit cell dimensions	a = 6.097(3) Å	α= 90°.
	b = 8.078(5) Å	β= 90°.
	c = 26.013(11) Å	γ = 90°.
Volume	1281.0(11) $Å^3$	
Z	4	
Density (calculated)	1.370 Mg/m^3	
Absorption coefficient	0.856 mm^{-1}	
F(000)	560	
Crystal size	0.38 x 0.04 x 0.02 mm^3	
Theta range for data collection	3.40 to 64.94°.	
Index ranges	-5<=h<=7, -8<=k<=7, -30<=l<=25	
Reflections collected	4019	
Independent reflections	1797 [R(int) = 0.1036]	
Completeness to theta = 64.94°	88.6 %	
Absorption correction	Semi-empirical from equivalents	
Max. and min. transmission	0.9831 and 0.7368	
Refinement method	Full-matrix least-squares on F^2	
Data / restraints / parameters	1797 / 0 / 97	
Goodness-of-fit on F^2	1.035	
Final R indices [I>2sigma(I)]	R1 = 0.1011, wR2 = 0.1648	
R indices (all data)	R1 = 0.4019, wR2 = 0.2508	
Absolute structure parameter	2(2)	
Largest diff. peak and hole	0.049 and -0.039 $e.Å^{-3}$	

Table 2. Atomic coordinates (x 10^4) and equivalent isotropic displacement parameters ($Å^2$x 10^3) for **16**. U(eq) is defined as one third of the trace of the orthogonalized U^{ij} tensor.

	x	y	z	U(eq)
C(1)	350(30)	3590(20)	791(6)	242(7)
C(2)	2690(30)	3840(30)	576(7)	233(8)
C(3)	990(30)	5740(20)	-26(7)	263(8)
C(4)	-1140(40)	4930(20)	2(7)	241(8)
C(5)	300(30)	4600(20)	1268(7)	281(9)
C(6)	100(20)	7520(20)	1485(5)	264(8)
C(7)	1456(17)	7473(13)	2001(3)	249(6)
C(8)	582(12)	6658(12)	2425(4)	251(7)
C(9)	1747(17)	6606(12)	2884(3)	263(6)
C(10)	3786(16)	7367(13)	2919(3)	285(7)
C(11)	4660(12)	8182(13)	2495(4)	273(7)
C(12)	3495(18)	8234(12)	2036(3)	268(7)
C(13)	1400(30)	6210(30)	-616(6)	276(8)
N(1)	-1460(17)	4000(20)	447(4)	253(7)
N(2)	2670(20)	4725(15)	145(4)	255(6)
O(1)	771(15)	6235(17)	1135(4)	276(5)
O(2)	4230(19)	3055(16)	755(3)	276(6)
O(3)	-2913(16)	5314(14)	-224(3)	281(7)
O(4)	1472(15)	4755(16)	-926(3)	292(6)

Table 3. Bond lengths [Å] and angles [°] for **16**.

C(1)-N(1)	1.457(14)	C(13)-H(13B)	0.9900
C(1)-C(5)	1.485(18)	N(1)-H(1A)	0.8800
C(1)-C(2)	1.547(18)	N(2)-H(2)	0.8800
C(1)-H(1)	1.0000	O(4)-H(4A)	0.8400
C(2)-O(2)	1.223(18)		
C(2)-N(2)	1.331(18)	N(1)-C(1)-C(5)	112.1(15)
C(3)-N(2)	1.386(16)	N(1)-C(1)-C(2)	116.6(14)
C(3)-C(4)	1.46(2)	C(5)-C(1)-C(2)	104.5(16)
C(3)-C(13)	1.599(19)	N(1)-C(1)-H(1)	107.7
C(3)-H(3)	1.0000	C(5)-C(1)-H(1)	107.7
C(4)-O(3)	1.270(19)	C(2)-C(1)-H(1)	107.7
C(4)-N(1)	1.392(17)	O(2)-C(2)-N(2)	127(2)
C(5)-O(1)	1.392(17)	O(2)-C(2)-C(1)	120(2)
C(5)-H(5A)	0.9900	N(2)-C(2)-C(1)	111.4(18)
C(5)-H(5B)	0.9900	N(2)-C(3)-C(4)	112.0(18)
C(6)-O(1)	1.442(16)	N(2)-C(3)-C(13)	109.5(15)
C(6)-C(7)	1.576(14)	C(4)-C(3)-C(13)	107.0(16)
C(6)-H(6A)	0.9900	N(2)-C(3)-H(3)	109.4
C(6)-H(6B)	0.9900	C(4)-C(3)-H(3)	109.4
C(7)-C(8)	1.3900	C(13)-C(3)-H(3)	109.4
C(7)-C(12)	1.3900	O(3)-C(4)-N(1)	113.3(18)
C(8)-C(9)	1.3900	O(3)-C(4)-C(3)	129(2)
C(8)-H(8)	0.9500	N(1)-C(4)-C(3)	114.2(19)
C(9)-C(10)	1.3900	O(1)-C(5)-C(1)	107.9(14)
C(9)-H(9)	0.9500	O(1)-C(5)-H(5A)	110.1
C(10)-C(11)	1.3900	C(1)-C(5)-H(5A)	110.1
C(10)-H(10)	0.9500	O(1)-C(5)-H(5B)	110.1
C(11)-C(12)	1.3900	C(1)-C(5)-H(5B)	110.1
C(11)-H(11)	0.9500	H(5A)-C(5)-H(5B)	108.4
C(12)-H(12)	0.9500	O(1)-C(6)-C(7)	111.7(12)
C(13)-O(4)	1.424(18)	O(1)-C(6)-H(6A)	109.3
C(13)-H(13A)	0.9900	C(7)-C(6)-H(6A)	109.3

O(1)-C(6)-H(6B)	109.3	C(13)-O(4)-H(4A)	109.5
C(7)-C(6)-H(6B)	109.3		
H(6A)-C(6)-H(6B)	107.9		
C(8)-C(7)-C(12)	120.0		
C(8)-C(7)-C(6)	119.1(10)		
C(12)-C(7)-C(6)	120.9(10)		
C(7)-C(8)-C(9)	120.0		
C(7)-C(8)-H(8)	120.0		
C(9)-C(8)-H(8)	120.0		
C(8)-C(9)-C(10)	120.0		
C(8)-C(9)-H(9)	120.0		
C(10)-C(9)-H(9)	120.0		
C(11)-C(10)-C(9)	120.0		
C(11)-C(10)-H(10)	120.0		
C(9)-C(10)-H(10)	120.0		
C(10)-C(11)-C(12)	120.0		
C(10)-C(11)-H(11)	120.0		
C(12)-C(11)-H(11)	120.0		
C(11)-C(12)-C(7)	120.0		
C(11)-C(12)-H(12)	120.0		
C(7)-C(12)-H(12)	120.0		
O(4)-C(13)-C(3)	110.7(16)		
O(4)-C(13)-H(13A)	109.5		
C(3)-C(13)-H(13A)	109.5		
O(4)-C(13)-H(13B)	109.5		
C(3)-C(13)-H(13B)	109.5		
H(13A)-C(13)-H(13B)	108.1		
C(4)-N(1)-C(1)	121.7(15)		
C(4)-N(1)-H(1A)	119.2		
C(1)-N(1)-H(1A)	119.2		
C(2)-N(2)-C(3)	126.6(17)		
C(2)-N(2)-H(2)	116.7		
C(3)-N(2)-H(2)	116.7		
C(5)-O(1)-C(6)	117.8(14)		

Symmetry transformations used to generate equivalent atoms:

Table 4. Anisotropic displacement parameters ($Å^2 x\ 10^3$)for **16**. The anisotropic displacement factor exponent takes the form: $-2\pi^2[\ h^2 a^{*2} U^{11} + ... + 2\ h\ k\ a^*\ b^*\ U^{12}\ ]$

	U^{11}	U^{22}	U^{33}	U^{23}	U^{13}	U^{12}
N(1)	201(10)	333(18)	225(11)	27(11)	-3(9)	-6(11)
N(2)	294(14)	256(15)	215(11)	34(11)	-13(11)	17(12)
O(1)	259(9)	254(13)	315(12)	-18(12)	-10(8)	-8(10)
O(2)	258(10)	311(15)	258(11)	-11(10)	-17(8)	31(11)
O(3)	218(10)	333(16)	291(10)	32(9)	-40(8)	40(10)
O(4)	300(10)	309(16)	266(9)	-25(10)	-65(8)	-18(10)

Table 5. Hydrogen coordinates (x 10^4) and isotropic displacement parameters ($Å^2$x 10^3) for **16**.

	x	y	z	U(eq)
H(1)	189	2406	892	290
H(3)	960	6775	185	316
H(5A)	-1163	4535	1431	337
H(5B)	1405	4186	1516	337
H(6A)	-1480	7390	1565	317
H(6B)	300	8613	1319	317
H(8)	-812	6138	2401	302
H(9)	1149	6049	3173	316
H(10)	4582	7331	3233	342
H(11)	6053	8702	2519	327
H(12)	4092	8791	1746	322
H(13A)	200	6938	-738	332
H(13B)	2796	6820	-649	332
H(1A)	-2789	3653	522	304
H(2)	3847	4661	-51	306
H(4A)	1202	3923	-743	437

Table 6. Hydrogen bonds for **16** [Å and °].

D-H...A	d(D-H)	d(H...A)	d(D...A)	<(DHA)
N(1)-H(1A)...O(2)#1	0.88	1.98	2.852(15)	173.6
N(2)-H(2)...O(3)#2	0.88	2.09	2.895(19)	151.2
O(4)-H(4A)...O(2)#3	0.84	2.00	2.686(16)	138.4

Symmetry transformations used to generate equivalent atoms:
#1 x-1,y,z #2 x+1,y,z #3 x-1/2,-y+1/2,-z

References

(1) Jonsson, B.; Lindman, B.; Holmberg, K.; Kronberg, B. *Surfactants and Polymers in Aqueous Solution*; John WIley & Sons: Chichester, 1998.

(2) Tanford, C. *The Hydrophobic Effect: Formation of Micelles and Biological Membranes*; 2nd ed.; John Wiley & Sons: New York, 1980.

(3) Myers, D. *Surfaces, Interfaces, and Colloids*; VCH Publishers: New York, 1991.

(4) Nagarajan, R. *Langmuir* **2002**, *18*, 31-38.

(5) Israelachvili, J.; Mitchell, D. J.; Ninham, B. W. *J. Chem. Soc., Faraday Trans. II* **1976**, *72*, 1525-1568.

(6) Messenga, R.; Schurtenberger, P.; Burbidge, A.; Michel, M. *Nat. Mater.* **2005**, *4*, 729-740.

(7) Cheng, Y.; Ho, D. M.; Gottlieb, C. R.; Kahne, D.; Bruck, M. A. *J. Am. Chem. Soc.* **1992**, *114*, 7319-7320.

(8) Virtanen, E.; Kolehmaninen, E. *Eur. J. Org. Chem.* **2004**, 3385-3399.

(9) Taotafa, U.; McMullin, D. B.; Lee, S. C.; Hansen, L. D.; Savage, P. B. *Org. Lett.* **2000**, *2*, 4117-4120.

(10) Zhang, Q.; Xingquan, M.; Ward, A.; Hong, W. X.; Jaakola, V. P.; Stevens, R. C.; Finn, M. G.; Chang, G. *Angew. Chem. Int. Ed.* **2007**, *46*, 7023-7025.

(11) Willemen, H. M.; Marcelis, A. T. M.; Sudholter, E. J. R. *Langmuir* **2003**, *19*, 2588-2591.

(12) Zhong, Z.; Yan, J.; Zhao, Y. *Langmuir* **2005**, *21*, 6235-6239.

(13) Barrett, D. G.; Gellman, S. H. *J. Am. Chem. Soc.* **1993**, *115*, 9343-9344.

(14) McQuade, D. T.; Barrett, D. G.; Desper, J. M.; Hayashi, R. K.; Gellman, S. H. *J. Am. Chem. Soc.* **1995**, *117*, 4862-4869.

(15) Stjerndahl, M.; Lundberg, D.; Zhang, H.; Menger, F. M. *J. Phys. Chem. B* **2007**, *111*, 2008-2014.

(16) Infante, M. R.; Perez, L.; Pinazo, A.; Clapes, P.; Moran, M. C.; Angelet, M.; Garcia, M. T.; Vinardell, M. P. *C. R. Chim.* **2004**, *7*, 583-592.

(17) Laughlin, R. G. *The Aqueous Phase Behavior of Surfactants*; Academic Press Inc: San Diego, 1994.

(18) Leo, A.; Hansch, C.; Elkins, D. *Chem. Rev.* **1971**, *71*, 525-616.

(19) Menger, F. M.; Zhang, H.; deJoannis, J.; Kindt, J. T. *Langmuir* **2007**, *23*, 2308-2310.

(20) Menger, F. M.; Zhang, H. *Langmuir* **2005**, *21*, 10428-10438.

(21) Kjellin, U. R. M.; Claesson, P. M.; Linse, P. *Langmuir* **2002**, *18*, 6745-6753.

(22) Pires, P. A. R.; El Seoud, O. A. *J. Colloid Interf. Sci.* **2006**, *304*, 474-485.

(23) Ohta, A.; Toda, K.; Morimoto, Y.; Asakawa, T.; Miyagishi, S. *Colloid Surface A* **2008**, *317*, 316-322.

(24) Gerova, M.; Rodrigues, F.; Lamere, J.-F.; Dobrev, A.; Fery-Forgues, S. *J. Colloid Interf. Sci.* **2008**, *319*, 526-533.

(25) Roy, S.; Dey, J. *J. Colloid Interf. Sci.* **2007**, *307*, 229-234.

(26) Rizvi, S. A. A.; Zheng, J.; Apkarian, R. P.; Dublin, S. N.; Shamsi, S. A. *Anal. Chem.* **2007**, *79*, 879-898.

(27) Billiot, E.; Agbaria, R. A.; Thibodeaux, S.; Shamsi, S.; Warner, I. M. *Anal. Chem.* **1999**, *71*, 1252-1256.

(28) Rizvi, S. A. A., Shahab A. S. *Electrophoresis* **2005**, *26*, 4172-4186.

(29) Ohta, A.; Ozawa, N.; Nakashima, S.; Asakawa, T.; Miyagishi, S. *Colloid Polym. Sci.* **2003**, *281*, 363-369.

(30) From Physical & Theoretical Chemistry Laboratory Oxford University: http://physchem.ox.ac.uk/~rkt/lectures/amphi.html; Accessed March 15, 2008.

(31) Feldman, K. S.; Bobo, J. S.; Ensel, S. M.; Lee, Y. B.; Weinreb, P. H. *J. Org. Chem.* **1990**, *55*, 474-481.

(32) Stephenson, B.; Solladie, G.; Mosher, H. S. *J. Am. Chem. Soc.* **1972**, *94*, 4184-4188.

(33) Menger, F. M.; Chlebowski, M. E. *Langmuir* **2005**, *21*, 2689-2695.

(34) Menger, F. M.; Galloway, A. L.; Chlebowski, M. E. *Langmuir* **2005**, *21*, 9010-9012.

(35) Oh, S. G.; Shah, D. O. *J. Phys. Chem.* **1993**, *97*, 284-286.

(36) Meyers, D. *Surfaces, Interfaces and Colloids: Principles and Applications*; VCH Publishers: New York, 1991.

(37) Furo, I. *J. Mol. Liq.* **2005**, *117*, 117-137.

(38) Olsson, U.; Soederman, O.; Guering, P. *J. Phys. Chem.* **1986**, *90*, 5223-5232.

(39) Carpena, P.; Aguiar, J.; Bernaola-Galvan, P.; Carnero Ruiz, C. *Langmuir* **2002**, *18*, 6054-6058.

(40) Mason, T. G.; Weitz, D. A. *Phys. Rev. Lett.* **1995**, *74*, 12501253.

(41) Cicuta, P.; Donald, A. M. *Soft Matter* **2007**, *3*, 1449-1455.

(42) Menger, F. M.; Caran, K. L.; Apkarian, R. P. *Langmuir* **2000**, *16*, 98-101.

(43) Lambert, J. B.; Shurvell, H. F.; Lightner, D. A.; Cooks, R. G. *Organic Structural Spectroscopy*; Prentice-Hall: Upper Saddle River, New Jersey, 1998.

(44) From University of Cambridge, Department of Materials Science and Metallurgy: http://www.doitpoms.ac.uk/tlplib/atomic-scale-structure/images/polariser2.gif; Accessed November 26, 2007.

(45) Yu, Q.; Frömmel, J.; Wolff, T.; Procházka, K. *Colloid. Polym. Sci.* **2004**, *282*, 1039-1043.

(46) Karlberg, M.; Stjerndahl, M.; Lundberg, D.; Piculell, L. *Langmuir* **2005**, *21*, 9756-9763.

(47) Akerlund, J.; Harmeier, S.; Pumphrey, J.; Timm, D. C.; Brand, J. I. *J. Appl. Polym. Sci.* **2000**, *78*, 2213-2218.

(48) de Vries, E. J.; Kellogg, R. M. *J. Chem. Soc., Chem. Commun.* **1993**, 238-240.

(49) Hanabusa, K.; Matsumoto, M.; Kimura, M.; Kakehi, A.; Shirai, H. *J. Colloid. Interf. Sci.* **2000**, *224*, 231-244.

(50) Mori, A.; Imanishi, Y.; Ito, T.; Sakaoku, K. *Biomaterials* **1985**, *6*, 325-337.

(51) Dagan, S.; Gottlieb, P.; Tzehoval, E.; Feldman, M.; Fridkin, M.; Yasumura, K.; Okamoto, K.; Yajima, H. *J. Med. Chem.* **1986**, *29*, 1961-1968.

(52) Montalbetti, C. A. G. N.; Falque, V. *Tetrahedron* **2005**, *61*, 10827-10852.

(53) Fava, G. G.; Belicchi, M. F. *Acta. Cryst. B.* **1981**, *37*, 625-629.

(54) Thea, S.; Guanti, G.; Hopkins, A. R.; Williams, A. *J. Org. Chem.* **1985**, *50*, 3336-3341.

(55) Eldo, J.; Heng, S.; Kantrowitz, E. R. *Bioorg. Med. Chem. Lett.* **2007**, *17*, 2086-2090.

(56) Bhattachar, S. N.; Deschenes, L. A.; Wesley, J. A. *Drug Discov. Today.* **2006**, *11*, 1012-1018.

(57) Megoulas, N. C.; Koupparis, M. A. *Crit. Rev. Anal. Chem.* **2005**, *35*, 301-316.

(58) Mourey, T. H.; Oppenheimer, L. E. *Anal. Chem.* **1984**, *56*, 2427-2434.

(59) From Cyberlipids: http://www.cyberlipid.org/images/pict106.gif; Accessed March 3, 2008.

(60) From American Instrument Exchange: http://www.americaninstrument.com/equipment/hplc/2942-hplc.asp; Accessed March 1, 2008.

(61) Moroi, Y.; Matuura, R. *Bull. Chem. Soc. Jpn.* **1988**, *61*, 333-339.

(62) Nishikido, N.; Kobayashi, H.; Tanaka, M. *J. Phys. Chem.* **1982**, *86*, 3170-3172.

(63) Khatua, D.; Gupta, A.; Dey, J. *J. Colloid. Interf. Sci.* **2006**, *298*, 451-456.

(64) Bales, B. L.; Benrraou, M.; Zana, R. *J. Phys. Chem. B* **2002**, *106*, 9033-9035.

(65) Ranganathan, R.; Tran, L.; Bales, B. L. *J. Phys. Chem. B* **2000**, *104*, 2260-2264.

(66) Seredyuk, V.; Alami, E.; Nyden, M.; Holmberg, K.; Peresypkin, A. V.; Menger, F. M. *Colloid Surface A* **2002**, *203*, 245-258.

(67) Han, F.; Zhang, G. *Colloid Surface A* **2004**, *237*, 79-85.

(68) Kralchevsky, P. A.; Danov, K. D.; Kolev, V. L.; Broze, G.; Mehreteab, A. *Langmuir* **2003**, *19*, 5004-5018.

(69) Hernainz, F.; Calero, M.; Blazquez, G.; Caro, A. *J. Chem. Eng. Data* **2006**, *51*, 1216-1219.

(70) Lin, S. Y.; Lin, Y. Y.; Chen, E. M.; Hsu, C. T.; Kwan, C. C. *Langmuir* **1999**, *15*, 4370-4376.

(71) Behme, M. T.; Cordes, E. H. *J. Org. Chem.* **1964**, *29*, 1255-1257.

(72) Lundberg, D.; Unga, J.; Galloway, A. L.; Menger, F. M. *Langmuir* **2007**, *23*, 11434-11442.

(73) Stejskal, F. O.; Tanner, J. E. *J. Chem. Phys.* **1965**, *42*, 288-292.

(74) Stilbs, P. *Prog. Nucl. Mag. Res. Sp.* **1987**, *19*, 1-45.

(75) Ginley, M.; Henriksson, U.; Li, P. *J. Phys. Chem.* **1990**, *94*, 4644-4648.

(76) Haffner, F. D.; Piccione, G. A.; Rosenblum, C. *J. Phys. Chem.* **1942**, *46*, 662-670.

(77) Kim, Y. A.; Chung, H. M.; Park, J. S.; Choi, W.; Min, J.; Park, N. H.; Kim, K. H.; Jhon, G. J.; Han, S. Y. *J. Org. Chem.* **2003**, *68*, 10162-10165.